Centrifugal Turbopumps

Flow Physics and Modelling

Carl Eriksson
Hampus Henåker

Thesis for the degree of Master of Science in Engineering
Division of Thermal Power Engineering
Department of Energy Sciences
Faculty of Engineering | Lund University

Centrifugal Turbopumps

Flow Physics and Modelling

by Carl Eriksson and Hampus Henåker

LUND
UNIVERSITY

Thesis for the degree of Master of Science
Thesis advisor: Prof. Magnus Genrup

To be presented, with the permission of the Faculty of Engineering of Lund University, for public criticism on the online meeting at the Department of Energy Sciences on Monday, the 7th of June 2021 at 10:00.

This degree project for the degree of Master of Science in Engineering has been conducted at the Division of Thermal Power Engineering, Department of Energy Sciences, Faculty of Engineering, Lund University.

Supervisor at the Division of Thermal Power Engineering was Professor Magnus Genrup. Supervisor at GKN Aerospace Sweden AB was Jonathan Mårtensson.

Examiner at Lund University was Associate Professor Marcus Thern.

The project was carried out in cooperation with GKN Aerospace Sweden AB in Trollhättan.

Division of Thermal Power Engineering
Department of Energy Sciences
Faculty of Engineering, Lund University
Box 118
SE–221 00 LUND
Sweden

ISSN: <0282-1990>
LUTMDN/TMHP-21/5485-SE

Typeset in LaTeX
Lund 2021

Preface

This thesis deals with the flow-physics and all components of a centrifugal pump, both single- and multi-stage. The physics and engineering aspects of these components have been studied thoroughly throughout the years. To fully grasp and model the intricate flow phenomena of a single of these components could warrant a thesis of its own. Or, indeed, an entire professional career. The challenge, therefore, has primarily been to condense the vast amount of (sometimes contradicting) material into something useful and applicable.

We would like to thank prof. Magnus Genrup for encouraging us and shining a light on areas within the realm of fluid mechanics and turbomachinery that he knew we would find interesting. His passion for engineering and teaching is something we have seen every day.

We would also like to thank GKN Aerospace Sweden AB for the opportunity to pursue our interest in turbomachinery. Especially our point of contact, Jonathan Mårtensson, for his insights and feedback.

Lastly, we would like to thank our families and loved ones. Not only for their support during this thesis, but for all encouragement during the years leading up to it.

To summarise five years of studies at university is no easy task. Time has flown by and it is first at the end of the journey one sees what the accumulation of experiences has produced. Perhaps it is best left to the greek philosopher Plutarch in the 1st century AD:

"...and Alexander wept, seeing as he had no more worlds to conquer"

Abstract

Choices made in the early stages of a design process are crucial. They dictate many of the limitations and freedoms the designer has in later stages of the design. Informed decisions are therefore crucial at this stage. With the increasing computational power of modern computers, more and more designers utilise CFD software to design and evaluate performance of turbopumps. The simulations allow the designer to visualise intricate flow patterns and simulate effects of advanced 3D geometry. However, even with modern computers, CFD simulations are relatively slow and should, therefore, mainly be used to improve an already decent design.

Centrifugal pumps are complicated, and in order to perform fast calculations the flow is modelled in a simplified fashion. Analogies from the field of centrifugal compressors are utilised since research within this field has progressed further in certain areas. Generally, the flow in radial turbomachinery is not well understood, and many empirical correlations are still in use, at least in open literature. An extensive literature review has been made, detailing the flow through the pump. Ways to model these flows are presented and discussed.

The main aim of this degree project is to develop a computer-program for the early stages of new centrifugal turbopump development. In order to develop this software, the flow physics of a centrifugal pump has been studied and broken down in a way that allows the vital parts to be easily implemented in computer code. The developed tool achieves its main purpose, being able to quickly deliver a preliminary design with analysis regarding off-design performance.

The software developed from these models allows generation of a preliminary design, from specified design criteria, in less than a second. The program has been validated against a similar, commercial, program, with satisfactory results. All geometry created within the software can also be analysed in off-design, i.e. varied mass-flow and rotational speed. Another aspect regarding off-design is the stable operating-range, which is included in the analysis.

Sammanfattning

Val som görs tidigt i en designprocess kan vara avgörande. De dikterar många av de begränsningar och friheter som konstruktörer har i senare skeden av processen. Informerade beslut är därmed viktiga i detta skede. Med den ökande beräkningskraften hos moderna datorer använder fler och fler konstruktörer CFD-programvara för att utforma och utvärdera prestanda hos turbopumpar. Simuleringarna gör det möjligt för konstruktören att visualisera invecklade flödesmönster och simulera effekter av avancerad 3D-geometri. Även med moderna datorer är CFD-simuleringar relativt långsamma och bör därför huvudsakligen användas för att förbättra en befintlig design.

Centrifugalpumpar är komplicerade och för att kunna göra snabba beräkningar behöver flödet modelleras på ett förenklat sätt. Analogier från centrifugalkompressorer har använts eftersom forskningen har kommit längre där i vissa avseenden. Flödet i radiella turbomaskiner saknar en tydlig beskrivning, och många empiriska samband används fortfarande, åtminstone i allmänt tillgänglig litteratur. En omfattande litteraturstudie har genomförts, i vilken flödet genom pumpen beskrivs. Alternativ för att modellera dessa flöden presenteras och diskuteras.

Huvudsyftet med detta examensarbete är att utveckla ett datorprogram för de tidiga stadierna i utformningen av en ny centrifugal turbopump. För att utveckla denna programvara har flödesfysiken för en centrifugalpump studerats och förenklats på ett sätt som möjliggjort implementering i datorkod. Programmet uppnår sitt huvudsyfte, att snabbt kunna leverera en preliminär design med analys av prestanda vid varierande massflöden och rotationshastigheter.

Programvaran som utvecklats från dessa modeller möjliggör generering av en preliminär design, från specificerade designkriterier, på mindre än en sekund. Programmet har validerats mot ett liknande, kommersiellt, program med tillfredsställande resultat. All geometri som skapas i programvaran kan även analyseras vid olika operationspunkter. Ytterligare en aspekt som utvärderas är vilka operationspunkter som ligger inom det stabila arbetsområdet.

Popular Science Summary

During the 15th and 16th century mankind started exploring Earth. She sought out riches on far-away shores and thus required ships that could travel the oceans. The shipbuilders of the day had to develop new concepts in order for these vessels to withstand the voyage. Progress was made. This progress increased rapidly during the 18th and 19th century through marvellous engineering breakthroughs such as the piston-, and steam engine that paved the way for more daring explorations onto shores even farther away.

It lies in our nature to seek out the unknown and find answers to questions that trouble our minds. We are a curious specie and as such we cannot hinder progress - nor should we. In the 1950s we resumed our obsession for exploration and a new shore had emerged. Space. John F. Kennedy said: "We choose to go to the Moon in this decade and do the other things, not because they are easy, but because they are hard...". He captured the essence of engineering and what mankind is all about.

Space is still our frontier as far as exploration goes. In recent years, travelling to other planets is viewed by some as a calling. Some go as far as saying it is our destiny as a specie. Leaving Earth's atmosphere is no simple feat and requires shuttles with engines capable of immense thrust and power. These are known as rocket engines and lie at the forefront of engineering. At the heart of the rocket lies the turbopump, a centrifugal machine capable of high rotational speeds and flows. If we want to explore space and find the next shore, we will need advanced turbo-pumps. The task of developing a turbopump can seem daunting and good design tools are needed.

Developing a design tool able to capture the advanced flows with turbopumps require knowledge and experience within the field of fluid dynamics. The thesis accompanying this text serves as an introduction as well as a deep-dive into models and flow phenomena in turbopumps. More specifically, centrifugal pumps.

A new age of exploration is upon us and who knows what the consequences may. Will space-travel further our knowledge of the universe or will we spend a vast amount of Earths resources chasing dreams? It may be that the development of turbo-pumps will actually help us back here on Earth. There are many similarities between turbo-pumps and regular pumps used in the electric power generation and industry. An expected 20% of the electricity produced is spent pumping water. If these pumps can be replaced with more efficient ones, created with the knowledge gained from turbo-pump development, it will be a significant step in the combat of climate change.

Populärvetenskaplig sammanfattning

Under 1400- och 1500-talet började mänskligheten utforska jorden. Hon sökte rikedomar i fjärran och behövde därmed fartyg som kunde klara långa sträckor till havs. Dåtidens skeppsbyggare utvecklade nya koncept för att bygga dessa skepp vilket ledde till nya framsteg. Utvecklingen ökade snabbt under 1700- och 1800-talet med fantastiska tekniska genombrott som t.ex. kolv- och ångmotorn som banade väg för djärvare utforskningar.

Det ligger i vår natur att utforska det okända och hitta svar på våra frågor. Vi är en nyfiken art och som sådan bör vi inte hindra framsteg. På 1950-talet återupptog vi vår besatthet för utforskning och en ny dörr hade öppnats. Rymden. John F. Kennedy sa: Åe choose to go to the Moon in this decade and do the other things, not because they are easy, but because they are hard...". Han fångade ingenjörskonstens kärna och vad mänskligheten kan åstadkomma.

Det är fortfarande rymden som vi håller på att utforska. Under de senaste åren har resor till andra planeter börjat bli en upprepad realitet. Vissa går så långt som att säga att det är vår arts öde att bilda kolonier på andra planeter. Att lämna jordens atmosfär är ingen enkel bedrift och kräver raketer med motorer som har enorm kraft och effekt. Dessa raketmotorer ligger i framkant av dagens teknik. I hjärtat av raketen hittar man en turbopump, ofta en centrifugalmaskin, som har höga rotationshastigheter och flöden. Om vi vill fortsätta utforska rymden behöver vi turbopumpar som är än mer avancerade. Uppgiften att utveckla en turbopump kan verka omöjlig och det behövs därför bra designverktyg.

Att utveckla ett designverktyg som kan beskriva de avancerade flödena i turbopumpar kräver kunskap och erfarenhet inom fluidmekanik. Uppsatsen som medföljer denna text fungerar som en introduktion till, och en djupdykning i, modeller och flödesfenomen i centrifugala turbompumpar.

En ny era av utforskning ligger framför oss och vem vet vilka konsekvenser det kan få. Kommer rymdresor att öka vår kunskap om universum eller kommer vi att spendera en stor mängd av jordens resurser till att jaga drömmar? Det kan vara så att utvecklingen av turbopumpar faktiskt kan hjälpa oss här nere på jorden. Det finns många likheter mellan turbopumpar och vanliga pumpar som används i elproduktion och industri. En uppskattning är att 20 % av den el vi producerar går åt till att pumpa vatten. Om dessa pumpar ersätts av pumpar med högre verkningsgrad, skapade med kunskapen från turbopumpens utveckling, är det ett viktigt steg i kampen mot klimatförändringarna.

Contents

List of Figures

List of Tables

Nomenclature

Overall

A	Area, constant in axial force calculations
AK	Velocity profile coefficient
AR	Area Ratio
a	Acceleration
$\frac{a}{c}$	Point of maximum camber
$\vec{B}$	General vector quantity
B	Blockage $B = 1 - (A_{eff}/A_{geo})$
b	Width
C	Absolute velocity
C_D	Discharge coefficient $C_D = A_{eff}/A_{geo} = 1 - B$
C_f	Fricition coefficient
C_h	Enthalpy recovery coefficient
C_{L_0}	Design lift coefficient
C_p	Static pressure recovery coefficient
C_T	Through-flow velocity in volute
C_{slip}	Slip velocity
c	Chord length
DR	Diffusion Ratio

d	Diameter
d_H	Hydraulic diameter
E	Energy
e	Specific energy
$\vec{e}$	Unit vector
F	Force
f	Frictional coefficient; specific force (throughflow)
g	Gravitational acceleration
H	Enthalpy; head
h	Specific enthalpy
I	Rothalpy
i	Incidence angle
L	Length; blade loading
L_s	Length of streamline
LC	Loss coefficient
M	Mach Number
$\dot{m}$	Mass flow rate
m	Mass; inverse swirl parameter
$NPSH$	Net positive suction head
$NPSHA$	Net positive suction head availiable
$NPSHR$	Net positive suction head required
N_{ss}	Suction specific speed
p	Pressure

p_T	Total rotational pressure
Q	Heat flux
R_c	Radius of curvature
Re	Reynolds number
r	Radial coordinate in cylindrical coordinate system
S	Entropy
s	Specific entropy
T	Absolute temperature
T_{foil}	Thickness altering constant for an airfoil
t	Time; thickness
t_{clr}	Tip clearance
U	Internal energy; blade speed
u	Specific internal energy
V	Volume
v	Specific Volume
$\dot{V}$	Volume flow
W	Relative velocity; work
$\dot{W}$	Power
w	Specific work
x	Cartesian coordinate; distance along chord
x_m	Location along chord for maximum thickness
y	Cartesian coordinate
Z	Number of blades or vanes

y_T Airfoil thickness

z Height; axial direction in cylindrical coordinates; cartesian coordinate

Greek Symbols

α Absolute flow angle axially defined

β Relative flow angle axially defined

γ Local camberline slope angle of airfoil

Δ Denotes difference

δ Deviation angle; boundary layer thickness

ε Secondary zone area fraction; surface roughness

ϵ Limiting factor for the Wiesner slip model

η Efficiency; effectiveness in TEIS-model

Θ Total energy of flowing fluid

θ Tangential coordinate in cylidrical coordinate system; specific energy of flowing fluid; camber angle

θ_C Divergence angle

κ Curvature

λ Swirl parameter, C_θ/C_m

μ Work input coefficient; dynamic viscosity

ξ Relative distance along impeller blade

ρ Density

σ Slip factor; solidity

σ_b Blade cavitation coefficient

τ Torque

Φ Inclination angle of flow; sweep angle

ϕ Flow coefficient; general property of fluid

χ Secondary flow mass flow fraction

ω Rotational speed

Subscripts

0 Total condition; plenum

1 Impeller inlet

2 Impeller outlet

3 Diffuser leading edge

4 Vaned diffuser throat

5 Diffuser exit; volute entry; return channel entry

6 180° from volute cutwater; return bend exit

7 Volute exit, Exit de-swirl vanes

8 Pump exit; stage exit

a Element a in TEIS-model

ave Average

BL Blade loading

b Blade property; element b in TEIS-model

c Property of camberline; cross-sectional property in volute

corr Corrected value

crit Critical value

dyn Dynamic property

F Front property axial force

f Flow property

h	Hub
i	Ideal; incidence
kin	Kinetic property
L	Lower coordinate of airfoil
m	Mixed-out property; meridional direction
max	Denotes max property
mix	Property at mixing
n	Normal direction
P	Polytropic
p	Primary zone
pot	Potential property
R	Rear property axial force
r	Radial property (cylindrical coordinate system)
SF	Skin friction
s	Insentropic property; secondary zone
seal	Seal
sep	Separation
sh	Shroud
stall	Property at stall
t	Tip
th	Throat location
ts	Total-to-static
tt	Total-to-total

u	Upper coordinate of airfoil
v	Vapour
w	Wake position
z	Axial property in cylindrical coordinate system
θ	Tangential component in cylindrical coordinate system

Superscripts and Overscripts

$-$	Average value
$\rightarrow$	Vector
$'$	Property behind seal; modified coordinate
$*$	Property at lowest incidence loss

Chapter 1

Introduction

1.1 Turbomachinery

1.1.1 What are Turbomachines?

Turbomachines are devices that transfer energy to or from a fluid in a continuous flow with a rotating part. This general description results in a lot of machines being classified as turbomachines, be it a feed-water pump in a power plant, a wind turbine supplying electrical energy, or a turbopump launching satellites to orbit earth. Even before the industrialisation, mankind has relied upon the work transfer made possible by turbomachines to aid them in their daily lives. The first wind-mill, for instance, is documented to have been in use around 500-900 AD in Persia or Mesopotamia [1]. The first record of a turbomachine to make use of thermodynamic principles, however, was perhaps the radial reaction steam-turbine showcased by Hero of Alexandria in the first century BC. The wind-mill and Hero's turbine operate on a different set of principles and thus they are divided into different sub-categories of turbomachinery.

One way to categorise these machines is to look at the path of the flow through the machine. A machine in which the flow enters and leaves in the axial direction is termed an 'axial' turbomachine. A machine in which the flow enters or leaves in the radial direction is termed a 'radial' turbomachine. To further classify turbomachines, a distinction is usually made between devices that extract energy from the flow and devices that transfer energy to the flow. The way energy is transferred to/from the flow is by decreasing/increasing the pressure level of the flow. Machines that lower the pressure level, thus extracting energy, are classified as turbines. Machines that increase the pressure level, thus increasing the energy level, are classified as compressors/pumps.

1.1.2 Centrifugal Pumps

Radial turbomachines that increase pressure are also known as 'centrifugal' turbomachines due to the influence of centrifugal effect on the pressure increase. This centrifugal effect

stems from an increase in radius and will be presented in detail in section 2.1.3. The difference between compressors and pumps is the state of the working fluid. Compressor is the term chosen for pressure increasing turbomachines that operate on gases while pumps operate on liquids. Compressors are commonly found in both the axial and radial sub-category of turbomachines while pump-designers usually favour the radial flow path. This is due to the higher density of the working fluid in pumps which leads to a lower volume-flow which corresponds to a low specific suction speed, section 2.5 goes into detail on this.

Gases have a lower density than liquids and thus, for a given pressure-ratio, experience a higher relative change in density. Liquids can, generally speaking, be considered incompressible i.e. constant density. This assumption has lead to different implementations of the governing equations for centrifugal turbomachinery. For most applications this is a perfectly reasonable assumption but for certain liquids experiencing significant pressure ratios the density variations become significant and compressible analysis is required. Designing compressible pumps, then, utilises techniques from both traditional pump and compressor design.

Given the complex 3D motion of the flow inside centrifugal turbomachinery, a complete design would require the full set of Navier-Stokes equations. These equations require advanced numerical methods in order to analyse fluid flows. Software running numerical solvers of the Navier-Stokes equation, also known as computational fluid dynamics (CFD), often require long computational times and can be an inefficient approach to a new problem. In order to simplify the fluid motion and obtain a first approximation of the design, the assumption is usually made that the flow is uniform over a given cross section. This reduces the description of the flow from 3D to 1D, for which simple models can be used. By choosing these cross sections carefully, the flow through the pump can be calculated and with loss models, gathered from empirical data, the design can be related to real pump performance. In the end, the result of both CFD and 1D-models depend on models and empirical data.

1.1.3 Geometry

During system or cycle design each component is often viewed as a control volume since engineers often only concern themselves with the input and output of each component. When designing components, however, it is useful to divide the component into parts since models are often developed separately for each part. The notations of the centrifugal pump geometry presented here will be used throughout this text. What each number is referencing, however, depends on whether it is a single- or a multistage pump.

Single-stage

Figure 1.1 shows the meridional cross-section of a single-stage pump featuring a vaned diffuser and figure 1.2 the axial cross-section featuring a vaneless diffuser. If the pump does not feature a vaned diffuser, sections 2-5 represents the vaneless diffuser. What each cross-section represents is described below.

1 Inlet to Impeller
2 Impeller outlet
3 Leading edge of vaned diffuser
4 Trailing edge of vaned diffuser
5 Volute entry
6 180 ° from volute cutwater
7 Volute exit
8 Pump exit

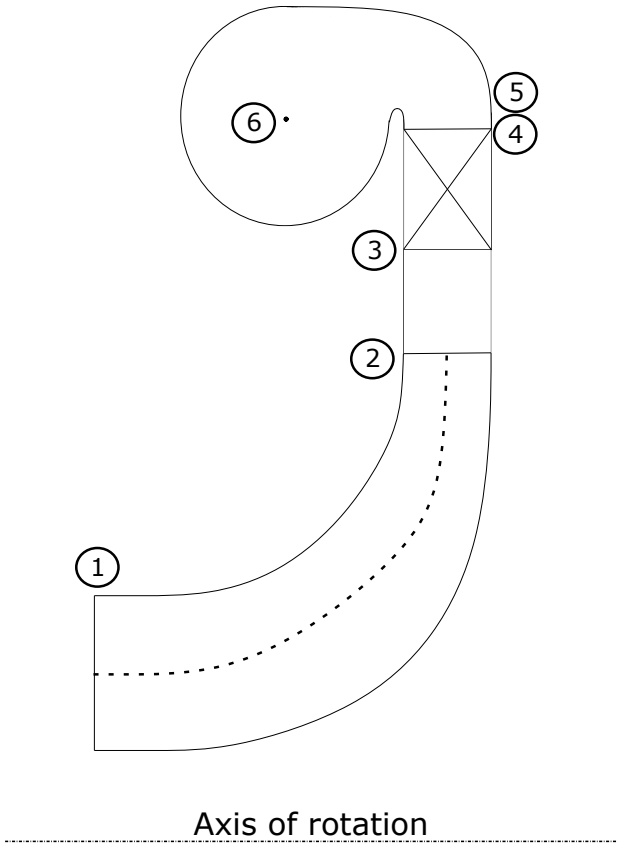

Figure 1.1: Meridional cross section of a centrifugal pump, with volute.

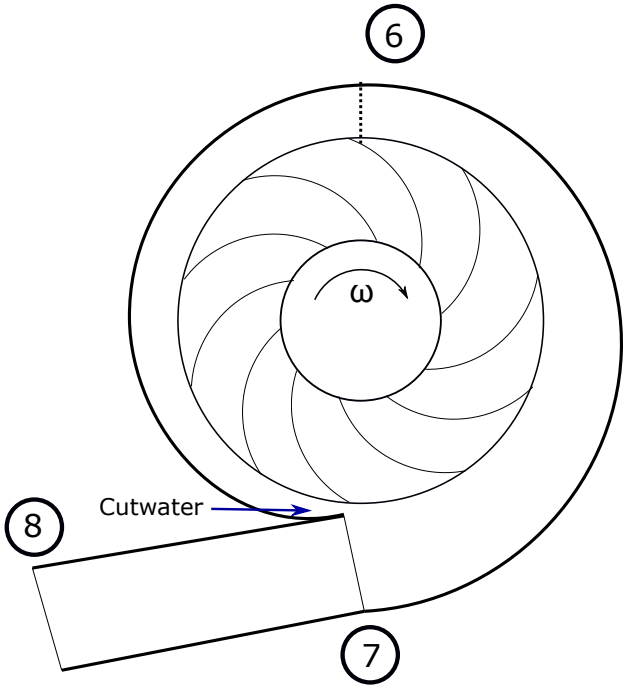

Figure 1.2: Axial cross section of a centrifugal pump, with volute.

Multistage

Figure 1.3 shows the division of a pump-stage for a pump with multiple stages. What separates the division of a single- and multistage pump is what happens after cross-section 5. In the single-stage pump, section 5 is the entry to the volute which collects the flow and leads it out of the pump at section 8. In the multistage pump, section 5 is the entry to the return-channel which guides the flow to the next stage. The last stage of a multistage pump has the same division as a single-stage. What each cross-section represents is described below.

1 Inlet to Impeller

2 Impeller outlet

3 Leading edge of vaned diffuser

4 Trailing edge of vaned diffuser

5 Return channel entry

6 Exit of first bend, entry to de-swirl vanes

7 Exit de-swirl vanes

8 Stage exit

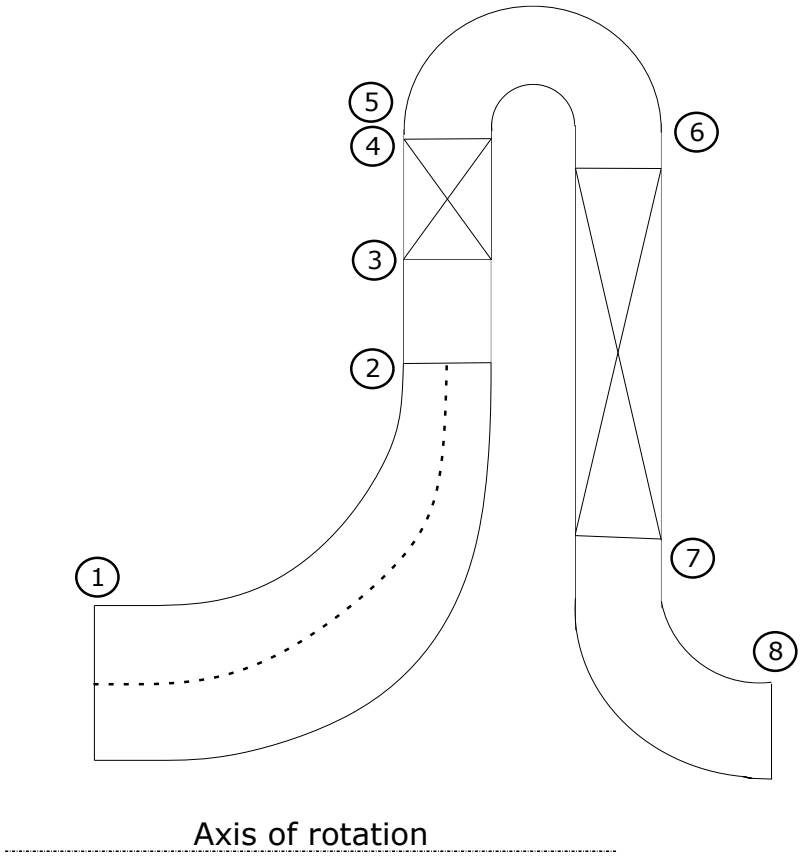

Figure 1.3: Meridional cross section of a centrifugal pump, with return channel.

The Concept of Pump Design

Each cross section depicted in figures 1.1, 1.2, and 1.3 represents the borders of a control volume, i.e. 1-2 is the first control volume and 2-3 the second control volume. The total control volume of the pump, then, is described by seven smaller control volumes. To design and determine the performance of a centrifugal pump each control volume must be solved sequentially. This is a simplified view of the design procedure for centrifugal pumps. As will be shown later, each control volume is often divided into separate regions (e.g. primary and secondary zone in the impeller). Nevertheless, for a first, holistic, view it can be helpful to regard the pump as a series of control volumes.

1.1.4 Rocket Science

Due to export control on rocket turbopumps, some details have been omitted from this report. Furthermore, water has been chosen as the working fluid of the pump due to

these restrictions. However, the design process described in the report is valid for any centrifugal pump.

Rockets are mainly utilised in the field of space exploration. A main identifier for a rocket is that both fuel and oxidiser is brought with the vehicle, i.e. not supplied from the surroundings as is standard for the air-supply to many engines, both automotive and aeroplanes.

Thrust is needed to propel a rocket and it is achieved by accelerating the fluid leaving the combustion chamber through a nozzle, see figure 1.4 . The force exerted to achieve this acceleration is equal and opposite the force acting on the rocket itself, i.e. the thrust. This is in line with Newton's third law.

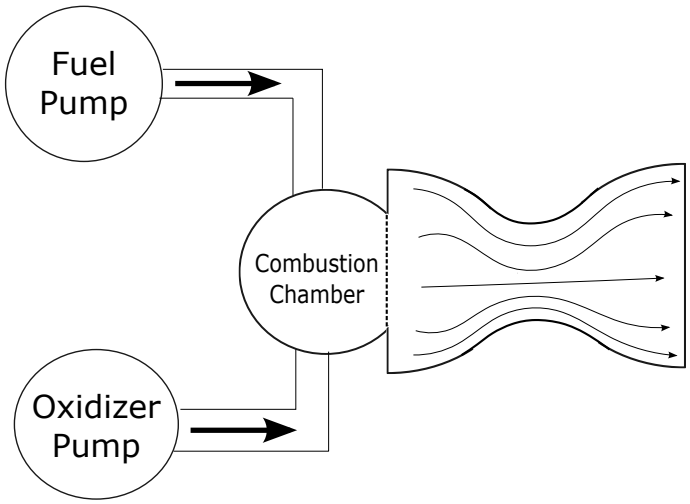

Figure 1.4: Simple schematic of a rocket engine.

The velocity and mass flow are both important parameters to generate thrust. In order to burn fuel and increase the energy level of the fluid, utilised in the acceleration, fuel and oxidiser need to be supplied to the combustion chamber at a desired state (pressure). A conventional way of achieving this is by using pumps, or turbopumps to be exact.

Turbopumps differ from ordinary pumps. For one, the turbopump is often driven by a turbine, hence its name, but electrically driven rocket-pumps also exist. It usually has a high rotational speed, compared to stationary pumps. Additionally, life time has not been as important, since the rocket stages were left to burn when they had done their part of the launch. A pump that constantly is pumping water, i.e. in a district heating system has high requirements on life time, since a high number of operating hours is desired. However, with the current trend of landing and reusing rockets, the life time of rocket turbo-pumps may be of a greater importance in the near future.

Restrictions regarding weight is put on the whole rocket engine. To reduce the weight of the fuel-, and oxidiser tanks it is desirable to have low pressure in the tanks as this reduces the required thickness of the tank and thus the weight. Low pressure in the tank can pose a problem for the inlet section of the pump, an area further discussed in chapter 3.

1.2 Aim of the study

The objective of this master's thesis is to develop a 1D design tool for preliminary design of centrifugal pumps. Preliminary design is meant to aid heavy 3D calculations performed in software running CFD. The idea is that the complex 3D flow field should only be solved for geometry having passed the 1D design phase. As the tool will be used in an iterative manner, emphasis is put on speed and stability. In order to develop this tool, the authors seek to:

- Understand the flow physics in each element of a centrifugal pump.
- Perform a literary review of models describing these flow physics.
- Implement these models in computer-code and create an interface for control.

1.2.1 Delimitations

Due to time restrictions the scope of this thesis has been limited. The authors have focused on rapid 1D calculations, neglecting aspects such as e.g. boundary layers, turbulence, and transient aspects. The focus have been on the theory and modelling of the centrifugal pump components depicted in figures 1.1, 1.2, and 1.3.

1.3 Outline

The report will start with a chapter on relevant concepts for fluid flow in centrifugal turbomachinery. Following chapters will focus on the different components of the machine, tracing a fluid-element's path. Chapter 10 will detail a quasi-three-dimensional model for a more detailed design of the rotating part of the impeller. Chapter 11 compares and validates the developed design program against Japikse [2].

Chapter 2

Fluid Mechanics in Turbomachinery

In order to describe the one dimensional fluid flow through a centrifugal turbomachine, something must be said about how the fluid and the flow is modelled. This chapter starts with a review of these models before introducing the governing equations and equations of state. The chapter ends with a section relevant for pump considerations.

2.1 Frame of Reference

2.1.1 Fluid elements

Consider the infinitesimal fluid element shown in figure 2.1. It has a differential volume $\partial x \partial y \partial z$ but contains enough molecules so that it can be viewed as a continuous medium. In this macroscopic point of view the fluid element can be described by macroscopic properties such as pressure, density, and temperature. Now consider a region in space with volume V constructed of fluid elements. This region is known as a control volume and can either be fixed in space or moving with the fluid. If the volume is fixed in space, also known as the Eulerian approach, fluid elements are constantly moving across the surface S of the control volume. Otherwise the fluid elements inside V remains constant but their properties change, this is known as the Lagrangian approach [3] [4].

In a three dimensional description of the flow field, the macroscopic properties vary in every direction inside the flow field. This means each fluid element inside the control volume has its own unique set of properties. In a cartesian coordinate system a fluid property can be described by $\phi = \phi(x, y, z, t)$, where ϕ is the property (density, pressure, temperature etc.) and t is time. Changes to the property inside the fluid element can be described by its total derivative, see equation (2.1).

$$\frac{D\phi}{Dt} = \frac{\partial \phi}{\partial t} + \frac{\partial \phi}{\partial x}\frac{dx}{dt} + \frac{\partial \phi}{\partial y}\frac{dy}{dt} + \frac{\partial \phi}{\partial z}\frac{dz}{dt} \tag{2.1}$$

A three dimensional level of detail is necessary to grasp the complicated flow phenomena

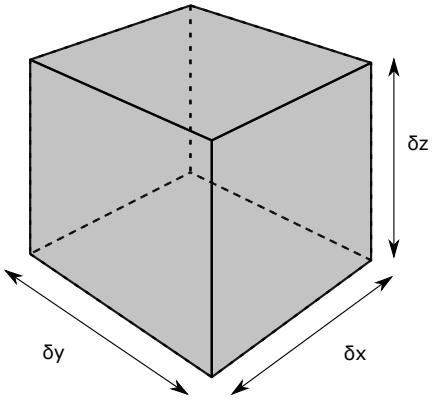

Figure 2.1: Fluid element in a cartesian coordinate system.

and to determine critical regions inside the flow field. However, for preliminary design and understanding of the fundamental flow it is often sufficient to consider a 2D or a 1D flow field. In a 1D flow field the fluid properties are constant for each cross-section of the control volume and are only subject to change in the flow direction i.e $\phi = \phi(x, t)$ taking x as the flow direction. Furthermore, if the flow is assumed to be steady there are no changes to the flow with respect to time and hence properties are constant for a given position along the flow path. In such cases, changes to properties are given by equation (2.2).

$$\frac{D\phi}{Dt} = \frac{\partial \phi}{\partial x}\frac{dx}{dt} \tag{2.2}$$

2.1.2 Coordinates

Before diving any further into the theory of centrifugal pumps something must be said about the coordinate system often employed when working with turbomachines and, in addition, the relative reference frame. As turbomachines include a rotating part (rotor) it is common to introduce a cylindrical coordinate system when describing them.

Cylindrical Coordinates

As for a great number of objects and machinery, the cartesian coordinate system *(x, y, z)* is not always the most suitable. For turbomachinery, amongst other things, the cylindrical coordinate system is beneficial to use. The cylindrical coordinate system is given by *(r, θ, z)*. The radial coordinate, r, is the distance from a centre-axis. The angular coordinate, θ, is the angle which the radial coordinate is at, compared to a chosen reference state.

Lastly, the axial coordinate, z, is the distance away from the chosen origin along the centre-axis.

The benefit from using cylindrical coordinate is due to the approximate axi-symmetric design of turbomachines. It is therefore easier to describe using cylindrical, e.g. the outer radius is given by a coordinate r (angular coordinate needed if a specific point on outer radius is to be specified), whereas in cartesian coordinates two coordinates are generally needed $x^2 + y^2 = r^2$. This is just one of many examples where this coordinate system is useful.

The velocity of a fluid flow through a turbomachine has components of velocity in all directions and its quantity can be calculated through equation (2.3).

$$C = \sqrt{C_z^2 + C_r^2 + C_\theta^2} \tag{2.3}$$

The turbomachinery-flow is often considered axi-symmetric meaning there is no variation in velocity in the tangential direction. The component of velocity normal to an axi-symmetric surface is called meridional velocity and it can be calculated through equation (2.4). When the velocity has components in the tangential direction, the flow is said to have swirl and the angle between the tangential and meridional components of velocity is termed the swirl angle, α. The swirl angle can be calculated through equation (2.5).

$$C_m = \sqrt{C_z^2 + C_r^2} \tag{2.4}$$

$$\alpha = \tan^{-1}\left(\frac{C_\theta}{C_m}\right) \tag{2.5}$$

2.1.3 Rotating System

Due to the rotating nature of turbomachinery it is helpful to have a coordinate system that fits into this. Cylindrical coordinates, describing radius, tangential angle and axial depth is a suitable choice, as mentioned above. The rotating coordinate system can be visualised as what the blades of the turbomachine experiences, and will therefore be dependent on the speed of rotation.

Greitzer et. al [5] mentions that working with such a coordinate system allows one to work with steady fluid motions, but the price one has to pay is that the system is not inertial. In an inertial coordinate system, the acceleration of a fluid particle and the force acting upon it can be related by Newton's second law, shown in equation (2.11). In the rotating coordinate system, which is about to be described, Coriolis and centrifugal accelerations must also be accounted for when using Newton's second law in a rotating

frame of reference. The velocity in the absolute frame, and the perceived velocity in the relative frame is related below, in equation (2.6). Where $\vec{C}$ denotes the absolute velocity vector, $\vec{W}$ is the relative velocity vector, ω is the rotational speed of the relative coordinate system and $\vec{r}$ is the position vector from the origin of rotation. The product $\omega\vec{r}$ is the local blade speed. This is easily visualised with help of velocity diagrams.

$$\vec{C} = \vec{W} + \omega\vec{r} \tag{2.6}$$

Velocity diagrams

One common tool for analysing the flow through a turbomachine is to look at the velocity diagrams for the flow through the machine. Velocity diagrams are constructed by inserting the absolute and relative velocities into the same diagram. As the absolute and relative velocities are related by the blade speed, the diagram closes and forms a triangle which is why velocity diagrams are also known as velocity triangles. Figure 2.2 shows an example of a velocity diagram for the inlet section of a centrifugal pump at the tip position. In the figure it can be seen that there is a difference between the blade angle (β_{1bt}) and the relative flow angle (β_{1t}). This difference is called incidence (i) and is a measure of how well the geometry matches an oncoming fluid. When the flow angle of the fluid leaving the blade section differs from the angle of the blade the flow is said to deviate and hence the difference between the blade angle and the relative flow angle is called deviation.

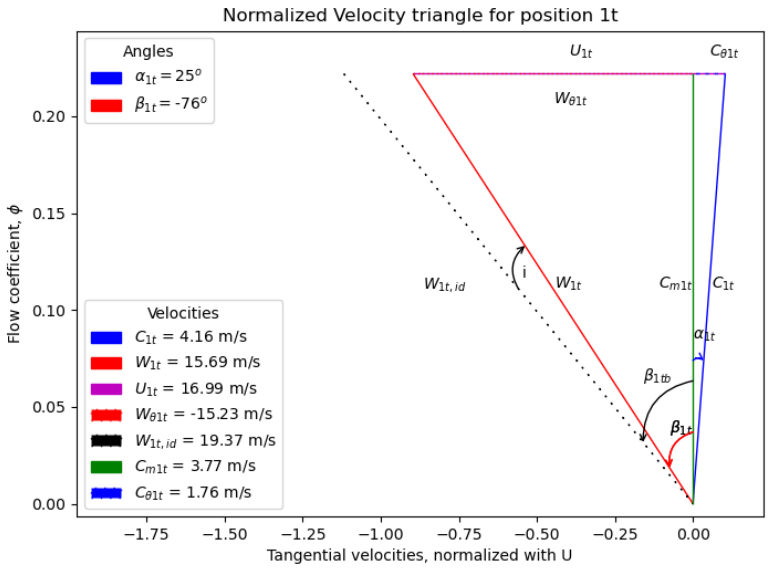

Figure 2.2: Example of a Velocity Triangle

Mathematical Description

To accurately describe and model objects and machinery a common notation is needed, whether it is a drawing sent to manufacturing or a CAD-model created and translated to a mesh for use in CFD. The most common system is the cartesian, which the reader may be familiar with, described by the spatial coordinates *(x, y, z)*, where all three axis lie orthogonal to each other. There are other systems which may be beneficial and easier to use for certain geometries, e.g. polar coordinates when describing circular objects.

The general transformation, as described by Greitzer [5], is shown in equation (2.7) below. If $\vec{B}$ is set to be the positional vector $\vec{r}$, equation (2.6) is obtained.

$$\left(\frac{D\vec{B}}{Dt}\right)_{absolute} = \left(\frac{D\vec{B}}{Dt}\right)_{relative} + \omega \times \vec{B} \tag{2.7}$$

The substantial derivative for a scalar quantity is, as shown by Greitzer [5], the same in both absolute and relative frames. This includes density and entropy amongst other scalar properties.

To give the reader a good intuition about Coriolis acceleration, and an intuitive acceptance, an illustrative example will be conducted, rather than just deriving equations and watch the term fall out due to maths.

Imagine standing on a disk, which is able to rotate around its centre point, as a merry-go-round. In this first scenario, you are standing on the outer rim of the disk, facing inwards, with the disk being stationary. You will now throw a ball, aiming for the centre. In this case the ball will go in a straight line in your frame of reference (which is the same as the absolute frame). In the next scenario the disk will be spinning with a constant angular velocity ω, and you, standing on the disk, will follow along as it rotates. In your frame of reference, the disk is stationary and the world is spinning the other direction, i.e. in a relative sense.

If you now throw the ball again, aiming for the centre, the ball will curve in your frame of reference. It will start with a tangential velocity, equal to rotational speed multiplied with the distance from the centre. As the ball moves inward, the local relative velocity of the disk will be lower than that for the ball, and the ball will seem to speed up. In the absolute frame of reference the ball will be seen travelling in a straight line.

The Coriolis acceleration can be visualised with the help of figures 2.3 and 2.4, depicting the reverse situation of the analogy above. The change in velocity can then be calculated, see equation (2.8).

$$\frac{dC_\theta}{dt} = 2\omega W \tag{2.8}$$

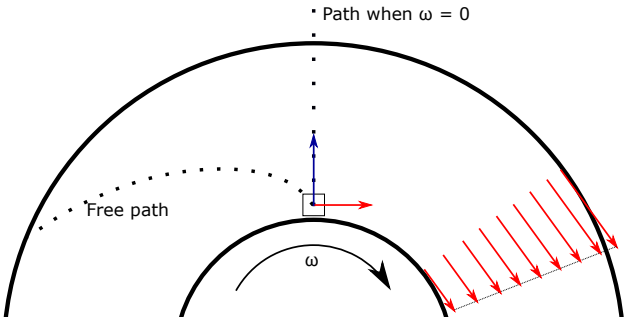

Figure 2.3: The path of a stationary disk and the relative path of a fluid element on a rotating disk.

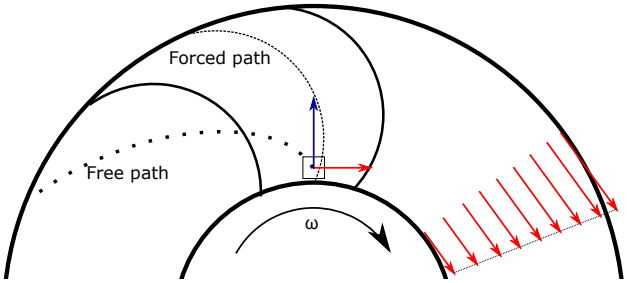

Figure 2.4: The effect blades on the impeller has on the flow path

There are other forces at play inside an impeller and the intuitive Coriolis acceleration requires some alteration. The Coriolis acceleration works normal to the relative velocity, towards the pressure surface of the blades. This creates a pressure gradient towards the pressure surface and thus a secondary flow towards the suction-side. Without the blades, the Coriolis acceleration would have moved the fluid in the opposite direction to the rotational speed but due to the pressure build-up on the blades, the fluid will move in the same direction as the rotational speed.

2.2 Equations of State

Once two properties of a substance (not in the saturated region) are known, the state of the fluid is fixed. This is useful in thermodynamic analysis as it closes a system of equations containing fluid elements. As described earlier in this chapter, a fluid element is defined such that it can only have one specified state, i.e. only one temperature, pressure, enthalpy, etc. This allows for iterative solutions, when the state does not change considerably between calculation points (with allowable tolerance) the solution has converged. For information about how fluids are modelled and choices made in the developed design program the reader is directed towards appendix A.

2.3 Governing equations

The laws of the universe applies to everything. Conservation of energy and mass are two fundamental cornerstones to all of science, and many useful expression can be obtained from combining and re-casting equations describing fundamental accepted laws. With knowledge about fluid elements and control volumes it is possible to look at the governing equations for one dimensional flow in a centrifugal pump.

2.3.1 Continuity

Continuity represents the notion that mass can neither be created nor destroyed. If a certain amount of fluid enters the region, the same amount must exit the region as well. The continuity equation is given in equation 2.9, where $\dot{m}$ is mass flow, A_f flow area, ρ density, and C velocity of the fluid. The flow area A_f is the area normal to the flow direction, i.e the direction of C.

$$\dot{m} = \rho A_f C \tag{2.9}$$

For an incompressible assumption, the mass continuity can be re-written to volume-continuity, see equation (2.10). This is usually an assumption made for many pumps in a preliminary design stage. However, it is useful to have the continuity-equation on a mass basis to account for compressible effects in the flow. The volume flow through a machine in which the density changes (compressible effects) will not be constant, as the volume of each fluid element change as the density change. The mass flow, however, will always be constant when dealing with steady flows.

$$\dot{V} = A_f C \tag{2.10}$$

2.3.2 Momentum

The momentum equation is Newton's second law applied to fluid elements. Newton's second law, see equation (2.11), states that the resulting force on a body is equal to its mass times the acceleration.

$$F = ma \tag{2.11}$$

The momentum equation can be written in a more general sense with equation (2.12). For a fluid element with constant mass, equation (2.12) reduces to Newton's second law since acceleration is the time derivative of velocity. The change in momentum over time

for a fluid element, which is equal to the force exerted on the fluid, is thus proportional to the change in velocity.

The forces F that cause a change in momentum inside a pump are primarily surface forces, stemming from the rotating impeller, that acts on the surface of the control volume.

$$F = \frac{d}{dt}(mC) = \dot{m}\Delta C \tag{2.12}$$

2.3.3 Energy

The energy is a vital property of the flow and fluid elements. To properly model the flow, laws governing the transfer of energy will be summarised in this section. For detailed descriptions of these fundamental laws, the reader is directed towards any textbook in thermodynamics e.g. Çengel and Boles [6].

First Law of Thermodynamics

The first law of thermodynamics describes the conservation of energy. The reader may familiar with the expression: "Energy cannot be created, nor destroyed", which captures the essence of the first law. The equation below, equation (2.13), describes the change of energy in the system as the difference of the heat supplied to the system and the work done by the system.

$$\Delta U = Q - W \tag{2.13}$$

Total Enthalpy

The first law of thermodynamics states that energy cannot be created or destroyed, only converted. Energy exists as internal energy U, kinetic energy E_{kin} or as potential energy E_{pot}. For fluid flow there is an additional form of energy: flow energy. Flow energy, or flow work, W_f is the work required to push the fluid element into the control volume. Imagine a control volume full of fluid elements, in order for a fluid element to enter the control volume it must push out an already existing fluid element. The force required to push the fluid element is pressure times area and the resulting flow work thus becomes pressure times volume, see equation (2.14).

$$F = pA_f, \qquad W_f = pAL = pV \tag{2.14}$$

The total energy of a flowing fluid (Θ) can then be described as the sum of internal, kinetic, potential, and flow energy see equation (2.15). Enthalpy (H) is defined as $U + pV$ which reduces the total energy of a flowing fluid to equation (2.16). Potential energy is often neglected when considering the flow through a machine thus reducing equation (2.16) into $H + KE$. Specific properties are obtained by dividing both sides with the mass of the fluid element, see equation (2.17). The combination specific enthalpy and specific kinetic energy is denoted stagnation (or total) enthalpy (h_0) which is the energy level of the fluid flow if it would be isentropically put to rest i.e. without losses.

$$\Theta = U + E_{\text{kin}} + E_{\text{pot}} + pV = U + \frac{mC^2}{2} + E_{\text{pot}} + pV \tag{2.15}$$

$$\Theta = H + \frac{mC^2}{2} + E_{\text{pot}} \tag{2.16}$$

$$\theta = h + \frac{C^2}{2} + e_{\text{pot}} = h_0 + e_{\text{pot}} \tag{2.17}$$

Energy can either be transferred as heat or as work. Heat is the energy transfer associated with a change in temperature, whilst work is the energy transfer associated with a force acting over a distance. In pumps, work is supplied in order to increase the pressure level of the fluid. If the pump is assumed to be adiabatic (i.e no heat transfer) the specific work supplied to the fluid is equal to the increase in stagnation enthalpy, $w = \Delta h_0$.

Second Law of Thermodynamics

The first law only describes the fundamental outline of a process. In order for a process to occur it must also satisfy the second law of thermodynamics [6]. An inequality of great importance is the Clausius inequality, see equation (2.18). It states that the cyclic integral of $\frac{\delta Q}{T}$ is always less or equal to zero, which is valid for both reversible and irreversible cycles [6].

$$\oint \frac{\delta Q}{T} \leq 0 \tag{2.18}$$

Consider a traditional heat engine where heat is supplied and work extracted. More units of heat needs to be supplied to the engine than the units of work we are able to retrieve from it. This is due to *irreversibilities* within the engine, such as i.e. friction. These irreversibilities makes it impossible to reverse the process. Entropy is a useful property which quantifies the irreversibility of a process. If more entropy is generated, the efficiency of said process is lower. It is the change in entropy that is of interest during analysis. Entropy is defined in equation (2.19) and is used to evaluate the *quality* of energy [6].

$$dS = \left(\frac{\delta Q}{T}\right)_{\text{int rev}} \tag{2.19}$$

Hence, the change in entropy can be described by equation (2.20). If the entropy of a system increases, there have been more irreversibilities at work, and we have lost some of the potential work from our initial state.

$$\Delta S = S_2 - S_1 = \int_1^2 \left(\frac{\delta Q}{T}\right)_{\text{int rev}} \tag{2.20}$$

The differential form of equation (2.13) for a closed and stationary system is described in equation (2.21), for an internally reversible process.

$$\delta Q_{\text{int rev}} - \delta W_{\text{int rev, out}} = dU \tag{2.21}$$

With the following expressions known

$$\begin{aligned} \delta Q_{\text{int rev}} &= T\,dS \\ W_{\text{int rev, out}} &= p\,dV \end{aligned}$$

equation (2.21) can now be re-written, with intensive properties, in equation (2.22), known as the first *Gibbs equation*.

$$T\,ds = du + p\,dv \tag{2.22}$$

$$dh = T\,ds + v\,dp \tag{2.23}$$

The second Gibbs equation, seen in equation (2.23), is obtained by eliminating du from the first Gibbs equation, utilising the definition of enthalpy in differential form, see equation (2.24).

$$\begin{aligned} h &= u + pv \\ dh &= du + p\,dv + v\,dp \end{aligned} \tag{2.24}$$

2.3.4 Essential Concepts in Turbomachinery

Euler's equation

One additional physical principle that can be derived from Newton's second law is the conservation of angular momentum. Consider a control volume in which the fluid flow enters at radius r_1 and tangential velocity $C_{\theta 1}$ and leaves at radius r_2 with tangential velocity $C_{\theta 2}$. The force that the fluid exerts on its surrounding is, according to equation (2.12) $F_\theta = \dot{m}\Delta C_\theta$ and hence the angular momentum $\tau = F_\theta r = \dot{m}\Delta(C_\theta r)$. In the case of no force acting on the fluid element, the change in angular momentum is zero and thus $rC_\theta = constant$, which is the conservation of angular momentum principle.

For centrifugal pumps, work is being exerted on the fluid and the work transfer can be calculated through the change in angular momentum: $\Delta w = \Delta(\tau\omega)$. The work transfer multiplied by the mass flow yields the required pumping power, $\dot{W} = \dot{m}\Delta w$. Combining these principles yields an expression for the pumping power described by the change in angular velocity, tangential velocity and radius shown in equation (2.25).

$$\dot{W} = \dot{m}\Delta(\omega r C_\theta) \tag{2.25}$$

As the angular velocity multiplied by the radii gives the blade speed of the rotor ($U = r\omega$) equation (2.25) can be rewritten as: $\dot{W} = \dot{m}\Delta(UC_\theta)$. Combining angular momentum with the definition for stagnation enthalpy yields the Euler work equation:

$$w = \Delta(UC_\theta) = \Delta h_0 \tag{2.26}$$

The Euler work equation is one of the principle equations for centrifugal turbomachinery as it links the energy equation to the momentum equation. The Euler equation is valid for adiabatic steady flows and holds for any streamline through the turbomachine.

Rothalpy

One implication of the Euler work equation is that the difference between stagnation enthalpy and the product of blade speed and tangential velocity stays constant along a streamline, see equation (2.27). This constant quantity is often referred to as rothalpy (or trothalpy in some texts) and is useful for analysing fluid flows through any turbomachine.

$$h_0 - UC_\theta = \text{constant} = I \tag{2.27}$$

Bernoulli equation

The Bernoulli equation is helpful in describing flow-diffusion for incompressible flow between two points in space. It can be derived from both the momentum and energy equation. Equation (2.28) shows the Bernoulli equation between points 1 and 2. Neglecting changes in potential energy it is clear that a reduction in velocity at point 2 implies an increase in static pressure at the same point. This coupling between velocity and pressure is fundamental in the analysis of turbomachinery.

$$p_1 + \frac{\rho C_1^2}{2} + gz_1 = p_2 + \frac{\rho C_2^2}{2} + gz_2 \tag{2.28}$$

2.4 Evaluation of Performance

2.4.1 Efficiency

The second law of thermodynamics covers that which the first law does not; The quality of energy. In an adiabatic flow, there is no heat transfer from the surrounding to the system. Any heat generated within the system is due to irreversibilities occurring within the flow e.g. friction. The magnitude of these irreversibilities determine how much heat is generated and in the end how much work potential is lost during the process. Entropy is a thermodynamic property that is used to determine how much work potential has been lost during a process.

Since entropy is a function of the state once two other properties of the state are known so is the entropy. Assuming an adiabatic process the lost work potential can be calculated as the increase in entropy between two states. In an isentropic process the entropy remains constant i.e. there are no irreversibilities. To determine the performance of a real process it can be compared to the ideal, isentropic, process. From the Euler work equation it can be seen that the stagnation enthalpy increases for a fluid as it moves through the pump. Hence, to determine the isentropic efficiency of a pump, one can compare the isentropic increase in enthalpy to the actual increase, see (2.29) in which s denotes the isentropic increase.

$$\eta_P = \frac{\Delta h_{0s}}{\Delta h_0} \tag{2.29}$$

When calculating the efficiency it is important to know if the kinetic energy leaving the impeller is useful or not. If the kinetic energy is not useful and cannot be recovered it should be considered a loss. In that case, one should use the static enthalpy at impeller exit instead of the total enthalpy. Considering the total-to-static change in enthalpy

results in the total-to-static efficiency, equation (2.30). The total-to-total efficiency is shown in equation (2.31), between general stations a and b.

$$\eta_{ts,a-b} = \frac{h_{bs} - h_{0a}}{h_b - h_{0a}} \tag{2.30}$$

$$\eta_{tt,a-b} = \frac{h_{0bs} - h_{0a}}{h_{0b} - h_{0a}} \tag{2.31}$$

2.4.2 Loss Models

When analysing the components inside a centrifugal pump and determining their individual performance one needs to look at the losses generated inside the component. In order to compare different pumps and different flow conditions dimensionless loss-coefficients are commonly used to relate the generated losses. Loss-coefficients provide the designer with a criteria for optimisation but one must avoid sub-optimising the components. The overall performance of the pump outweighs the performance of individual components. In preliminary design, loss-coefficients are necessary to relate the state between different components. These loss-coefficients are obtained from empirical data and the available data is scarce as performance of individual components are tightly kept secrets of pump-manufacturers. The most common loss-coefficients in centrifugal turbomachinery is the total pressure loss coefficient which relates a drop in total pressure to the initial dynamic pressure, see equation (2.32).

$$LC_{a-b} = \frac{p_{0a} - p_{0b}}{p_{0a} - p_a} \tag{2.32}$$

Another coefficient, commonly accompanying the loss-coefficient, is the pressure recovery coefficient. Velocity and pressure are closely linked, a reduction in velocity leads to an increase in pressure and vice versa. The pressure-recovery coefficient relates the change in static pressure to the dynamic pressure, see equation (2.33). As it is possible for the static pressure to either increase or decrease in a component, C_p can be both negative and positive.

$$C_{p,a-b} = \frac{p_b - p_a}{p_{0a} - p_a} \tag{2.33}$$

2.4.3 Off-Design

How a turbomachine behaves at mass-flows and rotational speeds different from design values is an important aspect during performance evaluation. Within which mass-flow the machine is able to operate is known as its range. Section 2.5.2 goes into more detail about how the range of the pump must match the range of the system it is placed in.

2.5 Pump Consideration

The core of this chapter has been describing the general flow physics coupled to a radial turbomachine, containing both compressors and pumps. However, when solely considering pumps, a number of simplifications can be made, but there is also a need for extra consideration of some aspects that are not a problem for compressors.

An assumption, leading to multiple simplifications down the line, is the assumption of a incompressible working fluid, i.e. the density is considered constant. This is a valid assumption in many pump cases, but not all. Some cases, when a high pressure/head rise is needed, the compressible effects have a greater impact, and may need to be considered.

2.5.1 Head

In the field of pumps, pressure and mass flow are often mentioned in terms of head and volume flow, which is done by dividing by the density. This is possible due to the incompressible nature of fluids. Because of this convention, several useful parameters are defined from head, instead of a pressure, and it is important for a designer to take this into account.

2.5.2 Pump Curve

A benefit that pump curves, and the notation of using volume flow and head, is that the pump performance is not dependant on the fluid used. If the same volume per unit time of oil and water is pumped by the same pump, they may be pumped to the same height. However, both the mass flow through the pump and the pressure ratio over the pump will differ, due to the working fluid. When fitting a pump to a system, the pump will operate at that point where the system's curve intersects with the pump's curve. In figure 2.5 pump curves for different rotational speeds are shown. The design point is shown as a red star.

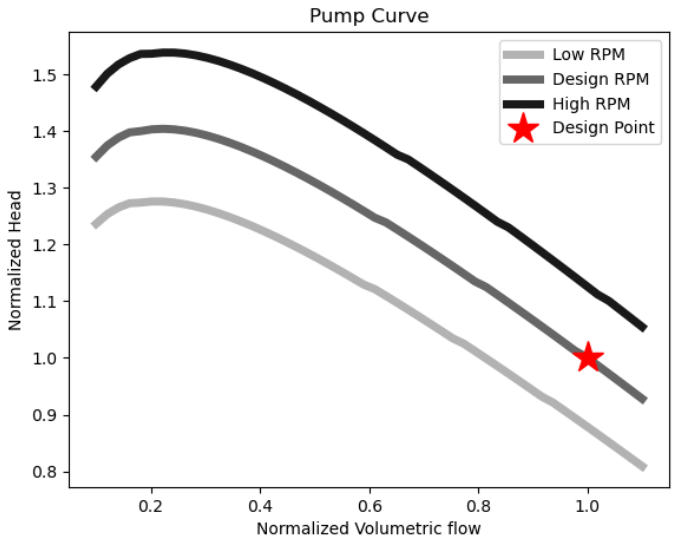

Figure 2.5: Example of a pump curve.

2.5.3 Cavitation

One phenomenon that needs to be considered in pump design, due to the working fluid being a liquid, is cavitation. Cavitation occurs when the static pressure decreases below the vapour pressure, for the current temperature, and vapour forms. When the pressure is increased again, the vapour bubble implodes, quickly. The implosion may impose stresses on the impeller and cause erosion.

The initiation of cavitation is often defined as when 3 % drop-off of the total delivered head (TDH) occurs. An increase of cavitation entails a rapidly lowered delivered head, and the pump is basically out of its range. The detrimental effects of cavitation, both in performance and life time deterioration, makes it needed to be considered from start of the pump design.

Since cavitation occurs when the static pressure falls beneath a certain pressure, cavitation is most likely to occur at inlet to the pump, before the impeller has put in work into the fluid and raised the pressure. It is, therefore, crucial to design the inlet with cavitation in mind.

One important parameter for pumps are the net positive suction head, NPSH. The required NPSH, NPSHR, is a parameter of the pump. It is the head the working fluid needs to have to just be at cavitation. A safety margin is recommended.

2.5.4 Specific Suction Speed

A useful parameter in pump design is the specific suction speed, N_{ss}, defined in equation (2.34). It it used to define the suction characteristics for pumps. The NPSH of two pumps can not be used directly to compare their suction performance. However, the specific suction speed allows these two pumps to be compared from a suction performance perspective.

$$N_{ss} = \frac{\omega \dot{V}^{1/2}}{(g\text{NPSHR})^{3/4}} \tag{2.34}$$

2.5.5 Rotational Pressure

As previously mentioned, the working fluid for a pump can in many cases be considered incompressible. From this assumption the rothalpy can be rewritten to something named rotational pressure, used by Japikse [2].

Let us once again divert our attention to one of the most fundamental equations in thermodynamics, the 2nd Gibbs equation, stated before in equation (2.23). If the assumption of incompressibility is made, the dynamic pressure can be expressed by the kinetic energy of the flow times the density. The total pressure is re-iterated below, in equation (2.35).

$$p_0 = p + p_{\text{dyn}} = p + \rho \frac{1}{2} C^2 \tag{2.35}$$

Thus making it possible to rewrite (2.23) in terms of total states.

The total enthalpy can now be rewritten to rothalpy, by subtracting work input on both sides, see equation (2.36).

$$dI = dh_0 - \omega d(rC_\theta) = dp_0 + Tds - \omega d(rC_\theta) \tag{2.36}$$

Rothalpy is constant along a streamline, as mentioned previously in this chapter. It can now be seen, that in the case of an isentropic streamline, the left hand side terms will be equal to the rothalpy, i.e. constant along the stream line. In simple terms, the rotational pressure can be seen as the incompressible version of rothalpy, where we have multiplied it with the density. It is, however, only valid for isentropic streamlines.

2.6 Additional Flow Phenomena

2.6.1 Turbulence

Turbulence is a property of the flow and a measure of turbulence is the dimensionless Reynolds number Re. It is a measure of the inertial forces to the viscous forces. A higher Re indicates a more turbulent flow. Re is an important parameter when modelling the flow, since it is incorporated in many models. It is defined in equation (2.37) where d is the characteristic length and μ the dynamic viscosity.

$$Re = \frac{\rho C d}{\mu} \tag{2.37}$$

2.6.2 Pipe Flow

The flow in pipes have been extensively researched and empirically tested. When analysing other flow regions it can be helpful to correlate the flow to pipe-flow for these reasons. The friction coefficient in pipe-flow can be modelled in numerous ways. Two of the most common modelling formulas are those of Haaland and Coolebrook, see equations (2.38) and (2.39) [7].

$$\frac{1}{\sqrt{f}} = -1.8log\left[\left(\frac{\varepsilon/d_H}{3.7}\right)^{1.11} + \frac{6.9}{Re}\right] \tag{2.38}$$

$$\frac{1}{\sqrt{f}} = -2log\left(\frac{\varepsilon}{3.7d_H} + \frac{2.51}{Re\sqrt{f}}\right) \tag{2.39}$$

The hydraulic diameter, D_h, used to calculate the friction factor is given by equation (2.40). For a circle the equation for the hydraulic diameter would yield the actual diameter of the circle and for a square it would yield the length of one of the sides. The hydraulic diameter is a measure to utilise non-circular cross-section in pipe-flow calculations.

$$d_H = 4\frac{A_f}{L_{\text{wet,per}}} \tag{2.40}$$

Chapter 3

Inlet Design

3.1 Basic Principles

The purpose of the inlet-section of the pump is to guide the flow towards the impeller entry and ensure stable operation and a sufficiently wide range in mass flow. The inlet section starts at Plenum, station 0 in figure 1.1. The inlet guide vanes (IGVs) are located at station 0.5, their role is to impart swirl of the incoming flow. It is not always desired to increase the swirl of the incoming flow and thus the IGVs are not always included in design. Between the IGVs and the inducer the flow is generally accelerated, due to the reduction of flow area due to impeller/inducer eye. At the start of the impeller the interaction between fluid and blade may cause cavitation of the fluid, and the designer should take these aspects into consideration.

3.1.1 Upstream of impeller

Upstream of the impeller there may be a tank, pool or similar, containing the working fluid at a certain thermodynamic state. For a compressor that may be the ambient air, i.e. no tank and atmospheric conditions apply. However, for a pump connected to a tank, the configuration may be of great importance. The location of the tank may add or subtract to the head available (NPSHA) by either being located at a higher or lower elevation relative to the pump. The thermodynamic state within the tank is also of great importance for the designer, due to the safe operational range outside cavitating range is altered due to these.

In power plants, it is not rare to have the feed-water tanks a couple of floors above the pumps, which are most commonly placed at or below ground level. This creates a fluid (water) column, increasing the pressure/head at the inlet of the pump.

The inlet guide vanes (IGVs), if present, may induce a swirl to the flow. Looking at the Euler turbomachine equation (2.26), this may either increase of decrease the amount of work that is possible to input into the fluid. Having a variable guide vane may also

increase the range of operation. However, it is not only the work input that is of interest for the designer. By inducing a swirl, the relative velocity, i.e. the velocity experienced by the impeller, is also changed. The impact the relative velocity has on cavitation will be shown later in this chapter. In figure 3.1 velocity triangles at inlet are shown for different level of swirl. The velocity triangles are created from the design tool created as part of this master thesis.

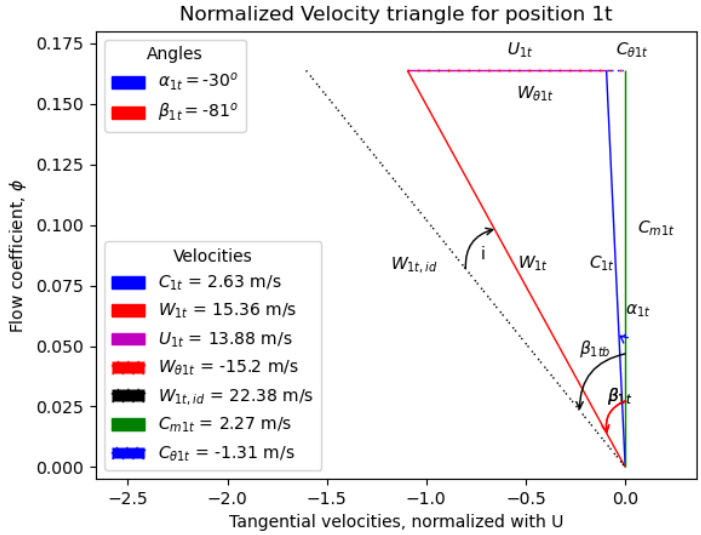

(a) Negative swirl

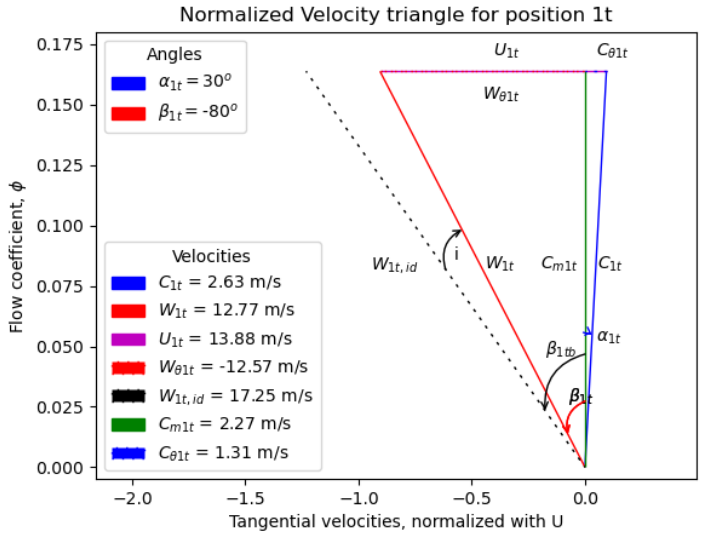

(b) Positive swirl

Figure 3.1: Inlet velocity diagrams with different level of inlet swirls

The effect of swirling the flow can be seen in the velocity triangles shown in figure 3.1. A positive swirl, i.e. in the direction of blade rotation, will decrease the relative velocity,

experienced by the blade, but the amount of work input available will also be reduced, as mentioned above. If instead the swirl is in opposite direction of blade rotation, the amount of work the impeller may transfer to the fluid is increased. However, the relative velocity is increased, which may present other problems to the designer, which will be discussed below (low W_{1t} desired, and large cavitation margin). If the IGVs are variable, i.e. able to move, the amount of swirl may be changed to suit the current mass flow.

In the above paragraphs, different velocity depending on radius has not been discussed. The effect of boundary layer build-up, components up-stream and interaction with the impeller may cause an uneven velocity profile. The effects of these are hard to simulate in 1D, and simplifications about the velocity field will be made in the preliminary design tool created.

3.1.2 Inducer

Firstly, a note regarding terminology must be made. In pump terminology an inducer is, often, a separate set of blades which may allow a cavitating flow. However, in centrifugal compressor terminology all blade inlet regions are referred to as inducers [2]. NASA [8] describes the inducer as the axial inlet portion of the turbopump rotor. This subsection will mainly refer to the additional structure for pump impellers.

The inducer may have several different roles, depending on what turbomachine it is mounted on [2]. It is the first rotating part that interacts with the working fluid, which means it has a critical role in e.g. guiding the flow.

Pumps having a high specific speed, often has separate inducers, designed to accept a cavitating flow, i.e. a two-phase flow. Japikse [2] mentions that in a well-designed inducer the first mode of cavitation occurs as tip vortex cavitation, followed by sheet cavitation at the leading edge which then is led into the core of the flow, in the middle of the flow passage. Due to this design, blade damage can be avoided, since the collapsing bubbles are not attached to the blade surface.

The main objective for cavitation accepting inducers are to capture the flow in the relative frame of reference and increase the pressure gradually, until the pressure exceeds cavitation pressure everywhere. Therefore, little blade turning is used, and the most common configuration is of a helical or screw shape, according to Japikse [2].

3.1.3 Cavitation at Inlet

Even though cavitation is a crucial phenomenon, it has not yet been fully understood, and modelling of cavitation uses many empirical correlations.
Inlet optimised for best efficiency is done by minimising the relative tip velocity. However, if the designer wishes to design the inlet for best performance in an NPSH-perspective,

this mindset needs to be altered, i.e minimising NPSHR.
At inlet the flow accelerate to pass through the impeller passage, which has some blockage from the blades. During this acceleration the static pressure is decreased, and as mentioned above, if this pressure is reduced below vapour pressure cavitation may occur.

The cavitation is an effect of the required NPSH exceeding the available. It is therefore of importance for the designer to know what the constraints and freedoms are before designing the pump. The absolute value of NPSHR of the pump does not single-handedly tell if the pump will cavitate. If the supplies fluid has an inlet head of a NPSH, i.e. has an available NPSH (NPSHA), that is equal to the NPSHR, that pump will remain at the inception of cavitation, assuming the cavitation coefficient, σ_b, was correctly chosen. The cavitation coefficient will be described in section 3.2.2 where cavitation is modelled.

NPSHA, i.e. the head above vapour pressure, is dependent on temperature. A higher temperature leads to boiling at a higher pressure, and an increased temperature of the working fluid would therefore entail a lower NPSHA. This is of utmost importance to the designer when determining the margin to cavitation. A pump designed to pump lake water at 10 °C might have problem if the temperature is increased to 20 °a hot summer day. It is important to consider cases that lie outside what the pump is designed for, i.e. off-design.

Another case of off-design is a varied mass flow. An increased mass flow will increase the velocity of fluid through the pump and reduce the static pressure. This results in an increase of NPSHR. At a certain mass flow, cavitation will occur and the upper limit for the pump is reached.

3.2 Modelling and Performance

In this section, equations based on both laws of conservation and empirical data describing the flow at inlet are presented. However, before the effects of the impeller are implemented the state of the fluid approaching the impeller must be determined.

The flow state at the impeller inlet can be calculated from the specified thermodynamic state upstream of the pump. However, before the fluid reaches the impeller it may accelerate or decelerate and encounter losses. Therefore the state at impeller inlet may not be the same as the state prescribed in the tank. The velocity is calculated in equation (3.1). The loss is described by a prescribed loss coefficient, see equation (3.2).

$$C_{m1} = \frac{\rho_0}{\rho_1} \mathrm{AR}_{01} C_{m0} \tag{3.1}$$

$$p_{01} = p_{00} - \mathrm{LC}_1 (p_{00} - p_0) \tag{3.2}$$

For a general case, some iterations may be needed to correctly determine the state at station 1, due to the unknown density in equation (3.1).

3.2.1 At Impeller

The speed of the impeller is calculated by multiplying the rotational speed with the radius, as seen in equation (3.3).

$$U_1 = r_1 \omega \tag{3.3}$$

The meridional velocity is obtained in equation (3.4), which is obtained by re-casting the continuity equation. The flow area utilised to calculate the meridional velocity is found through equations (3.5) and (3.6), by a specified inlet blockage factor and inlet sweep angle.

$$C_{m1} = \frac{\dot{m}}{\rho_1 A_{f1}} \tag{3.4}$$

$$A_{f1} = \frac{C_D \pi (r_{1t}^2 - r_{1h}^2)}{\sin \Phi_1} \tag{3.5}$$

$$C_D = 1 - B \tag{3.6}$$

For a more realistic description of the flow field, the meridional component will be allowed to vary in the radial direction. The meridional velocity at inlet tip radius is calculated in equation (3.7). AK may be empirically determined by experiments and simulations conducted. According to Japikse [2], a common range of AK is between 1.0 and 1.25.

$$C_{m1t} = AK \times C_{m1} \tag{3.7}$$

Since $C_{\theta 1}$ is set from guide vanes, both components of the absolute flow velocity is known. The magnitude of this velocity is calculated by the Pythagorean theorem, seen in equation (3.8). The relative velocity is calculated in a similar manner, seen in equation (3.9).

$$C_1 = \sqrt{C_{m1}^2 + C_{\theta 1}^2} \tag{3.8}$$

$$W_1 = \sqrt{(C_{\theta 1} - U_1)^2 + C_{m1}^2} \tag{3.9}$$

Once the relative velocity is known, the relative flow angle may be calculated by equation (3.10). The blade angle may then be calculated, for a set value of incidence, in equation (3.11).

$$\sin\beta = \frac{C_{m1}}{W_1} \tag{3.10}$$

$$i = \beta_b - \beta \tag{3.11}$$

It should be noted, that the local blade speed depends on the radial location. This implies that an even absolute flow field will result in a relative flow field which varies in radial direction.

3.2.2 Empirical Cavitation

An empirical approach correlating acceleration effects to the cavitation phenomenon exists and is essential for preliminary design [2]. The static pressure at inlet tip is described by equation (3.12).

$$p = p_{1t} - \sigma_b \left(\frac{1}{2} \rho W_{1t}^2 \right) \tag{3.12}$$

σ_b is the blade cavitation coefficient. It represents the fraction of the relative dynamic pressure which contributes to cavitation, by reducing the static pressure. At cavitation, the coefficient is defined according to equation (3.13). Some recommended values of σ_b are shown below [2].

$$p = p_v = p_{1t} - \sigma_b \left(\frac{1}{2} \rho W_{1t}^2 \right) \tag{3.13}$$

$0.2 \leq \sigma_b \leq 0.4$ Dixon (1978)
$0.1 \leq \sigma_b \leq 1.0$ Practice
$\sigma_b \leq 0.1$ Rocket Turbopumps

The static pressure at tip can be rewritten, assuming incompressible flow, as seen in equation (3.14). Due to the low mach numbers experienced by liquids, and the empirical nature of cavitation modelling, this is deemed sufficient, even for a liquid of more compressible nature.

$$p_{1t} = p_{01} - \frac{1}{2}\rho C_{1t}^2 = p_v + \sigma_b\left(\frac{1}{2}\rho W_{1t}^2\right) \tag{3.14}$$

To calculate the margin to cavitation, the difference of total pressure of fluid and vapour pressure is analysed, seen in equation (3.15) described by the blade cavitation coefficient and velocities.

$$\text{NPSH} = \text{NPSHR} = \frac{p_{01} - p_v}{\rho g} = \frac{\frac{1}{2}C_{1t}^2 + \sigma_b\frac{1}{2}W_{1t}^2}{g} = \frac{\frac{1}{2}C_{1t}^2(1+\sigma_b) + \frac{1}{2}\sigma_b U_{1t}^2}{g} \tag{3.15}$$

We can now optimise the inlet for a minimum of required NPSH, and be further away from cavitation at a given NPSHA. Optimising according to a minimum NPSHR will be in conflict with minimising the relative tip velocity, which can be shown analytically for a incompressible fluid.

3.2.3 Brumfield Criteria

If the performance parameters are known for the pump to be designed, i.e. ω, $\dot{V}$ and NPSHR, then the specific suction speed is known. For this specific suction speed there is a maximum value of cavitation coefficient at a specific flow coefficient, see figure 3.2. This relationship is obtained from equation (3.16). One might say that we could choose another, lower cavitation coefficient, if our blades allow it, however, from the definiton of NPSHR in equation (3.15) it can be observed that a higher value of σ_b allows for a lower relative tip velocity. The lower tip velocity is desired as it is the design goal for optimum efficiency.

The optimum cavitation coefficient can be found as a function of flow coefficient, i.e. the Brumfield criteria, see equation (3.17).

$$\frac{N_{ss}}{\sqrt{1-(\frac{r_{1h}}{r_{1t}})^2}} = \frac{2^{3/4}\pi^{1/2}\phi^{1/2}}{(\sigma_b + (\sigma_b+1)\phi^2)^{3/4}} \tag{3.16}$$

$$\sigma_b = \frac{2\phi^2}{1-2\phi^2} \tag{3.17}$$

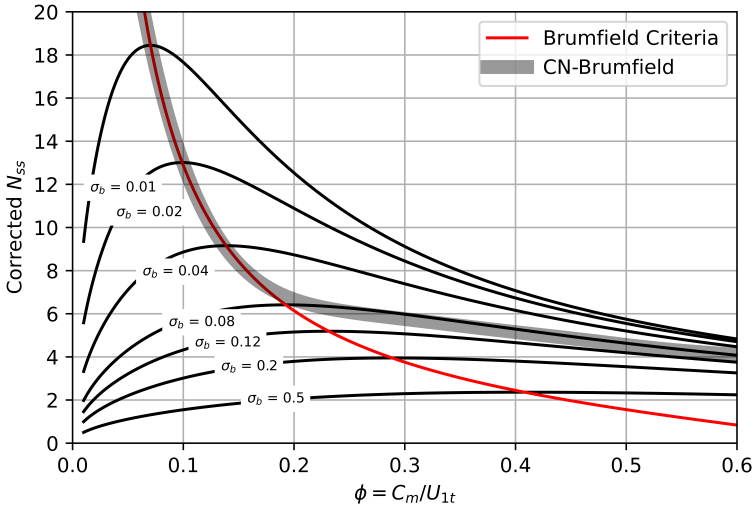

Figure 3.2: Relation of Specific suction speed and flow coefficient, for different values of blade cavitation coefficient. The Brumfield criteria is also shown.

The NPSHR for the current inlet design can be found by using equation (3.15) together with the calculated velocities. An estimate for σ_b is required. An example of how the variations may look like is presented in figure 3.3. It should be obvious to the reader that the two ways of optimising the impeller does not coincide. To summarise, for a set N_{ss}, a maximum σ_b is obtained from the Brumfield criteria. This also results in obtaining the corresponding flow coefficient, ϕ. The flow coefficient can be used, together with the specified performance parameters, to calculate the dimensions of the impeller inlet. Thus the inlet design is achieved from this N_{ss}.

3.3 Design Choices

The inlet of the impeller can, in machines operating on a liquid working fluid, be optimised in two aspects. Either to minimise the relative tip speed, i.e. optimise for best efficiency, or to optimise for minimum NPSHR, i.e. being as far away from cavitation as possible. These two conditions does not coincide, and for a first stage pump, the NPSHR optimisation is often chosen, due to the detrimental effects of cavitating flow, both in performance and life time. However, if a multistage pump is to be designed, the inlet of the following stages may be optimised in an best efficiency aspect, due to the pressure of the working fluid being far from vapour pressure. This design procedure will be explained further in the following section.

A high efficiency is always desired. However, if cavitation occurs, both life time and performance of the pump is severely reduced. Thus, a cavitating pump does not have high efficiency. An impeller designed for best efficiency will be the design which corresponds

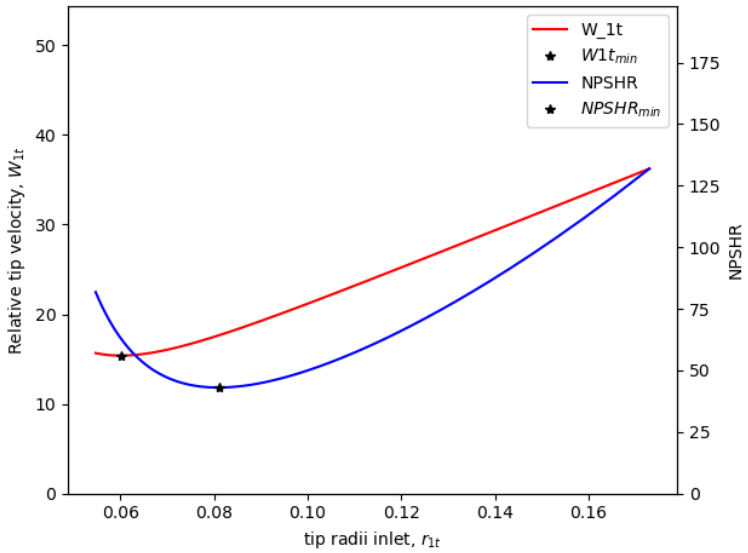

Figure 3.3: The variation of relative velocity at tip and the NPSHR for different geometries. Calculated for water for an arbitrary pump in the design tool.

to the lowest relative tip velocity W_{1t}.

The parameter NPSHR has already been discussed above. A popular design choice is to optimise the impeller to have the lowest NPSHR possible for the given parameters. A pump with set volume flow rate and rotational speed will have increased N_{ss} for decreasing NPSHR since NPSHR is in the denominator in equation (2.34). This relationship is also shown in figure 3.2, and discussed above.

However, the designer always desire an impeller with as high efficiency as possible, i.e. a low relative tip velocity W_{1t}, which is discussed above. It can be seen that, when the cavitation coefficient σ_b is reduced, the relative tip velocity must increase to maintain the NPSHR, see equation (3.15).

3.4 Design Procedure

To find a design yielding either a minimum NPSHR or a minimum relative velocity, a number of designs are computed and evaluated. The design corresponding to the chosen method of optimisation is then chosen. It is possible to solve for the inlet design analytically, if simplifications are made, e.g. incompressible flow. Explicit equations are presented by Japikse [2] for both efficiency and NPSHR optimisation. The Brumfield criteria could also be utilised to determine the design of the inlet. These designs, although derived from a simplified case, could provide decent starting values to quickly find the sought optimum, which will be described below.

When the above equations are used, the state is needed at all radial locations used, i.e. the computational points. These are often hub, mean, and tip radius. However, the specified thermodynamic state is often the state of the fluid far upstream, in a relative manner. Therefore, an iterative procedure is done to find the state just upstream the blades, due to losses and changes in flow are in the inlet duct.

Numerical Approach

In order to find the the inlet design suitable for the chosen design criteria a parametric study is conducted. A velocity is set upstream of the impeller eye, at station 0, where the thermodynamic state is specified. By specified loss and area ratio the density and velocity of the fluid at impeller inlet is found through some iteration.

Once the fluid velocity at impeller inlet is determined, equations (3.4) to (3.6) are utilised to calculate the inlet dimensions, given either the hub radius or the hub-tip-ratio. A meridional velocity profile may be acquired from equation (3.7) before calculating the absolute and relative velocities at desired radii. The NPSHR is computed with equation (3.15). A new velocity is then set upstream of the impeller and the procedure is repeated.

The relative velocity at tip radius and the NPSHR is then compared for the different cases, shown in figure 3.3 In figure 3.4 a flow chart for the design procedure is shown.

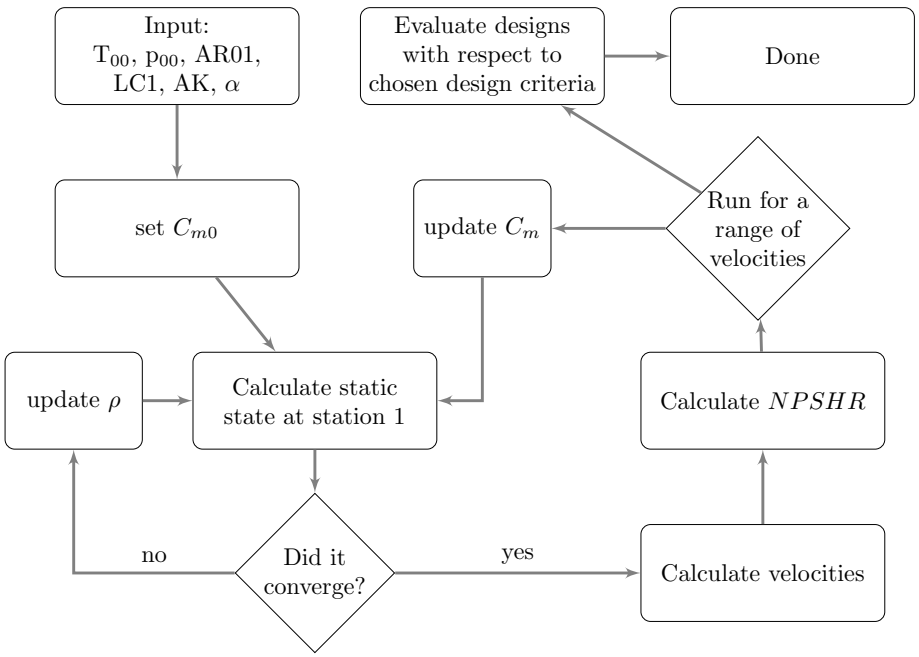

Figure 3.4: Flow chart for the numerical design procedure

Combining with Brumfield-Criteria

Another mean to determine the inlet geometry is to utilise the Brumfield graph, shown in figure 3.2. However, the pump will then be designed with a simplistic approach, assuming an incompressible working fluid, an even velocity profile and no blockage from impeller blades.

If the designer wishes to maintain a realistic view, the Brumfield criteria may serve as an approximation. In figure 3.5 the effect of these parameters are shown. E.g. in figure 3.5b the difference of the design points achieved from Brumfield and numerical computations are clearly seen. A velocity profile is applied, which entails a higher velocity of the fluid at the tip, following from equation (3.7). This would result in a higher NPSHR, given by equation (3.15) and therefore a lower specific suction speed. In the figure shown water is used a working fluid, which does not experience much compressibility. However, for liquid hydrogen, a fuel used in rocket propulsion [8], the compressibility causes the lines to diverge.

According to NASA [8] there are several starting points when designing, i.e. combinations of input parameters. The Brumfield criteria provides a useful tool when translating these different input parameters to another set of quantities which can be utilised in the equations above.

The numerical approach, described by the equations above, is always solving for tip velocities, with rotational speed and mass flow/volume flow known. However, these may not be known by the designer, but an NPSHR may be chosen as input instead. NASA describes two cases, **A** and **B**, [8]. In case **A**, all performance parameters, (rotational speed, mass- or volume flow and NPSHR) are all specified by the designer and the specific suction speed is known. The Brumfield plot can then be utilised by drawing a line from the corrected specific suction speed to find the flow coefficient, ϕ, which correlates to the maximum cavitation coefficient, σ_b. The numerical approach, however, will not utilise the specified NPSHR. Instead, the cavitation coefficient, σ_b found with Brumfield criteria will be utilised relating the velocity to NPSHR. The numerical approach uses rotational speed and flow to determine the velocity and NPSHR.

In the other case (**B**), where not all three performance parameters are known, another approach is needed. When two of the three parameters are specified by the designer, the specific speed becomes a function which is only dependant on the last parameter. The specific speed will be related to the flow coefficient, according to the Brumfield criteria. To do this, an estimated value of σ_b is required. This allows to calculate the specific suction speed, and therefore the last remaining unknown. The numerical approach can now be conducted in the same way as above, due to rotational speed and flow are determined through Brumfield, if they were not specified by the designer.

The flow chart of inlet design calculation is seen in figure 3.6.

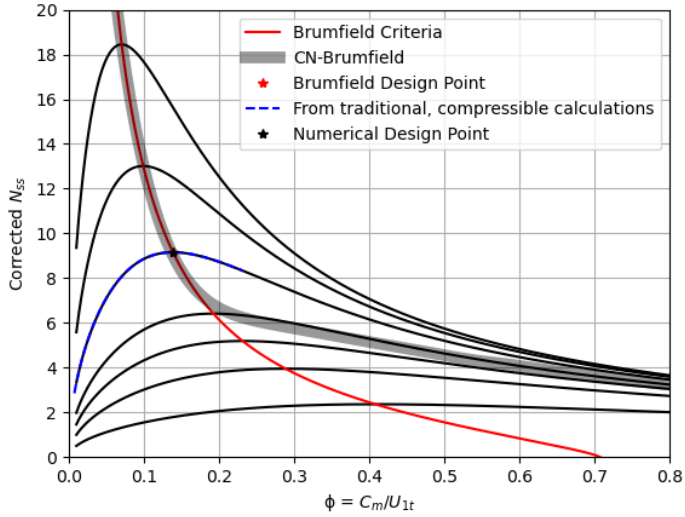

(a) With AK

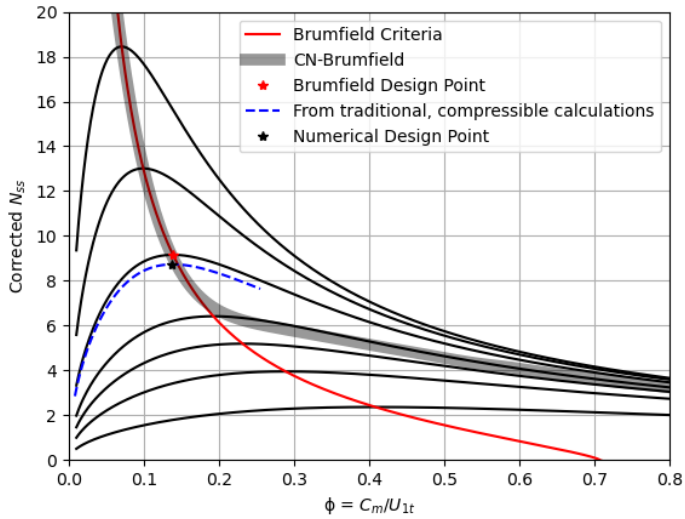

(b) No AK

Figure 3.5: Brumfield plots showing the numerical calculation, the Brumfield design point and the actual design point. Both cases have the same specified parameters, with exception for the velocity profile, *AK*.

3.5 Off-Design Considerations

At higher than design mass flows the absolute velocity is increased, following the continuity equation. The dimensions are set from the generated geometry, and the performance may be calculated for a given absolute velocity. At high mass flows

the NPSHR will be increased, and cavitation may be encountered. Considering the detrimental effects of cavitation, the off-design range should be considered early in the design process.

At lower than design mass flows, the absolute velocity is reduced which alters the aerodynamic performance of the blades. The flow will begin to separate on the suction side of the blade if the flow is further reduced. The flow separation creates zones of re-circulation and if conditions worsen, the inlet may stall [2].

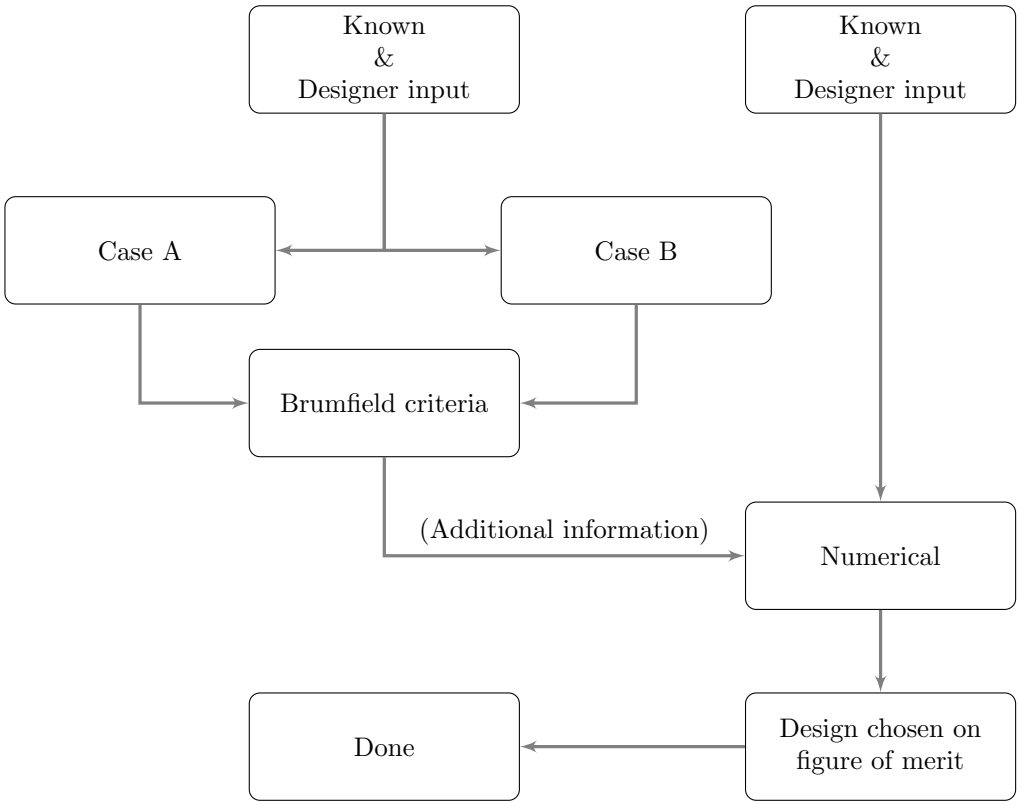

Figure 3.6: Flow chart of inlet design

Chapter 4

Impeller Flow Physics

The impeller, also known as the rotor, is the part of the pump that supplies work to the working fluid. The aim of this chapter is to initially explain the geometry of the impeller, followed by a simplified view of how the fluid is affected, i.e. the fluid at station 2. Lastly a more thorough view of the internal flow physics will be described.

The modelling of the flow will be conducted in the subsequent chapter.

4.1 Detailed Impeller Geometry

To obtain a complete view of the impeller and possible interactions with other part of the pump the impeller and surrounding components will be discretised. A meridional view of an impeller is shown in figure 4.1. The sketch shows a shrouded impeller, but it is possible to use an un-shrouded impeller, also known as an open impeller. The open impeller does not have a shroud, and is thereby open to the front cavity.

As seen in the figure 4.1, it is possible to have a sweep-angle ($\phi_1 < 90°$) resulting in a mixed flow into the impeller. Similarly for station 2, the designer has the option to have the discharge going in a more axial direction. Seals are present both between the shroud-cavity and inlet, i.e. front seal, and between rear of the disk and shaft, i.e. rear seal. Pumps are often designed with a blade angle at impeller tip, called back sweep due to being in the opposite direction of rotation. This is utilised to minimise the effect of slip, discussed later in this chapter.

4.2 Basic Principles

The main purpose of the impeller in a pump is to increase the pressure of the working fluid by supplying work to it. The impeller is driven by an external machine, be it an electrical motor or a turbine. Torque is transferred through the shaft to the fluid. As described above, the outlet of the pump impeller, i.e. the impeller tip, lies at a greater

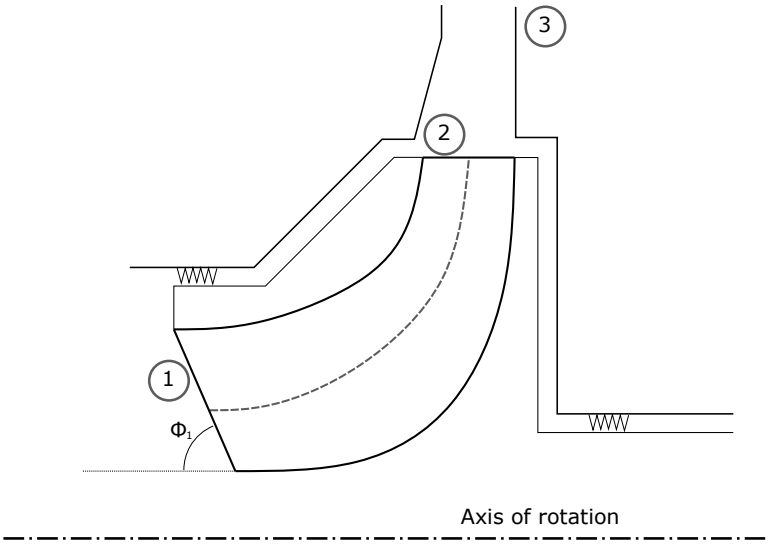

Figure 4.1: Meridional view of an impeller, including seals.

radius than the inlet. This increase of radius may be of benefit as it aids in the process of work input, as explained earlier in Euler's turbomachine equation (see equation (2.26)).

When visualising the flow through the impeller it can be beneficial to work in a relative coordinate system, i.e. one rotating at same speed as the impeller. The flow can then be described in terms of relative velocities. The relative flow of the impeller may be allowed to diffuse through the impeller, in order to obtain a flow closer to the desired state.

4.2.1 Outlet State

At the impeller tip, where the flow leaves the impeller, the flow can be visualised by utilising velocity triangles. For an ideal flow, in which the flow completely follows the blades, the relative flow angle is equal to the exit blade angle, given by the back-sweep. The velocities are dependant on the work supplied and the relative diffusion taking place within the impeller. This will be related with modelling and equations in the next chapter.

Deviation/Slip Phenomenon

The relative flow leaving the impeller will deviate from the blade angle, even in ideal (inviscid and isentropic) conditions due to lack of guidance from the blades [9]. A perfectly guided flow could theoretically be achieved by an infinite number of infinitely thin blades, thus giving perfect guidance. This is practically impossible, but this reasoning should distinguish slip from other losses and inefficiencies.

Dixon [9] mentions a concept to visualise the origin of slip. Imagine inviscid fluid

entering the impeller without swirl. The absolute flow at outlet should maintain the zero swirl from inlet. The impeller is rotating with rotational speed ω and relative to the impeller the fluid has a rotation of $-\omega$. This is called the *relative eddy*. The outlet flow can be viewed as a through-flow following the blading with the relative eddy superimposed, thus creating a difference in flow angle and blade angle.

This difference in angles is referred to as deviation. This deviation is present, even in a loss-free case, and as seen in figure 4.2, it reduces the tangential velocity in the absolute frame. The slip factor is defined as the ratio of the actual and theoretical absolute tangential velocities.

Velocity Diagram

In figure 4.2 an arbitrary velocity triangle of the mixed-out, average, state flow leaving the impeller is visualised. The blade speed is from left to right, i.e. a clockwise turning impeller. The slip is visualised in the figure through the difference between ideal and actual relative velocity. The actual velocity does not follow the blading, resulting in a subsequent decrease of the tangential absolute velocity, C_θ.

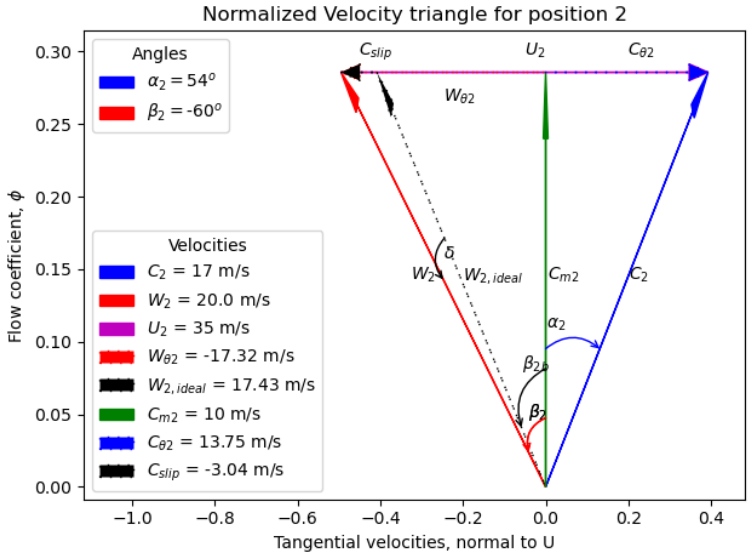

Figure 4.2: Arbitrary velocity triangle created by the design tool created by the authors. (Text on x-axis wrong)

4.3 Internal Flow

The reader should now have a general view of the overall achievements accomplished by the impeller. The flow within the impeller is, however, of great importance to accurately describe and understand the impeller and pump as whole.

During the passage, centrifugal and Coriolis forces affect the flow and distorts the flow field. Later in this chapter it will be shown that low-momentum fluid is relocated to certain areas within the passage. This phenomenon will be utilised in the modelling of the flow in chapter 5.

4.3.1 Primary Flow

The primary flow in the impeller, or in any other flow, can be thought of as the flow doing what is intuitive [10]. For the impeller this means following the blades through the passage. Experiments has shown the presence of a virtually loss-free (isentropic) zone at the outlet of the impeller, referred to as the primary zone [2].

4.3.2 Secondary Flow

The secondary flow is defined as all non-primary flow. This implies that the secondary flow is not a unified state, but a multitude of velocities combined. The reader may get an intuitive feel for secondary flows from the following example. When reading this thesis, the *primary flow* could be thought of the direction along which the page numbers increase. The other *movements* such as going to nomenclature or another section, be it for clarification or repetition, could be seen as a secondary flow of reading.

Another famous example of visualising secondary flows was done by Edward S. Taylor [10]. He describes a cup of tea, with tea leaves, and what happens if one were to stir it. A first intuition would be that the leaves would be thrown outwards onto the cup edge due to centrifugal force. However, the leaves goes towards the middle of the cup. This phenomenon is described by secondary flows. As the denser leaves are brought to the bottom, the secondary flows carry them towards the centre.

The secondary flows inside the centrifugal impeller is extremely difficult to describe. In order to obtain a grasp of this concept, the inviscid and incompressible case is discussed at first, originally done by Johnson [11]. Consider a velocity triangle, described in equation (4.1) in vector notation and the definition of absolute vorticity, shown in equation (4.2).

$$\vec{C} = \vec{W} + \vec{U} \tag{4.1}$$

$$\Omega_s = \vec{\nabla} \times \vec{C} = \vec{\nabla} \times \vec{W} + 2\omega \tag{4.2}$$

Substituting equation (4.1) into equation (4.2), taking the divergence and some further manipulation yields the expression shown in equation (4.3). The equation describes the streamwise vorticity, and the parameters inside the equation are given below [11]:

- Ω_s = streamwise vorticity
- x = direction along the rotational axis
- b = binormal to the relative streamline

$$\frac{\partial}{\partial s}\left(\frac{\Omega_s}{\rho W}\right) = \frac{2}{\rho W^2}\left(\frac{1}{R_c}\frac{\partial p_T}{\partial b} - \frac{\omega}{W}\frac{\partial p_T}{\partial x}\right) \tag{4.3}$$

By fixing the coordinate system to the rotating fluid element, described in section 2.1, the following expression, seen in equation (4.4) is obtainable. This equation describes the twisting of the secondary flow field, ϕ, in terms of the angular coordinate along the flow path.

$$\begin{aligned}\frac{\partial^2 \phi}{\partial \theta^2} = S_{\text{rtp}}\Bigg[\cos\phi - \frac{1}{Ro}(\omega_x \sin\phi cos\theta + \omega_y \cos\phi + \omega_z \sin\phi \sin\theta)\Bigg] \\ -\frac{1}{Ro}(\omega_x \cos\theta + \omega_z \sin\theta)\end{aligned} \tag{4.4}$$

Where:

$$S_{\text{rtp}} = \text{Strength of the relative total pressure gradient} = \frac{\Delta p_T}{\rho W^2}\frac{R_c}{D}$$

$$Ro = \text{Rossby Number} = \frac{W}{\omega R_c}$$

The Rossby Number, Ro, can be seen as the fraction of relative influence that either the curvature or rotational effects has. As Johnson mentions, if the Rossby number is low, the flow will be dominated by rotational effects, and a large Rossby number tells of a flow dominated by curvature.

Johnson [11] has applied these equations to simplified cases in order to increase the understanding of secondary flow development.

Flow in Bends

Johnson [11] mentions that, for a potential flow, the rotational total pressure, p_T, is uniform in the flow field. However, for a real flow, even for a flow with uniform rotational relative pressure, areas of low p_T will develop, either due to separation of flow or viscous losses in boundary layers. In the report by Johnson, however, the consideration is for inviscid flow and how an already developed gradient of p_T is convected through the flow. The geometry of the rotating bend is depicted in figure 4.3.

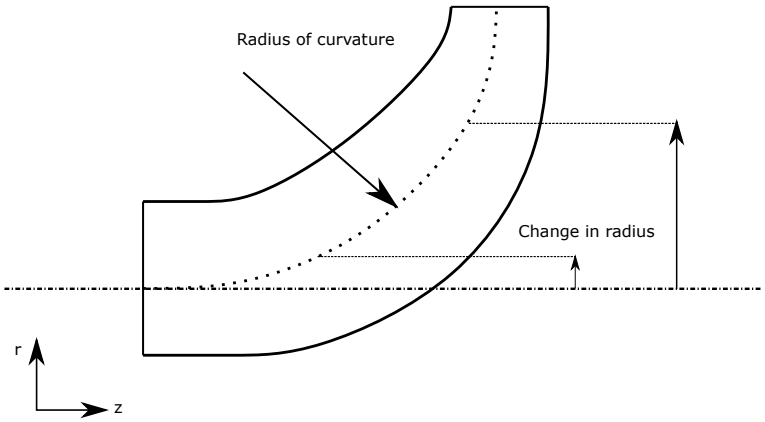

Figure 4.3: A 90 °bend used in the two scenarios. The rotation is around the z-axis, in the second scenario.

Johnson [11] presents stable locations for fluid having low p_T, and the movement associated when not being in this stable position. The stable location of low p_T is defined by Johnson as the point on the wall of a passage, either rotating or stationary, where the gradient of p_T may exist in the boundary layer without any creation of streamwise vorticity. Three main points about stable locations, according to Johnson, are:

- At the stable position, the value of $\frac{\partial}{\partial s}\left(\frac{\Omega_s}{\rho W}\right)$ is zero.
- The stable location of low p_T is also the point where all fluid with low relative pressure tends to move.
- The stable location for low p_T coincides with the position of minimum reduced static pressure, $p_r = p - \frac{1}{2}\omega^2 r^2$

The reduced static pressure and and total rotational pressure are related in equation (4.5).

$$p_T = p_r + \frac{1}{2}\rho W^2 \tag{4.5}$$

Below, two examples from Johnson will be presented. The first is a stationary bend and thereafter a rotating bend. The flow is still assumed inviscid.

For a stationary bend, i.e. having no rotational speed $\omega = 0$, equation (4.4) above can be reduced. The simplified equation is presented below in equation (4.6).

$$\frac{\partial^2 \phi}{\partial \theta^2} = S_{\text{rtp}} \cos \phi = \frac{\Delta p_T}{\rho W^2} \frac{R_c}{D} \cos \phi \tag{4.6}$$

In this scenario, flow is going through a 90° bend, and a fluid particles path though the bend is analysed. The flow path depends on the initial conditions, especially the pressure gradient. For a flow, with initial pressure gradient pointing (positive) in opposite direction of the upcoming bend, the flow will be stable.

This stable location is intuitive by the following reasoning. The turning of the flow requires a force acting upon it, this equates to having a pressure side on the outside of the bend. If the same bend now rotates around the axial direction the second scenario is reached. Applying equation (4.4) to this scenario equation (4.7) is obtained.

$$\frac{\partial^2 \phi}{\partial \theta^2} = S_{\text{rtp}} \cos \phi - \frac{S_{\text{rtp}}}{Ro} \sin \phi \sin \theta - \frac{1}{Ro} \sin \theta \tag{4.7}$$

The stable locus position is now dependent on the Rossby number. For Rossby numbers greater than unity it will be located on the suction surface, otherwise the stable location is located on the pressure surface.

By comparing equation (4.7) to the equation of the stationary bend, equation (4.6), the effects of the Rossby number can be easily visualised, and a general intuition made. E.g. for large values of Ro, the two equations will be approximately the same, i.e. rotational effects are in that case negligible. To obtain a grasp how this is connected to secondary flows inside an impeller passage it is important to note the several bends the flow experiences though the impeller.

Eckardt's Impeller

For the impeller passage in a centrifugal machine three main contributors of streamwise vorticity generation is mentioned [2].

Firstly the inlet, or inducer, bend is mentioned, where the low momentum fluid is convected from the boundary layers of the shroud and hub walls to the suction surface, due to secondary flows caused by the bend's curvature.

The exact location is dependent on the influence from either of these parts. Johnson also mentions that the Rossby number is about 0.25 for this initial bend for most impellers. Since Ro is small, rotational effects will dominate the secondary flow. The stable location should therefore be closer to the centre of the suction surface for the inlet bend.

In the axial to radial bend the curvature induces secondary flows which carries low p_T fluid towards the shroud. The rotation of the passage also generates secondary flows, caused by Coriolis acceleration, which moves low p_T fluid to the suction surface. The Rossby number is around unity for this part of the impeller, for Eckardt's impeller $Ro = 0.7$. Which entails that aspects of curvature is of the same significance as rotational aspects in terms of secondary flow generation.

Thirdly, the basic passage rotation increases in strength as the flow passes through the impeller to the radial direction. Secondary flow is generated by coriolis forces, which moves low momentum fluid from hub and shroud walls, and from the unstable pressure surface, onto the suction surface.

It has now been shown that both the curvature of the flow and rotational aspects generate secondary flow, which in turn move low p_T fluid to certain areas. This fluid is most commonly found within boundary layers, as it is there friction causes a reduction in p_T. This gives rise to what is called the secondary zone. At the tip of the impeller, i.e. outlet, there will be both a primary zone and a secondary zone.

4.3.3 Mixing Flow

After leaving the impeller, there is no phenomena that collects low momentum fluid in separate, stable locations, i.e. there is no active segmentation of the flow. Due to turbulence, viscosity etc. the two zones will eventually mix and merge into one mixed-out state. Japikse [2] mentions that the separate zones may continue their formation after the impeller. At a radius, about 30 % greater than impeller outlet, the flow field can be seen as essentially mixed-out. The mixing of the two zones is associated with a loss of total pressure and an increase in static pressure.

Chapter 5

Impeller Modelling

In the preceding chapter the impeller and the flow within was presented. To obtain a quantitative measure of the pump and its performance, these flow phenomena need to be modelled. This chapter will introduce two ways of modelling the impeller. Firstly, a well known simplistic approach will be presented. Thereafter, a more realistic way of modelling, taking the internal flow physics into account, is presented.

5.1 One-Zone Modelling

In this way of describing the impeller, all fluid entering the control volume is described by a single state. The same is true for the exit stage. Conservation equations, Euler work equation and impeller efficiency is utilised to determine the exit state of the fluid from the inlet state.

The simplicity stems from the neglection of the internal flow, i.e. no information is gained about the internal flow field. It is required to describe the inlet and outlet as one averaged thermodynamic state each. It can easily be distinguished, that this simplistic way of describing the impeller is inferior to more advanced models. However, it does provide a mean to quickly determine the exit state, even possible to do by hand. It is a well know procedure, mentioned in most turbomachinery literature and utilised by both students and engineers to estimate an exit state [2].

5.1.1 Slip Models

The slip phenomenon described in section 4.2.1 can be modelled in a multitude of ways. They apply to different scenarios and ranges.

Stanitz slip model [9] is shown in equation (5.1).

$$\sigma = 1 - \frac{0.63\pi/Z}{1 - \phi_2 \tan \beta_{2b}} \tag{5.1}$$

A popular slip model, originally proposed by Wiesner, is seen in equation (5.2). This model is valid within a limited range, defined in equation (5.3). If the radius ratio exceeds ϵ a correction for the slip factor may be obtained through equation (5.4) [9].

$$\sigma = 1 - \frac{\sqrt{\cos \beta_{2b}}}{Z^{0.7}(1 - \phi_2 \tan \beta_{2b})} \tag{5.2}$$

$$\frac{r_1}{r_2} \leq \epsilon = \exp\left(\frac{-8.16 \cos \beta_{2b}}{Z}\right) \tag{5.3}$$

$$\sigma_{\text{corr}} = \sigma\left[1 - \left(\frac{r_1/r_2 - \epsilon}{1 - \epsilon}\right)^3\right] \tag{5.4}$$

A slip model proposed by Stodola is shown in equation (5.5) [9].

$$\sigma = 1 - \frac{(\pi/Z)\cos \beta_{2b}}{1 - \phi_2 \tan \beta_{2b}} \tag{5.5}$$

5.1.2 One-Zone Calculations

The outlet is described as an averaged mixed-out state [2]. To calculate this state, the Euler turbomachine equation, conservation of mass, velocity triangles and definition of impeller efficiency is utilised.

The meridional velocity at impeller outlet is found in equation (5.6), where the whole circumferential area is used, i.e. no blockage from vanes [2]. The impeller tip speed may be calculated in equation (5.7). The slip velocity, described in section 4.2.1, is calculated in equation (5.8), utilising the slip factor from a slip model of choice. With these velocities now known, the actual absolute tangential velocity may be calculated, see equation (5.9).

$$C_{m2m} = \frac{\dot{m}}{\rho_2 A_{f2}} \tag{5.6}$$

$$U_2 = \omega r_2 \tag{5.7}$$

$$C_{\text{slip}} = U_2(1 - \sigma) \tag{5.8}$$

$$C_{\theta 2m} = U_2 - \frac{C_m 2m}{\tan \beta_{2b}} - C_{\text{slip}} \tag{5.9}$$

The velocity triangle at outlet is now fully defined. Using this velocity triangle and known inlet state in the Euler turbomachine equation (5.10) and applying it in the energy equation (5.11), together with parasitic losses, the total enthalpy rise through the impeller is acquired.

$$w_{\text{Euler}} = U_2 C_{\theta 2} - U_1 C_{\theta 1} \tag{5.10}$$

$$w = \Delta h_0 = w_{\text{Euler}} + w_{\text{friction}} + w_{\text{backflow}} + w_{\text{leakage}} \tag{5.11}$$

Below, in equation (5.12), is an incompressible description of the isentropic efficiency. The equation may also be used to find the total pressure after the impeller if the efficiency is specified.

$$\eta_{0-2} = \frac{(p_{02m} - p_{00})/\rho}{w} \tag{5.12}$$

By utilising the equations above the state at impeller exit may be approximated.

5.2 Two-Zone Model

In traditional meanline design seen above, the work transferred from impeller to the fluid may be described by isentropic efficiency, which may be found from loss models. In the following section, however, it will be described how the impeller flow can be modelled by utilising characteristics of the flow physics described in section 4.3. Losses will naturally arise from this method of modelling.

The flow through the impeller has, as previously stated, a primary and a secondary zone. A conceptual representation of these zones is shown in figure 5.1. However, it should be noted that this figure is just a concept, and does not necessarily represent the exact locations of physical zones within the impeller. It indicates the presence of a primary zone with isentropic streamlines, and an averaged secondary zone with non-isentropic streamlines. This is the essential concept behind two-zone modelling. Actual flow physics are considered, unlike the calculations for single-zone modelling.

The state after the impeller cannot be easily described by one of these zones. Some form of mixing is needed to reach a reasonable flow characteristic. This mixing can be reached in a multitude of ways, e.g. mixing by taking a mass average of the primary

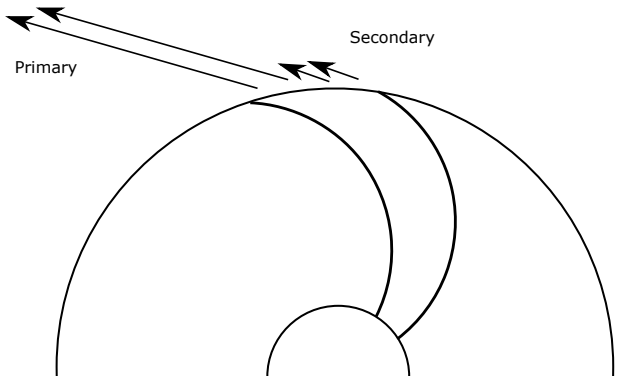

Figure 5.1: Conceptual representation of the primary zone and secondary zone. Reworked from [2].

and secondary flow conditions or by performing mixing calculations, which is described later, in section 5.2.4.

To find the thermodynamic state of the fluid exiting the impeller from either zone, conservation equations are utilised. The relative velocity out of the impeller, for the isentropic streamlines, are calculated by the diffusion ratio for the impeller. This diffuision ratio may be calculated by utilising the **T**wo **E**lements **I**n **S**eries model (TEIS-model).

5.2.1 TEIS

The knowledge about an isentropic core flow permits the definition of parameters describing the acceleration or deceleration of the core. A convenient parameter for this purpose is the ratio of relative velocities at impeller inlet and exit. It is conventional to use the relative velocity at inlet tip [2].

$$W_{1t}/W_{2p}$$

This ratio gives a good description of the the most critical streamlines in the impeller. If this ratio is greater than one, the core flow has been decelerated, i.e. diffused. If the ratio is less than one, it has been accelerated. To achieve a good design, the designer wishes to have considerable diffusion of the core flow within the impeller.

The impeller passage may be seen as a rotating diffuser. For a conventional diffuser, parameters as area ratio and length to width, for each stream tube, are important. To obtain a sufficient description of the flow diffusion through the impeller passage a two step diffusion model is employed. A principle sketch of these two elements are visualised in figure 5.2.

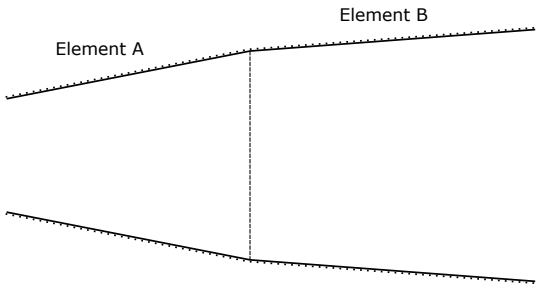

Figure 5.2: Principle sketch of the TEIS-model. Reworked from [2].

The first element can be either a nozzle or diffuser in character, as it has a variable geometry, depending on the level of incidence. The second element most often has a diffusive character. The first element is described by an inlet area and a throat area, whilst the second element is described by the same throat area and exit area.

The inlet area to the impeller passage, i.e. to the first element, is dependent on the flow. At high flow the relative flow angle is reduced and flow area is increased, thus making the first element into a nozzle, accelerating the flow. At low flows, the relative flow angle is increased and the inlet area is reduced accordingly. The reduction of the flow area means that a diffusive character is obtained in the first element.

The second element, which is being fed by the first one, is of constant geometry, i.e. the flow areas are not dependant of the flow. However, Japikse [2] mentions that the actual fluid dynamic throat is able to move to various positions in the vicinity of the geometric throat, depending to the particular flow. To relate the exit and inlet tip the diffusion ratio parameter can be utilised.

$$DR_2 = W_{1t}/W_{2p}$$

A higher value of the diffusion ratio indicates that more diffusion has occurred. If the value is below unity, the flow has accelerated in the impeller passage. If the passage is modelled without effects of viscosity and a flow that follows the blading perfectly an ideal diffusion ratio is obtained. A comparison of the ideal and actual values may be instructive to the pump designer.

A simple analytical model can be written for these two elements. Each of the elements is treated as a diffuser with constant effectiveness (η). The following equations are valid for a compressible flow. If an incompressible assumption is sufficient, coefficients of pressure recovery may be used instead of coefficients of enthalpy recovery. This is

described by having the density ratio set to unity. The ideal diffusion ratio, for element a, is described in equation (5.13). It can be seen that the diffusion ratio is a function of the relative flow angle at inlet.

$$DR_{ai} = \frac{\rho_1}{\rho_a} \frac{A_{annular,1} \cos(\beta_{1t})}{A_{th}} = \frac{W_{ai}}{W_{1t}} \tag{5.13}$$

The ideal enthalpy recovery coefficient can be found with the ideal diffusion ratio, see equation (5.14). As previously mentioned, in the case of incompressible fluid assumption this reduces to the pressure recovery coefficient, as the ideal diffusion ratio is described solely by the area ratio.

$$C_{h,ai} = 1 - DR_{ai}^2 \tag{5.14}$$

The actual diffusion ratio in the first element, equation (5.15), is obtained from the ideal coefficient of enthalpy recovery and an effectiveness, which is assumed constant through the element.

$$DR_a^2 = \frac{1}{1 - \eta_a C_{h,ai}} = \left(\frac{W_a}{W_{1t}} \right)^2 \tag{5.15}$$

The relative velocity in the throat is now found, and can be utilised to determine the thermodynamic state in this position. By utilising the isentropic definition of the primary zone, only one other property is needed to determine the thermodynamic state, as mentioned in chapter 2. By utilising the constant property rothalpy, the enthalpy in the throat may be found. The density can now be calculated as a function of the state. The above equation can be repeated with the newly calculated density and the process is repeated until the state has converged.

The second element, element b, is described in a similar manner, where the ideal diffusion is obtained from the ratios of densities and flow areas in equation (5.16). The ideal enthalpy recovery coefficient in element b is then obtained by equation (5.17), which is used in equation (5.18) together with the constant effectiveness of element b to obtain the actual diffusion ratio of the second element.

$$DR_{bi} = \frac{\rho_a}{\rho_b} \frac{A_{th}}{A_{\text{annular,exit}} \cos(\beta_{2b} + \delta_{2p})} = \frac{W_{bi}}{W_a} \tag{5.16}$$

$$C_{h,bi} = 1 - DR_{bi}^2 \tag{5.17}$$

$$DR_b^2 = \frac{1}{1 - \eta_b C_{h,bi}} = \left(\frac{W_b}{W_a}\right)^2 \tag{5.18}$$

In a similar manner as above, the state at outlet may now be found, to calculate the density, and iterate until convergence.

When the actual diffusion ratios are found for each element, the total diffusion ratio for the impeller passage may be calculated, according to equation (5.19).

$$DR_2^2 = DR_a^2 DR_b^2 = \left(\frac{W_b}{W_{1t}}\right)^2 \tag{5.19}$$

A flow chart for computational process for TEIS is shown below in figure 5.3. The iterative method it not needed in an incompressible case.

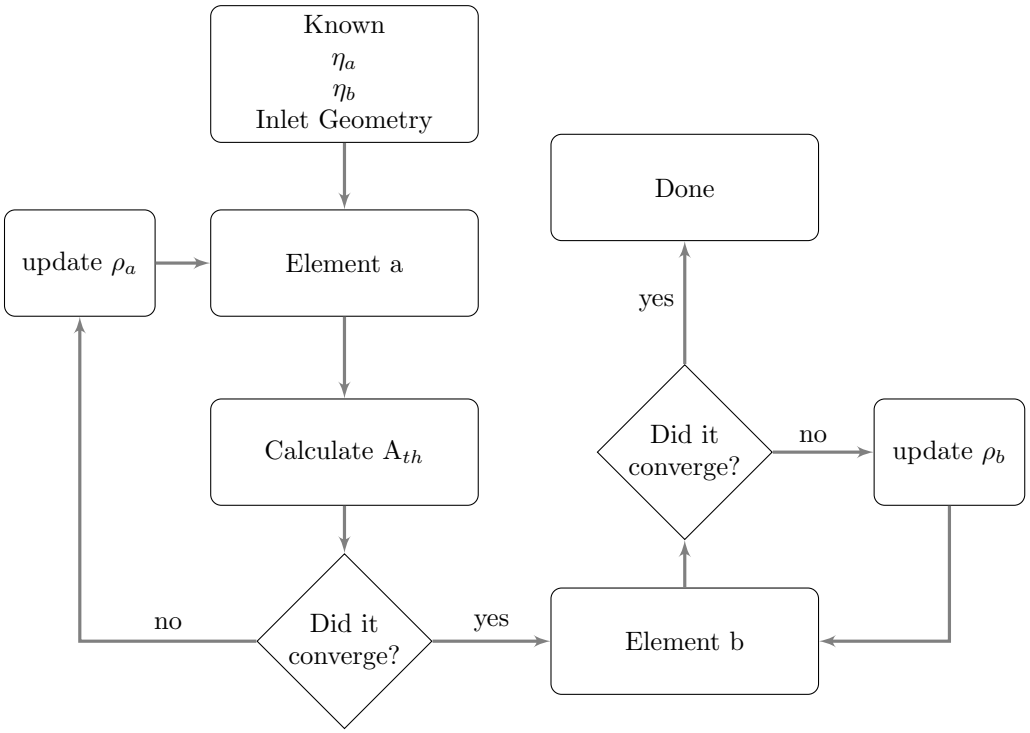

Figure 5.3: Flow chart of TEIS-model calculations.

5.2.2 Primary Zone

With known isentropic relative velocity leaving the impeller, the property known as rothalpy or, in the case for incompressible flow, rotational pressure may be utilised to determine the enthalpy or pressure at the outlet, since the state at inlet is completely known. This in done by re-arranging either equation (5.20) or (5.21), for compressible and incompressible case, respectively.

$$I = h_{2p} + \frac{1}{2}W_{2p}^2 - \frac{1}{2}U_2^2 = h_{1t} + \frac{1}{2}W_{1t}^2 - \frac{1}{2}U_{1t}^2 \tag{5.20}$$

$$p_T = p_2 + \frac{1}{2}\rho_{2p}(W_{2p}^2 - U_2^2) = p_{1t} + \frac{1}{2}\rho_{1t}C_{1t}^2 - \rho_{1t}U_{1t}C_{\theta 1t} \tag{5.21}$$

Where U_2 is the wheel speed at impeller tip, shown in equation (5.22).

$$U_2 = \omega r_2 \tag{5.22}$$

With the enthalpy or pressure known, the thermodynamic state is fully defined, due to the isentropic nature of the primary zone streamlines. The entropy is constant from inlet and can be used to calculate other properties of the primary zone, e.g. density.

With blade angle known, and a set deviation, the complete velocity triangle can be determined. The meridional velocity component is related to the relative velocity in equation (5.23). The relative tangential velocity is found in the same manner, see equation (5.24). The absolute tangential velocity can now be calculated from the blade speed and relative tangential velocity, equation (5.25), and thereafter, the total absolute velocity is calculated with the Pythagorean theorem in equation (5.26).

$$C_{m2p} = W_{m2p} = W_{2p}\cos\beta_{2p} \tag{5.23}$$

$$W_{\theta 2p} = W_{2p}\sin\beta_{2p} \tag{5.24}$$

$$C_{\theta 2p} = U_2 + W_{\theta 2p} \tag{5.25}$$

$$C_{2p} = \sqrt{C_{m2p}^2 + C_{\theta 2p}^2} \tag{5.26}$$

The relative flow angle, used in the equations above, is calculated in equation (5.27), with blade angle and deviation known.

$$\beta_{2p} = \beta_{2b} + \delta_{2p} \tag{5.27}$$

The geometric area at impeller outlet is given by the circumferential area, minus the area attributed to blade thickness, given by equation (5.28).

$$A_{f2} = 2\pi r_2 b_2 - \frac{Z_R b_2 t_{2b}}{\cos \beta_{2b}} \tag{5.28}$$

In order to evaluate the flow, both containing primary and secondary flow, descriptions of the sizes of them are required. The size of the secondary zone is described by the fraction of mass flow and flow area, defined by equations (5.29) and (5.30), respectively. The mass fraction in secondary zone is, usually, the specified parameter. A common value in preliminary design is 0.15, but it may be altered if more knowledge is acquired, e.g. from similar pumps.

The value of ε may be calculated from χ and continuity equation applied to the primary zone at impeller outlet, described below in equation (5.31).

$$\chi = \frac{\dot{m}_s}{\dot{m}} \tag{5.29}$$

$$\varepsilon = \frac{A_s}{A_{f2}} \tag{5.30}$$

$$\varepsilon = 1 - \frac{\dot{m}(1-\chi)}{(\rho_{2p} W_{m2p} A_{f2})} \tag{5.31}$$

With the absolute velocity and static enthalpy known, the total enthalpy can be found through equation (5.32). With the pre-made assumption about isentropic streamlines in the primary zone, the complete state can be found at outlet of the primary zone. For the incompressible case the total pressure may be calculated directly by equation (5.33).

$$h_{02p} = h_{2p} + \frac{C_{2p}^2}{2} \tag{5.32}$$

$$p_{02p} = p_{2p} + \rho_{2p} \frac{C_{2p}^2}{2} \tag{5.33}$$

In order to close this system without the assumption that the primary zone occupies all of the impeller a description of the secondary zone and mixing process is needed.

5.2.3 Secondary Zone

The secondary zone contains losses, and is therefore not isentropic. The thermodynamic state can not be defined by the known entropy (at inlet) as in the primary zone. Because of this, some iteration may be necessary to achieve a converged solution. In theses cases, when a state property is needed, the initial guess will be the same value as for the primary zone. Subsequent values for these parameters are taken from the previous iteration, until convergence.

An assumption made, is that the tip is unloaded, i.e. the static pressures in primary and secondary zones are equal, seen in equation (5.34).

$$p_{2p} = p_{2s} = p_2 \tag{5.34}$$

The meridional velocity of the fluid in the secondary zone can be determined by the use of the continuity equation and the secondary zone flow area fraction, ε, shown below in equation (5.35).

$$\rho_{2s} C_{m2s} \varepsilon + \rho_{2p} C_{m2p} (1 - \varepsilon) = \frac{\dot{m}}{A_{f2}} \tag{5.35}$$

The average flow angle describing the secondary zone is given in a similar manner as for the primary zone and can be seen in equation (5.36).

$$\beta_{2s} = \beta_{2b} + \delta_{2s} \tag{5.36}$$

With the calculated meridional velocity, the velocity triangle can be determined from the secondary zone flow angle. The relative velocity in the tangential direction is found from the trigonometric relationship, seen in equation (5.37), and the relative velocity of the secondary zone is acquired from the Pythagorean theorem, in equation (5.38). The absolute velocities are described in equations (5.39) and (5.40), in a similar manner as for the primary zone.

$$W_{\theta 2s} = W_{m2s} \tan \beta_{2s} \tag{5.37}$$

$$W_{2s} = \sqrt{W_{m2s}^2 + W_{\theta 2s}^2} \tag{5.38}$$

$$C_{\theta 2s} = U_2 + W_{\theta 2s} \tag{5.39}$$

$$C_{2s} = \sqrt{C_{m2s}^2 + C_{\theta 2s}^2} \tag{5.40}$$

The energy equation, seen in equation (5.41), relates the inlet state of the impeller to the outlet by utilising Euler turbo machinery equation from inlet tip to outlet of secondary zone and ascribing losses from front cover to the secondary zone.

$$h_{02s} = h_{00} + U_2 C_{\theta 2s} - U_{1t} C_{\theta 1t} + w_{\text{front cover}} \tag{5.41}$$

The front cover friction for shrouded impellers, seen in equation (5.41), is hard to estimate [2]. Even though the number of studies is limited, it has been shown that a good approximation is to equate it with the rear disk friction, described by Daily and Nece [12]. The rear disk friction is described in section 5.2.5.

With the definition of total enthalpy, the static enthaply for the secondary zone may be calculated, as shown in equation (5.42).

$$h_{2s} = h_{02s} - \frac{C_{2s}^2}{2} \tag{5.42}$$

The static thermodynamic state is now fully defined for the secondary zone, both static enthalpy and pressure is know. This allows for a computation of the density and iteration until density convergence is necessary as previously mentioned.

When the primary and secondary zones are fully defined, the mixing process tying them together must be described.

5.2.4 Mixing

As previously stated, the isentropic core flow or the secondary flow is not sufficient to single handedly described the mixed out state. The mixed state can be obtained either by mass averaging of the two states obtained by primary and secondary flow calculations or by performing mixing calculations, stated by Japikse [2].

These methods are not the same, because the mixing calculations includes entropy generation. The mixing method allows to evaluate the losses associated to the mixing and attribute these to the impeller, which is the cause of primary and secondary flow zones.

It should be noted, again, that mixing is not an instantaneous process and the mixing process may extend into the diffuser. Japikse [2] mentions that the flow field is substantially mixed out at a radius approximately 30 % greater of the impeller tip radius. Therefore, the mixing equations must be thought of giving an effective mixed-out station,

needed to proceed with the calculations.

The direct result of this mixing process is a loss in total pressure and an increase in static pressure. The loss in total pressure can be found if the mixed out state is compared to the state of mass averaged properties from the primary and secondary zone.

Mixing Equations

The exit process may be calculated correctly by setting up a control volume. This was done by Johnston and Dean, later by Dean, Wright and Runstadler, and later corrected by Japikse [2].

The following mixed-out state equations are obtained. Momentum, continuity and energy equations.

$$\int_0^t \left\{ \oiint_{c.v.} \rho(t)\vec{C}(t)\left[\vec{C}(t)\cdot d\vec{A}\right] \right\} dt = \int_0^t \sum \vec{F}(t)dt \tag{5.43}$$

$$\int_0^t \left\{ \oiint_{c.v.} \rho(t)\vec{C}(t)d\vec{A} \right\} dt = m \tag{5.44}$$

$$\int_0^t \left\{ \oiint_{c.v.} \Delta h_0(t)\left[\rho(t)\vec{C}(t)\cdot d\vec{A}\right] \right\} dt = \sum_i E_i \tag{5.45}$$

where,

$$\vec{C}(t) = C_m(t)\vec{e_m} + C_\theta(t)\vec{e_\theta}$$

and

$$d\vec{A} = dz r d\theta \vec{e_m}$$

Taking the scalar product of the velocity and the infinitesimal area, results in the following expression:

$$\vec{C}(t)\cdot d\vec{A} = \pm C_m(t) r d\theta dz$$

When integrating over time, the meridional velocity is partially described by the secondary zone and partially by the primary zone. This is due to the temporal dependency of

the rotating impeller passage. The computation of the mixing process is essential. It provides closure to the system of equation and allows important parameters, describing the flow field, to be calculated.

From the integrals equations of momentum, in both meridional and tangential direction, continuity and energy are derived. The final thermodynamic state is unknown and some iteration may be needed, as for the secondary zone. An initial guess for the density is the mass averaged density of the primary and secondary zone, described by equation (5.46).

By manipulating the radial momentum, shown in equation (5.47), the static pressure after mixing may be obtained, seen in equation (5.48).

$$\rho_{2m} = \rho_{2p}(1 - \chi) + \rho_{2s}\chi \tag{5.46}$$

$$\dot{m}_p C_{m2p} + \dot{m}_s C_{m2s} = \dot{m} C_{m2m} + (p_{2m} - p_2) 2\pi r_2 b_2 \tag{5.47}$$

$$p_{2m} = p_2 + \frac{\dot{m}_p C_{m2p} + \dot{m}_s C_{m2s} - \dot{m} C_{m2m}}{A_2 m} \tag{5.48}$$

However, in order to calculate this pressure, the meridional velocity is needed. This can be calculated by the continuity equation applied to the mixing zone, seen in equation (5.49).

$$\dot{m} = 2\pi r_2 b_2 C_{m2m} \rho_{2m} \tag{5.49}$$

By conserving angular momentum, the tangential velocity after mixing can be found from equation (5.50). The complete velocity triangle can now be decided with the the Pythagorean theroem, shown again in equation (5.51).

$$\dot{m}_p C_{\theta 2p} + \dot{m}_s C_{\theta 2s} = \dot{m} C_{\theta 2m} \tag{5.50}$$

$$C_{2m} = \sqrt{C_{m2m}^2 + C_{\theta 2m}^2} \tag{5.51}$$

By utilising the energy equation and attributing losses connected to the impeller at this stage, the total enthalpy of the mixed state can be found, through equation (5.52). Through total enthalpy and velocity, the static enthalpy may be calculated with equation (5.53). This provides information about the thermodynamic state since both static pressure and static enthalpy is known. Density for this state may now be calculated and the procedure can be repeated until convergence is achieved.

$$\dot{m}_p h_{02p} + \dot{m}_s h_{02s} + \dot{W}_{\text{disk friction}} + \dot{W}_{\text{re-circulation}} = \dot{m} h_{02m} \tag{5.52}$$

$$h_{02m} = h_{2m} + \frac{C_{2m}^2}{2} \tag{5.53}$$

Once convergence is achieved, the impeller flow may be evaluated by some dependent variables shown below. A slip factor, found from velocity triangles and dependent on the chosen deviation angles, is seen in equation (5.54). This may be related to a chosen slip factor to evaluate whether the deviation chosen is correct.

Another useful variable is the swirl parameter, described in equation (5.55). It is a measure of the swirl leaving the the impeller. This parameter may be used by the designer to quickly evaluate the impeller performance.

A third parameter obtainable at this stage is the work input coefficient, seen in equation (5.56).

$$\sigma_{2m} = \frac{C_{\theta 2m}}{C_{\theta 2m} + C_{\text{slip}2m}} \tag{5.54}$$

$$\lambda_{2m} = \frac{C_{\theta 2m}}{C_{m2m}} \tag{5.55}$$

$$\mu_{2m} = \frac{C_{\theta 2m}}{U_2} - \frac{C_{\theta 1} U_1}{U_2^2} \tag{5.56}$$

A flow chart for the calculations for the two-zone-model is presented in figure 5.4.

5.2.5 Additional Losses

The losses within the impeller passage are ascribed to the secondary zone and mixing process. These losses stem from boundary layer growth, leakage, viscous forces etc.

Disk Friction

Disk friction on the rear of the impeller is complicated to describe, due to the incredibly complicated flow field arising between the rotating impeller and the stationary wall. The model used for this is by Daily and Nece [12] and is thought to be a reasonable assumption. The friction is described in equation (5.57), with friction coefficient and Reynolds number given in equations (5.58) and (5.59), respectively.

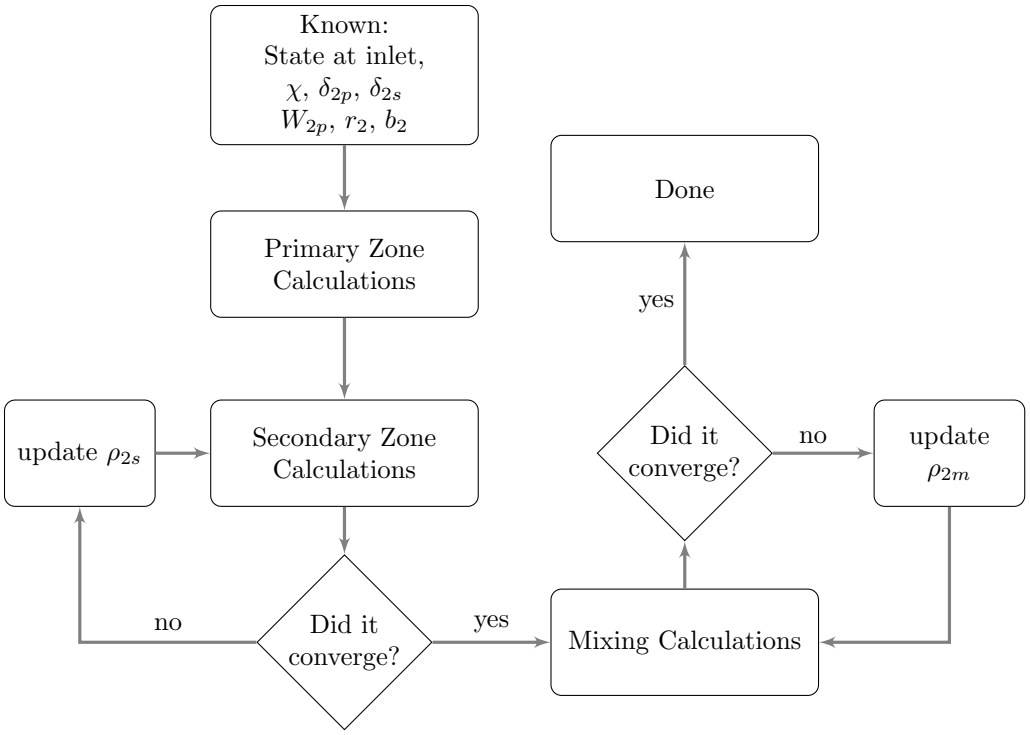

Figure 5.4: Flow chart describing the procedure for one Two-Zone calculation.

$$w_{\text{rear disk}} = \frac{C_{df}\rho_{2m}(U_2/r_2)^3 r_2^5}{\dot{m}} \tag{5.57}$$

$$C_f = \frac{0.0402}{Re_{2m}^{0.2}} \tag{5.58}$$

$$Re_{2m} = \frac{U_2 r_2 \rho_{2m}}{\mu_{2m}} \tag{5.59}$$

Seal Leakage

Leakage is caused by a pressure gradient over the seals. The theory behind leakage loss, is that the mass flow going through the seal already has some work attributed to it. The pressure is lost, but temperature increased, i.e. more energy is needed to obtain a specified pressure rise for a given mass of fluid. The leakage through an arbitrary seal is discussed below. A simple model is used to create an estimate of the leakage through the front seal, as presented by Japikse [2].

Firstly, a relationship between pressure and velocity at impeller tip and seal location is written in terms of total relative pressures, see equation (5.60), i.e. the fluid is approximated as incompressible.

$$p_T = p_2 + \left(\frac{W_2^2}{2} - \frac{U_2^2}{2}\right)\bar{\rho} = p_1' + \left(\frac{W_1'^2}{2} - \frac{U_1'^2}{2}\right)\bar{\rho} \tag{5.60}$$

The relative velocities, at both stations, are difficult to describe and accurately model. A simple approach is made by approximating the relative velocity to a fraction of the local wheel speed, see equation (5.61). This fraction is, for the sake of simplicity, set to be the same for both stations.

$$W_i = FU_i \tag{5.61}$$

Combining equations (5.60) and (5.61) yields the expression seen in equation (5.62).

$$p_T = p_2 + \left(\frac{(FU_2)^2}{2} - \frac{U_2^2}{2}\right)\bar{\rho} = p_1' + \left(\frac{(FU_1)'^2}{2} - \frac{U_1'^2}{2}\right)\bar{\rho} \tag{5.62}$$

Recasting equation (5.62) to solve for the pressure just before the seal finally gives us the expression seen in equation (5.63).

$$p_1' = p_2 + \frac{\bar{\rho}}{2}\left[U_2^2(F^2-1) - U_1'^2(F^2-1)\right] \tag{5.63}$$

The static pressure difference across the field, i.e. the pressure gradient driving the leakage flow, can now be solved for and related to a pressure loss in a similar manner as described earlier, as a fraction of the dynamic head/pressure through the seal. The following relationship may be found, seen in equation (5.64), using equation (5.63) and the general expression of pressure loss, mentioned before.

$$\frac{p_1' - p_1}{\rho} = \frac{p_2 - p_1}{\rho} + \frac{1}{2}\left[U_2^2(F^2-1) - U_1'^2(F^2-1)\right] = \frac{\Delta p}{\rho} = \frac{LC_{\text{seal}}C_{\text{seal}}^2}{2} \tag{5.64}$$

Where the loss term can be written on its own, as seen below in equation (5.65).

$$LC_{\text{seal}}C_{\text{seal}}^2 = \left[\frac{2(p_2 - p_1)}{\rho} + (U_2^2 - U_1'^2)(F^2-1)\right] \tag{5.65}$$

The value of the fraction F, relating wheel speed to relative velocity, is important as it

describes how the fluid behaves inside the cavity. A general understanding regarding the implications of F is critical to a pump designer using these simplifications. As seen in equation (5.66) F is in the range of zero to negative one. If F is set to zero the relative velocity will equate to zero as well, indicating that the absolute velocity is equal to the blade velocity, thus resulting in a solid body rotation. If F is negative one, the relative velocity is equal to the blade speed, but in opposite direction. The absolute velocity is then zero, analogous to a simple stagnation cavity flow, according to Japikse [2].

$$\begin{aligned} F &= -1 \quad \text{Cavity} \\ F &= -0.5 \quad \text{Couette} \\ F &= 0 \quad \text{solid body rotation} \end{aligned} \tag{5.66}$$

For pumps the value of F may vary between 0.3 and 0.9 (sign not important and is dropped). Through pressure-measurements inside the cavity a reasonable value of F may be deduced. A suggested, initial, value for preliminary design is somewhere around 0.75-0.85 [2].

The mass flow through the seal is obtained by applying the continuity equation to the seal, see equation (5.67).

$$\dot{m}_{\text{seal}} = \rho C_{\text{seal}} A_{\text{seal}} \tag{5.67}$$

The area of the seal is described by the annulus area, see equation (5.68).

$$A_{\text{seal}} = 2\pi r_{\text{seal}} t_{\text{clr,seal}} \tag{5.68}$$

The mass flow through seals, i.e. the leakage, may be in both direction, i.e. there may be either inwards-leakage or outwards-leakage. The generally accepted sign convention, adopted by Japikse [2], is positive mass flow when fluid is flowing away from impeller tip, i.e. outwards leakage, and negative mass flow when there is inwards-leakage.

The direction of leakage may be of great importance depending on the fluid requirements. Outwards leakage means that no external fluid is allowed to penetrate the seals to contaminate the working fluid, if the seal is separating two different fluids.

This general, simplistic approach does not account for additional effect that leakage may cause. If there is a big mass flow through the front seal, the leakage will have an effect on the velocity field of the incoming fluid, hence affecting the inlet performance. Japikse [2] advises that the impeller diffusion should be reduced if significant leakage is obtained.

The general approach for seal leakage above, which has been visualised for the front seal, may also be applied to the rear seal. The pressure behind the seal, which may be different from the front should be adjusted if that is the case. However, this is rare.

5.3 Design Procedure

The flow leaving the impeller may now be mathematically described for a given impeller and set deviation. In the design process, the designer will specify a pressure ratio and a value for the swirl parameter λ_{2m}, which the design process will search for. The search contains three nested loops, i.e. loops within loops. This design procedure is essentially an off-design analysis, where the program will try different geometries and with help from numerical algorithms change the design to get closer and closer to the desired performance. The procedure and the logic is visualised in figure 5.5.

The deviation is changed to match the estimated slip from a chosen slip model. When correct slip is acquired, the particular geometry is evaluated in terms of pressure ratio. The impeller tip radius is varied, and therefore the deviation analysis is repeated, until correct pressure ratio is found.

Once the pressure ratio is found, the width of the impeller tip is varied to match the desired swirl parameter. This changes in geometry entails that both a new radius is needed to find the correct pressure ratio (for this new width), and for each radius tried the deviation is matched to the slip for the current geometry.

Once the geometry yielding the desired performance is found the design process is done.

5.3.1 Design Criteria

The design criteria, briefly mentioned above, is chosen by the pump designer. The performance of the pump is specified (some information is already specified at inlet) and the particular parameters for impeller design is pressure ratio and swirl parameter.

5.3.2 Optimisation

The numerical method used for finding correct values of e.g. deviation is the Newton-Raphson method. The local derivative is used to estimate where the correct value should be. This method is described in deeper detail in appendix C.1.

The iteration for correct deviation runs the most, since it is deepest among the nested loops. A quicker convergence of this loop would entail a massive improvement of the

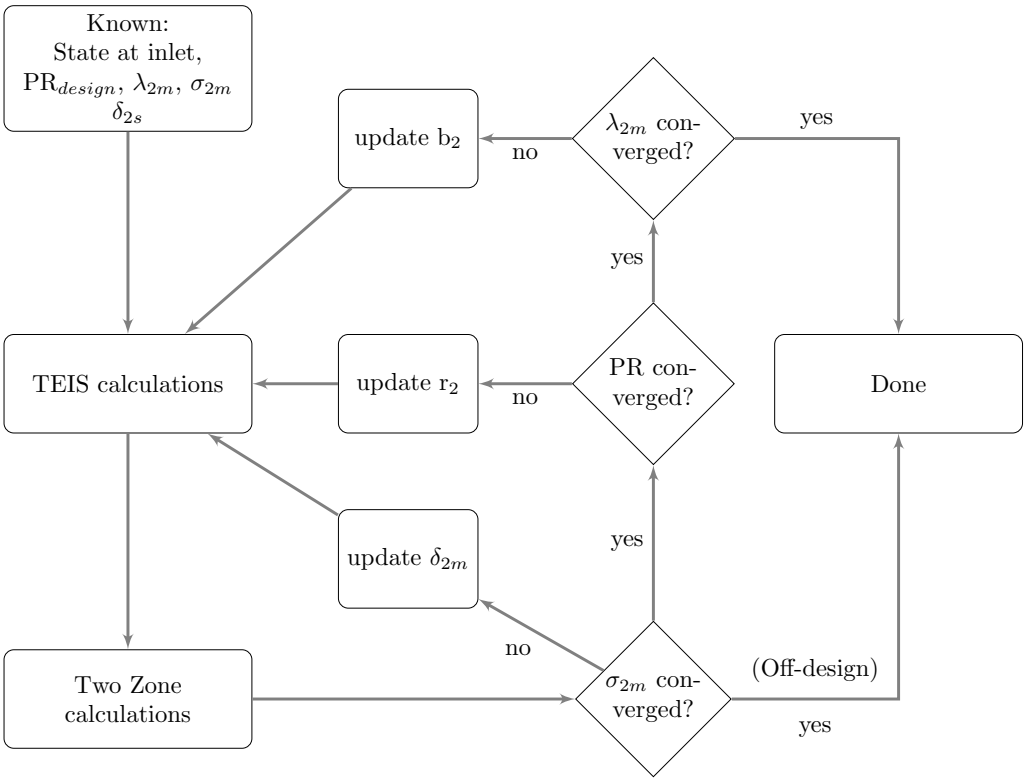

Figure 5.5: The impeller design procedure, containing both the TEIS and Two-Zone models.

overall computational time.

Relaxation, to ensure stable operation, may be tweaked to improve the computational time. The same can be said for tolerances, although the latter may lower the accuracy of the solution.

Analysis

As previously mentioned, the equations used in the design process describe the performance of a specific geometry. This means that the analysis for a given impeller, e.g. for a varied mass flow, utilises a similar procedure. To obtain an accurate value of the mixed-out state, the deviation is altered to match the slip with a chosen slip model. Afterwards, the performance can be analysed.

5.4 Additional Considerations

In this section additional information about the designed impeller is presented. These provide the designer with a means to compare the data to other analyses conducted. Some of the aspects mentioned is approximate due to the design only being preliminary. For instance, blade loading depends on the 3-D shape of the blade and axial force may be handled with various techniques, although this is out of the scope for a preliminary design.

5.4.1 Unified Loss-Correlation

Once the impeller is designed and the outlet state is calculated loss coefficients and efficiencies can be determined. This can be useful when comparing the performance to analyses done in other software.

The total-to-total efficiency, described in equation (2.31), may be applied to the mixed out state. This is shown in equation (5.69) for clarity.

$$\eta_{0-2} = \frac{h_{02m,s} - h_{00}}{h_{02m} - h_{00}} \tag{5.69}$$

A loss coefficient stemming from the two zone model is shown in equation (5.70).

$$LC_{\text{impeller}} = \frac{W_{2p}^2}{W_{1t}^2}\left(1 - \frac{W_{2s}^2}{W_{2p}^2}\right)\chi \tag{5.70}$$

5.4.2 Blade Loading

When the system of equation is solved for the primary, secondary, and mixing zones the internal flow physics of the impeller can be estimated. The blade loading of the impeller can be visualised in a plot, see figure 5.6.

Aungier [13] describes the flow from impeller inlet tip to outlet by following equations. The max velocity reached is described in equation (5.71), from the relative velocities at inlet tip and outlet primary zone, respectively. $\mu_{2\text{m}}$ is the work-input factor, which can be calculated according to equation (5.56).

$$W_{\max} = \frac{W_{1t} + W_{2p} + \Delta W}{2} \tag{5.71}$$

$$DR_{\text{eq}} = \frac{W_{\max}}{W_{2p}} \tag{5.72}$$

$$\begin{aligned} \int_0^{L_b} (W_{\text{suction}} - W_{\text{pressure}}) d\xi &= 2\pi \frac{r_2 C_{\theta 2p} - r_{1t} C_{\theta 1t}}{Z} \\ W_{\text{suction}} - W_{\text{pressure}} &= \Delta W \left[1 - \left| \frac{2\xi}{L_b} - 1 \right| \right] \\ \Delta W &= \frac{2\pi d_2 U_2 \mu_{2m}}{Z L_b} \end{aligned} \tag{5.73}$$

By assuming incompressibility, which allows the use of rotational pressure, the static pressure can be found as a function of the relative velocity found above. This results in the blade loading figure being described by pressures. If the temperature is assumed to be constant, which is a fairly good assumption, the vapour pressure can be shown. This can be seen in figure 5.6. The aim of this figure is to give the designer an idea of the performance and flow physics in the impeller passage.

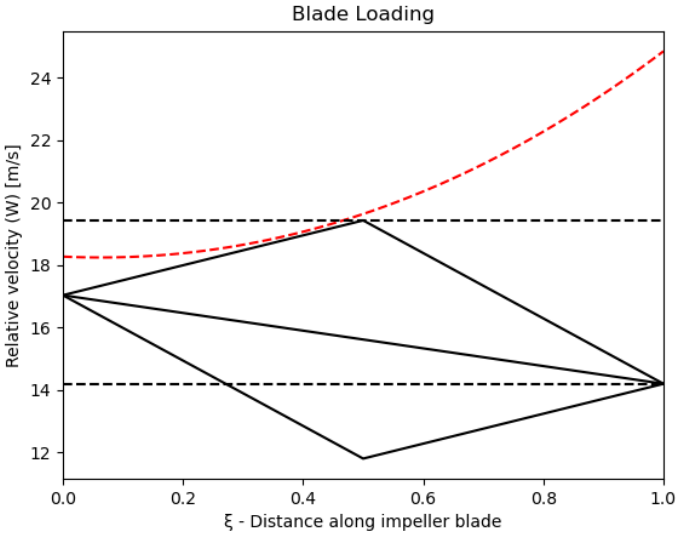

Figure 5.6: Preliminary blade loading. The red line is the relative velocity where cavitation would occur. The increase in this velocity is due to the increase in pressure due to work supplied by the impeller.

It should be re-iterated that the velocity/pressure distribution shown in the plots above are highly approximate, but give the designer a preliminary view of the blade loading. For a more thorough description of the internal flow it is recommended to use a through flow solver and finally 3-D CFD solver to obtain an accurate flow field and blade loading.

5.4.3 Axial Force

Axial thrust may be of great importance when designing pumps. There are several ingenious ideas where axial forces are lowered by redirecting pressures or creating specific configurations of several impellers. However, a preliminary estimate of the axial thrust produced can be computed.

The axial thrust can be calculated by considering the impeller as a control volume and analysing the momentum equation in axial direction. The shaft force is found by knowing that the impeller is axially stationary. Figure 5.7 shows the control volume over the impeller. Pressure forces are acting at inlet, outlet and in both front and rear cavity. The pressures at inlet and outlet are determined in other steps of the design calculations, and will be treated as known quantities here. The static pressure in the cavities will be described in a similar manner as for seal leakage. Since the wheel speed varies with radius, the static pressure in the cavity will be a function of radius.

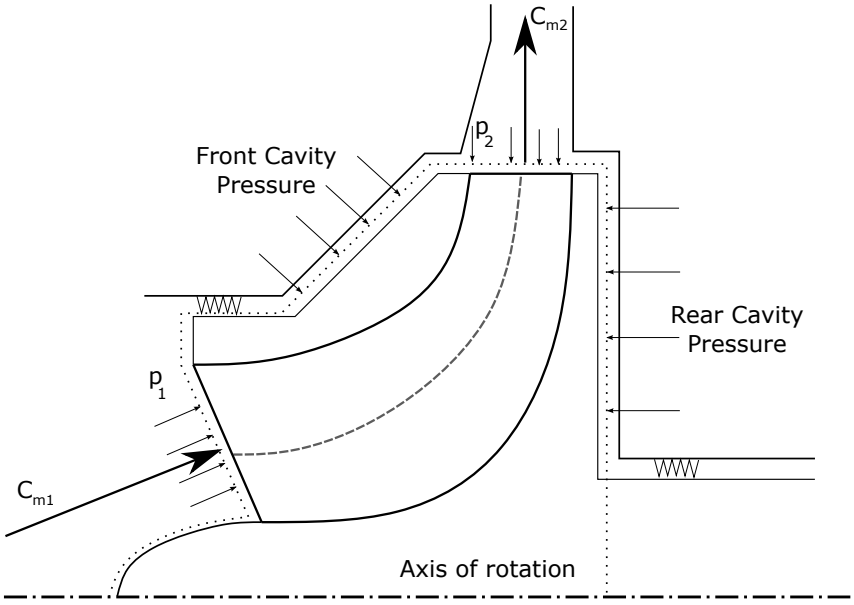

Figure 5.7: Control volume showing pressure forces acting on the impeller

$$p(r) = p_1' + (1 - F^2)\left(\frac{\rho}{2}\right)[U^2(r) - U_1'^2] \tag{5.74}$$

or rewritten as

$$\begin{aligned} p(r) &= \left(\frac{\rho}{2}\right)(1 - F^2)U^2(r) + \left[p_1' - \left(\frac{\rho}{2}\right)(1 - F^2)U_1'^2\right] \\ &= Ar^2 + B \end{aligned} \tag{5.75}$$

Where A and B are constants, described for each cavity in equation (5.77). The momentum equation in axial direction also needs the change in velocity occurring within the control volume, i.e. the acceleration, applied in the axial direction. Combining the pressure forces and change in velocity equation (5.76) is acquired.

$$\begin{aligned} F_z = \dot{m}C_{m1}\sin\phi_1 - \dot{m}C_{m2}\sin\phi_2 + p_0\pi r_{1h}^2 + \frac{p_{1h}+p_{1t}}{2}\pi(r_{1t}^2 - r_{1h}^2) \\ +\frac{\pi}{2}A_F(r_{2t}^4 - r_{1t}^4) + \pi B_F(r_{2t}^2 - r_{1t}^2) - \frac{\pi}{2}A_R(r_{2h}^4 - r_{8h}^4) \\ -\pi B_R(r_{2h}^2 - r_{8h}^2) - p_2\pi(r_{2t}^2 - r_{2h}^2) \end{aligned} \tag{5.76}$$

$$\begin{aligned} A_F &= \frac{\rho}{2}(1 - F_F^2)(2\pi\omega)^2 \\ A_R &= \frac{\rho}{2}(1 - F_R^2)(2\pi\omega)^2 \\ B_F &= p_1' - \frac{\rho}{2}(1 - F_F^2)U_1'^2 \\ B_R &= p_8' - \frac{\rho}{2}(1 - F_R^2)U_8'^2 \end{aligned} \tag{5.77}$$

Chapter 6

Vaneless Diffuser

6.1 Basic Principle

The kinetic energy leaving the impeller is roughly 20% to 40% of the total work input according to Japikse [2] and Braembussche [14] mentions that it can be as high as 50 %. This kinetic energy must be recovered in an efficient way if an efficient stage is desired.

6.1.1 Purpose of Vaneless Diffuser

Diffusers convert kinetic energy of the fluid into a rise of static pressure. There are two main principles that govern the diffusion of the flow, continuity and conservation of momentum. Diffusers are able to utilise both of these principles.

- Increasing the flow area, thus reducing the average velocity and increasing static pressure, e.g. see Bernoulli equation (2.28).
- Changing the mean flow path and giving an recovery in angular velocity according to conservation of angular momentum, $rC_\theta \cong$ constant.

The designer has several choices to utilise these methods to obtain a pressure recovery, which will be described in this chapter and chapter 7. This chapter will focus on vaneless diffusers, their usage, mathematical description and role in the pump. The range of stable operation and the effect design choices has on the range will also be described.

The vaneless diffuser is employed in various industries, as it is a cheap way to reach a reasonable pressure recovery. The absence of a geometric throat leads to a wider operation range. However, stall in a vaneless diffuser may still occur and will be discussed later in this chapter.

When designing a diffuser, it is important to note what exit state is desired. As Braembussche [14] expresses, there is no reason to reduce the velocity below what is needed in the pipe transporting the fluid or the sought velocity field to the next stage.

Japikse [2] mentions that the field of diffuser design in pumps is comparatively weak in comparison to centrifugal compressors. Technology, theory and advancements in the field of compressors will therefore be applied to pumps, which has been done by rocket turbopump designers for decades.

A simple vaneless diffuser is described by two parallel walls forming an open annular passage from the impeller tip to some limiting outer radius [2]. The lack of vanes also means that the vaneless diffuser will not cause any vane driven oscillation.

It should be noted that the flow coming into the vaneless diffuser is highly non-uniform as stated by Braembussche [14]. This is because of the boundary layers developing along walls and the secondary flow and flow separation in the impeller. The axial non-uniformity of the relative flow is responsible for the skewness of the absolute flow at diffuser inlet. This non-uniformity is enhanced by radial pressure gradient in the diffuser that can cause return flow and stall in the diffuser. This phenomenon will be discussed further in section 6.4.

6.1.2 Evaluation of Performance

Braembussche [14] states that diffuser performance is usually not stated in an efficiency, but rather a pressure coefficient and a loss coefficient, described in section 2.4.2 and re-iterated below in equations (6.1) and (6.2) for clarity.

$$C_{p,a-b} = \frac{p_b - p_a}{p_{0a} - p_a} \tag{6.1}$$

$$LC_{a-b} = \frac{p_{0a} - p_{0b}}{p_{0a} - p_a} \tag{6.2}$$

Some designers, when designing pumps with highly backswept blades, might completely omit the diffuser and use the volute as a diffuser to save cost and space. This approach comes at the expense of efficiency and pressure recovery.

6.2 Governing Equations

To efficiently describe the diffuser, a number of simplifications are made. These are in accordance with the literature and are deemed sufficient by the authors for a preliminary design. The following equations describe a vaneless diffuser:

$$rC_\theta \cong \text{constant} \tag{6.3}$$

$$\rho C_m 2\pi r b = \dot{m} \tag{6.4}$$

$$\lambda = \tan\alpha = \frac{C_\theta}{C_m} \cong \frac{\text{constant}/r}{\dot{m}/(\rho 2\pi r b)} = \text{constant} \times \frac{\rho b}{\dot{m}} \tag{6.5}$$

Equation (6.3) and (6.4) shows the conservation of angular momentum and mass, respectively. Equation (6.5) shows that the flow angle in the vaneless diffuser depends on the density, passage width and mass flow rate. If a constant width vaneless diffuser is considered, and the assumption of incompressibility is made, the flow angle is constant for a given mass flow rate. The flow path will then form a logarithmic spiral through the diffuser. This logarithmic path will be longer than a flow path in a vaned diffuser, and may therefore give greater losses [2], due to frictional losses to the walls. To form a better understanding of the flow in a general vaneless diffuser, the conservation equations governing the flow will be integrated through the diffuser. The vaneless diffuser is governed by the following partial differential equations.

The following form of conservation equation is finally reached, from Stanitz [15].

$$\frac{1}{\rho}\frac{\partial \rho}{\partial r} + \frac{1}{C_m}\frac{\partial C_m}{\partial r} + \frac{1}{b}\frac{\partial b}{\partial r} + \frac{1}{r} = 0 \tag{6.6}$$

$$C_m \frac{\partial C_m}{\partial r} - \frac{C_\theta^2}{r} + C_f \frac{C^2 \cos\alpha}{b \sin\Phi} + \frac{1}{\rho}\frac{\partial p}{\partial r} = 0 \tag{6.7}$$

$$C_m \frac{\partial C_\theta}{\partial r} - \frac{C_\theta C_m}{r} + C_f \frac{C^2 \sin\alpha}{b \sin\Phi} = 0 \tag{6.8}$$

The levels of skin friction is approximated by using equation (6.9), where k is usually set to 0.010, according to [2].

$$C_f = k\left(\frac{1.8 \times 10^5}{Re}\right)^{0.2} \tag{6.9}$$

Where Reynolds number is based on the flow at the inlet of the diffuser, seen in equation (6.10).

$$Re = \frac{\rho_{2m} D_2 C_{\theta 2m}}{\mu} \tag{6.10}$$

6.2.1 Code Implementation

The above governing equation can be re-cast in a manner shown below, and be directly used to calculate the flow state in the vaneless diffuser by numerically integrating with the Runge-Kutta method. By using a fourth order Runge-Kutta, a good approximation of the next step can be obtained and the end state can be calculated with a reasonable accuracy with relatively large step-size. For a more in-depth description of the numerical integration by the Runge-Kutta method the interested reader can see appendix C.2.

$$\frac{\partial C_m}{\partial r} = -C_m\left(\frac{1}{\rho}\frac{\partial \rho}{\partial r} + \frac{1}{b}\frac{\partial b}{\partial r} + \frac{1}{r}\right) \tag{6.11}$$

$$\frac{\partial p}{\partial r} = \rho\left(\frac{C_\theta^2}{r} - C_m\frac{\partial C_m}{\partial r} - C_f\frac{C^2\cos\alpha}{b\sin\Phi}\right) \tag{6.12}$$

$$\frac{\partial C_\theta}{\partial r} = -\frac{1}{C_m}\left(\frac{C_\theta C_m}{r} + C_f\frac{C^2\sin\alpha}{b\sin\Phi}\right) \tag{6.13}$$

From the results, i.e. the last step of the Runge-Kutta, a loss coefficient can be calculated in a similar manner as losses are described in other sections, as a fraction of the dynamic pressure. The values of pressure and velocity at different radii through the diffuser can be seen in figure 6.1.

The difference of a reversible and ireversible flow path through the diffuser can also be visualised by plotting the path for each of them, see figure 6.2.

The effect of compressibility is expressed in the term $\partial\rho/\partial r$, and was initially neglected with the assumption of incompressibility. However, the compressible effect can have an immense effect on the fluid behaviour.

When testing the incompressible version geometry for a vaneless diffuser applied to a compressor normally working on R-134a was utilised. When air was supplied to the same geometry, at the same conditions, the diffuser acted as a nozzle, accelerating the flow.

The compressible effects of water and other liquids are smaller than for the aforementioned gasses. However, for some liquids it can be of significant proportion. The application of the pump may also be of importance, where in some applications the level of accuracy is higher and the assumption of incompressibility may not be suitable.

For a less compressible working fluid, the convergence is faster. An assumption of incompressibility is not necessary because it will not significantly increase the speed of calculation and the compressible case can be used as a default setting, at least when using

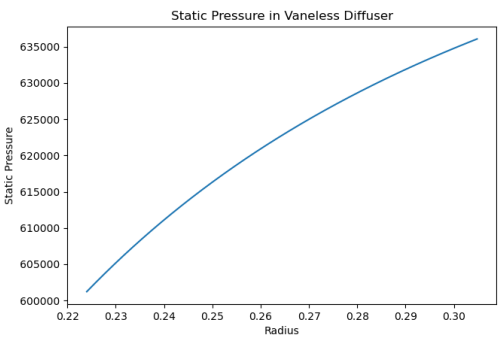

(a) Static pressure at different radii. Note the increase.

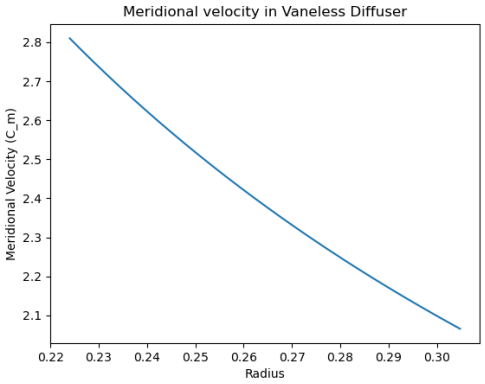

(b) Meridional velocity at different radii.

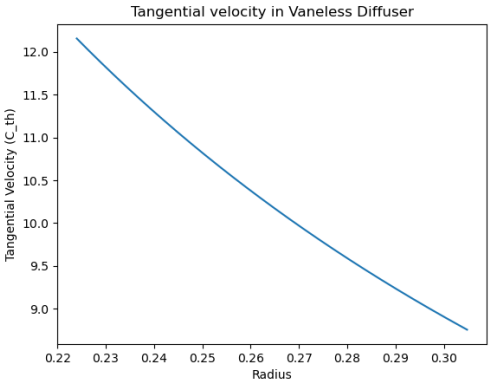

(c) Tangential velocity at different radii.

Figure 6.1: Pressure and velocity of fluid within the vaneless diffuser.

a pre-made matrix describing the thermodynamic properties (which is recommended for all fluids).

6.3 Design Options

This section will briefly mention some of the many options the designer may consider.

6.3.1 Pinch

Pinch is the notion used for the design option of varying the width of the diffuser to control the change of flow area. For an unpinched diffuser, the circumferential area is given by $2\pi rb$. For a diffuser utilising pinch, the circumferential area can be expressed as $2\pi rb(r)$, where the width is a function of the radius.

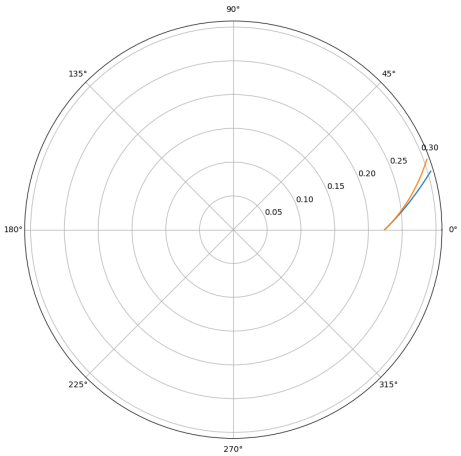

Figure 6.2: The effects friction has on the flow path within the diffuser. The orange curve is friction-less while the blue has friction. However, the friction has been exaggerated in order for clearer visualisation.

6.3.2 Matching the Flow

An additional effect of the diffuser is matching of flows between the impeller to some desired flow state downstream, either at a volute or a vaned diffuser. As mentioned previously, the flow leaving the impeller is highly-non uniform. By letting the flow go through a vaneless part, the flow is allowed to stabilise and a more stable flow field is obtained.

6.4 Off-Design Considerations

The governing equations are applicable for various types of inflow and can be used to determine the performance while within operating range. The lower limit of the operating range is estimated as the flow condition where the diffuser stalls.

6.4.1 Rotating Stall

At low flow rates the pump may experience stall in one or several of its components. This section aims to discuss rotating stall in the vaneless diffuser (VDRS).

Jansen [16] made the following main conclusions about rotating stall in a vaneless diffuser:

- Rotating stall is triggered by local return flow in the diffuser.
- It can exist with uniform inlet and outlet flows.
- The rotational speed, ω_σ, is between 5% and 22% of ω.

It is likely that these local return flows will first occur in the boundary layer. These return flows will create perturbations, which are damped by the core flow. This destabilising mechanism is confirmed by Fringe and Braembussche [17].

The theory Jansen [16] forged, combined with calculations of viscous flow combines into a practical stability limit. These calculations, of the boundary layer, was repeated by Senoo and Kinoshita [18] with the following modifications.

- The flow is no longer assumed to be symmetric with respect to the center of the diffuser.
- The inlet conditions account for distortions of radial and tangential velocity over the diffuser width.
- The boundary layer profiles are modified in such a way that merging of the two boundary layers does not necessarily lead to return flow.

The wall stream line angle, $\alpha_\infty + \gamma$ is seen to increase initially and then decrease when boundary layers have fully developed. Return flow occurs when the wall streamline angle exceeds 90 degrees, according to Senoo and Kinoshita [18]. Return flow will occur for a given inlet flow angle, when the free stream angle is high enough.

The geometric effect of the vaneless diffuser with parallel walls, i.e. various (b_2/r_2) and r_5/r_2 can be analysed. A segmentation may be made, distinguishing short diffusers from long diffusers. Short diffusers are considered to have a radius ratio of $r_5/r_2 = 1.2$, whilst long diffusers are defined as $r_5/r_2 \to \infty$, but more commonly $r_5/r_2 > 2$.

Different aspects, such as inlet Mach number, Reynolds number and velocity perturbations all have an impact on the critical inlet angle where VDRS will occur. The relative influence from each parameter is decided from the diffuser geometry, as seen in figure 6.3. If a vaneless diffuser without parallel walls is employed, i.e. pinching is used, a correction is needed to find the inlet angle where VDRS starts to occur. This is also true for diffusers employing different types of inlet shapes, due to e.g. stabilising/destabilising effects on the boundary layers.

Senoo and Kinoshita [18] has claimed that VDRS will occur when the flow angle entering the diffuser exceeds a critical value α_{crit}, described by equation (6.14), for an infinitely long diffuser i.e. radii ratio of more than 2.

$$\frac{90^\circ - \alpha_{\text{crit}}}{90^\circ - \alpha_r} = 0.88 \tag{6.14}$$

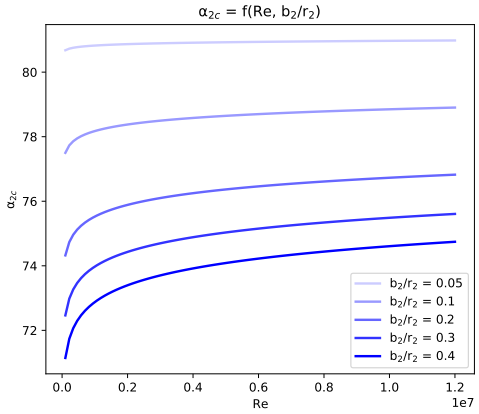

(a) Critical angle for different Re

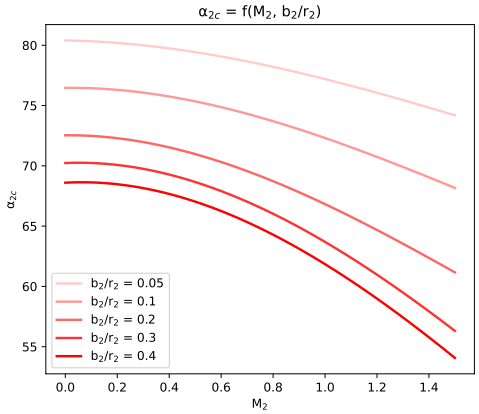

(b) Critical angle for different Mach-number

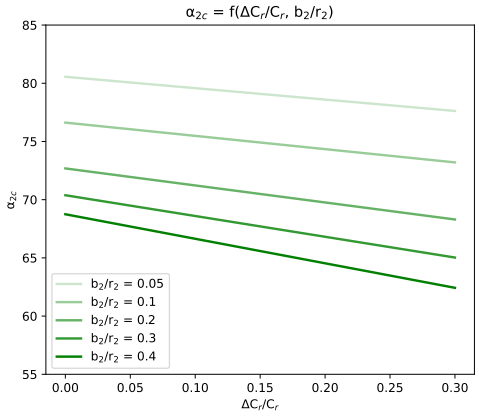

(c) Critical angle for different $\Delta C_r/C_r$

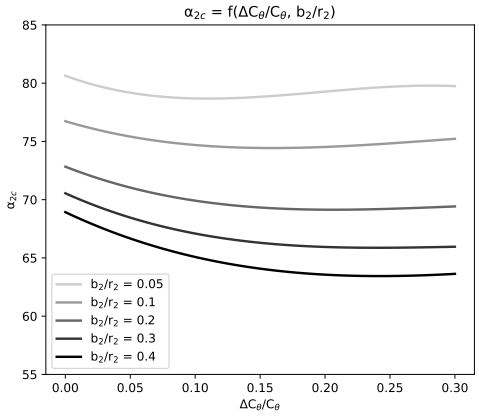

(d) Critical angle for different $\Delta C_\theta/C_\theta$

Figure 6.3: Effects on critical flow angle. Digitised plots from [2].

α_r is the inlet flow angle for which local return flow begins to occur.

Experiments conducted by Senoo and Kinoshita [18] has resulted in the expression shown in equation (6.14). In these experiments it was shown that the radius ratio is of great importance, as seen in figure 6.3. Braembussche [14] states that stabilising effect of a fully developed flow starts close to the inlet of a narrow diffuser and further down the passage for a wider one.

The multiple aspects that causes VDRS all need to be considered in a performance analysis, where geometrical aspects are of great importance, both radii ratio and width to inlet ratio. Flow perturbations and Reynolds number are also important. However, the flow perturbation may be difficult to estimate, and even measure.

Up until now, the stability has only been discussed for vaneless diffusers with parallel walls. However, as described above, the designer may choose to have a pinch, i.e. a

width reduction along an increasing radius. If a pinched diffuser is utilised the critical angle for stable operation has to be corrected to account for the pinching. Braembussche [14] proposes a correction angle according to equation (6.15) in which b_D denotes width at diffuser exit.

$$\alpha_{2,\text{crit,corr}} = 76 + (\alpha_{2,\text{crit}} - \Delta\alpha - 76)\frac{b_D}{b_2} \tag{6.15}$$

Other geometrical parameters that could have an effect on stability is the shape of the entry to the diffuser, e.g. round-off or a sharp edge. These aspects have not been considered for a preliminary design.

Chapter 7

Vaned Diffusers

Similar to vaneless diffusers, vaned diffusers are tasked with recovering the kinetic energy leaving the impeller. Vaned diffusers achieve this recovery in a shorter distance by turning the flow. There are primarily two kinds of vaned diffusers: channel and cascades. The channel type diffuser has, according to Japikse, the longest history out of all types of diffusers. However, the simple conical and simple wedge diffuser had not been applied to advanced pumps and compressors until more recent times. The range for this type of diffuser is, however, narrow, and is not as extensively used in pumps as other types of vaned diffuser. They are mentioned here to inform the reader that other types of diffusers exists, but they will not be covered.

This chapter deals with cascade diffusers of the NACA65 and circular arc type. Their geometric construction is described along with performance models, both at design and off-design mass-flows.

7.1 Basic Principle

From the continuity equation it is clear that an increase in flow area leads to a diffusion of the flow. The flow leaving the impeller has a large component of its velocity in the tangential direction and hence the flow area is equal to the annular area multiplied by the cosine of the flow angle. Thus, a turning of the flow in the radial direction leads to an increase in flow area and thus more rapid diffusion. This is the general idea behind vaned diffusers. Their purpose is to increase the diffusion compared to the vaneless diffuser by increasing the flow area more rapidly. This leads to shorter diffusers since the same pressure ratio can be achieved for a smaller radial increase. This is useful when the application calls for high pressure ratios or when the overall dimensions of the pump is a limiting factor. In many applications vaned diffusers often lead to increases in efficiency as well. This chapter deals with vaned diffusers and the two main designs commonly adopted; wedge diffusers and cascade diffusers.

Cascade diffusers, similar to axial turbomachinery, utilises airfoil profiles to turn the flow. There is vast amount of test data available for different categories of airfoil-proiles

but the ones most commonly adopted in cascade diffusers are the NACA65 airfoils. The design process of cascade diffusers include determining a desired flow path and then selecting a corresponding airfoil. Implementing cascade diffusers in a design tool requires knowledge about airfoil theory, geometric construction, and how to evaluate their performance.

7.2 Airfoils

Airfoil theory finds its origin in the early days of the airplane industry. Horatio F. Phillips was a British aviation enthusiast who experimented on airfoils in a wind tunnel and was able to patent the first airfoil shape in 1884. The Wright brothers followed soon after with their own experiments which resulted in their first flight in 1903. These first iterations of airfoils relied upon trial-and-error and were primitive in nature. In the 1930s NACA (now NASA) started a systematic design process which relied upon a numbering system to describe the geometry of the airfoils [3].

7.2.1 NACA 65

Figure 7.1a shows the basic geometry of a symmetric airfoil, namely the NACA65-0010. The mean camber line sits halfway between the upper and lower side of the foil and the chord is the minimum distance between the leading and trailing edge. For a symmetric airfoil the camberline and chord-line coincide. The flow approaches the airfoil in the figure from left to right and often at an angle to the chord-line. This angle is known as the angle of attack (AoA). Figure 7.1b shows the NACA65-1210 airfoil at 6° AoA. Another important angle in airfoil-theory is the incidence-angle, which is the angle between the flow and the camberline at the leading edge. The difference in direction between the flow and the camberline at the trailing edge is called deviation [3].

An airfoil turns the flow which generates a lift force through the moment of momentum equation. The difference in blade angles at the leading and trailing edge along with how well the flow follows the airfoil (i.e. the magnitude of the incidence an deviation) determines how much lift is generated. Airfoils performance in guiding the flow is why they are implemented in applications not requiring a lift-force to be generated. The numbers in the NACA65-serie represents the following:

- 1st: The name of the serie.
- 2nd: Location of minimum pressure along the chord.
- 3rd: Lift coefficient.
- 4th & 5th: Thickness of the foil.

(a) NACA65-0010 profile **(b)** NACA65-1210 profile

Figure 7.1: Two different models of the NACA65 airfoil.

Geometric Construction

To construct the geometry of a selected NACA65 airfoil one needs to modify the coordinates of a given airfoil. The coordinates of a profile with unity lift coefficient and a thickness distribution of 10% are usually given. The thickness (y_T) is given as a percentage of the chord, distributed along the camberline. In order to distribute the thickness, the slope of the camber line (dy_c/dx_c) must be known. This slope is predefined for the NACA65 with zero slope at 50% of the chord. The thickness distribution is given in equations (7.1) through (7.4).

$$x_u = x_c - y_T \sin\left(\frac{dy_c}{dx_c}\right) \tag{7.1}$$

$$x_L = x_c + y_T \sin\left(\frac{dy_c}{dx_c}\right) \tag{7.2}$$

$$y_u = y_c + y_T \cos\left(\frac{dy_c}{dx_c}\right) \tag{7.3}$$

$$y_L = y_c - y_T \cos\left(\frac{dy_c}{dx_c}\right) \tag{7.4}$$

The coordinates are rotated by the angle of attack (AoA) and in order for the leading and trailing edge to be placed on r_3 and r_5 respectively the length of the chord, given in equation (7.5), must be known. The parameter m is the inverse of the swirl parameter, λ.

$$c = \frac{m^2 + 1}{m\cos(AoA) + \sin(AoA)} \ln\left(\frac{r_5}{r_3}\right) \tag{7.5}$$

The coordinates are modified for the lift-coefficient and the chord according to equations (7.6) through (7.9). The parameter T_{foil} is used to alter the thickness and is determined by the chosen NACA65 airfoil.

$$x_c^{'} = cx_c \tag{7.6}$$

$$y_c^{'} = C_{L_0} c y_c \tag{7.7}$$

$$y_T^{'} = cT_{\text{foil}} y_T \tag{7.8}$$

$$\tan(\gamma^{'}) = C_{L_0} \tag{7.9}$$

Figure 7.2 shows the top-view of a vaned diffuser constructed using the method described above. The diffuser has 15 NACA65-0406 airfoils.

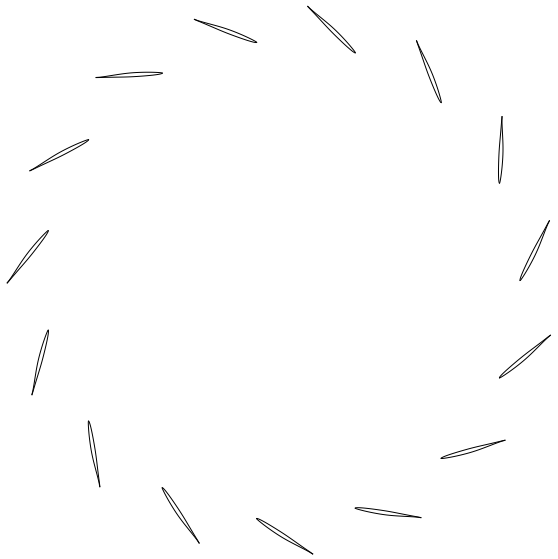

Figure 7.2: Top view of cascade diffuser with 15 NACA65-0406 airfoils.

7.2.2 Alternative Airfoils

An alternative approach to the NACA65 airfoils is to adopt the vane design suggested in Aungier [19]. Much like the NACA65 airfoils, Aungier constructs a mean camber line and places a thickness along the camber. The camberline is described by a natural logarithm in combination with a cubic polynomial and thus needs 4 boundary conditions.

Geometric construction

Defining η as $\eta = r/r_3$ the camberline is described by:

$$\theta(\eta) = A\ln(\eta) + B(\eta - 1) + C(\eta^2 - 1) + D(\eta^3 - 1) \tag{7.10}$$

Two of the boundary conditions are chosen so as to yield the blade angles at the leading and trailing edges. The angles along the camberline is given by equation (7.11) and (7.12).

$$\tan\alpha_b = \eta\frac{d\theta}{d\eta} \tag{7.11}$$

$$\frac{d\theta}{d\eta} = \frac{A}{\eta} + B + 2C\eta + 3D\eta^2 \tag{7.12}$$

The two remaining equations necessary to close the system of equations are provided by the blade loading. Aungier introduces a parameter K to control the distribution of the blade loading, see equation (7.13). Whether α_b is set to either α_{3b} or α_{4b} determines if K is K_3 or K_4.

$$K = \frac{\frac{r_4}{r_3} - 1}{\tan\alpha_{4b} - \tan\alpha_{3b}}\frac{d(\tan\alpha_b)}{d\eta} \tag{7.13}$$

The constants in equation (7.10) are now fully defined, see equation (7.14)

$$
\begin{aligned}
D &= \frac{(\tan\alpha_{4b} - \tan\alpha_{b3})(K_3 + K_4 - 2)}{3(\frac{r_4}{r_3} - 1)^3} \\
C &= \frac{(\tan\alpha_{4b} - \tan\alpha_{b3})(K_4 - K_3)}{4(\frac{r_4}{r_3} - 1)^2} - \frac{9D(\frac{r_4}{r_3} + 1)}{4} \\
B &= \frac{K_3(\tan\alpha_{4b} - \tan\alpha_{b3})}{\frac{r_4}{r_3} - 1} - 4C - 9D \\
A &= \tan\beta_3 - B - 2C - 3D
\end{aligned}
\tag{7.14}
$$

With the camberline fully defined, a thickness distribution is all that remains for the geometric description. Aungier proposes two options: constant thickness with linear reduction towards leading and trailing edge or a thickness distribution resembling the NACA66006 airfoil. The thickness distribution for the latter is given by the equations in (7.15).

$$
\begin{aligned}
t_0 &= \frac{t_{b3} + (t_{b4} - t_{b3}\frac{x}{c})}{t_{b,\max}} \\
\frac{t_b}{t_{b,\max}} &= t_0 + (1 - t_0)\left(2\frac{x}{c}\right)^n \qquad \text{for } \left(\frac{x}{c}\right) \leq 0.5 \\
\frac{t_b}{t_{b,\max}} &= t_0 + (1 - t_0)\left(2 - 2\frac{x}{c}\right)^n \quad \text{for } \left(\frac{x}{c}\right) > 0.5 \\
n &= 0.755\left(0.57 - \frac{x}{c}\right) \qquad \text{for } \left(\frac{x}{c}\right) \leq 0.539 \\
n &= 1.225\left(\frac{x}{c} - 0.52\right) \qquad \text{for } \left(\frac{x}{c}\right) > 0.539
\end{aligned}
\tag{7.15}
$$

7.2.3 Transformation to Match the Flow

It should be noted that airfoil theory and cascade testing has mostly been done on axial flow. To account for this in the swirling flow inside the diffuser, the airfoil needs to be distorted somewhat. The flow needs to experience the vaned diffuser in a similar manner as it would an axial airfoil during purely axial flow. The airfoil relative to the flow should have the same aerodynamic properties regardless of flow structure. This distortion is done by transforming the airfoil.

On a similar note, the solidity of a vaned diffuser is dependent on the distance between two adjacent foils. This distance varies with radii and in the developed program an average value has been utilised between leading and trailing edge. Solidity is key in the modelling of vaned diffusers, and if only one of the leading- and trailing edge values would be used, the empirical data could yield unrealistic performance.

7.3 Performance

The performance of the vaned diffuser is determined by the increase in static pressure as well as the losses in total pressure. The losses are due to friction and sub-optimal guidance of the flow by the airfoils. Approximations are needed to implement advanced effects such as boundary layer growth and friction losses. The model presented below relies upon the work presented in Aungier [13], and has been verified empirically. This section strictly deals with the performance of specified flow and geometry. Design considerations are detailed in section 7.4.

The procedure is iterative in nature. Initial estimations about blockage, deviation etc. which affect the velocities and losses must be updated. The process continues until the velocity leaving the diffuser satisfies continuity.

7.3.1 Design Mass-Flow

The performance of vaned diffusers is described in Aungier [13]. Aungier uses continuity and conservation of angular momentum alongside loss models to predict the state of the fluid leaving the vaned diffuser. The loss models predict losses stemming from incidence, blockage, and flow-mixing with the wake. Once the individual loss coefficients have been estimated, the total loss coefficient can be added together using equation (7.16). Similar to older performance prediction (e.q. Lieblein [20]) Aungier uses Howell's models for estimating the deviation of the flow leaving the vanes [21]. Furthermore, Aungier uses a blockage factor to factor in the effect of divergence angle and blade-loading on the discharge area from the vanes.

$$LC = \sum_{i=1} LC_i \tag{7.16}$$

Blockage

The divergence angle θ_C is estimated from equation (7.17) with w given by equation (7.18).

$$2\theta_C = 2 \arctan \left[\frac{2L_s}{\frac{b_4(w_4 - t_{b4})}{b3} - w_3 + t_{b3}} \right] \tag{7.17}$$

$$w = \frac{2\pi r \cos \alpha_b}{Z} \tag{7.18}$$

From empirical data it has been noted that the performance of vaned diffusers rapidly

decrease for $2\theta_C > 11°$. To account for this in the model, Aungier defines a correction factor, $C_{\theta,\text{corr}}$, described by the relation in (7.19). For divergence angles smaller than the critical value $C_{\theta,\text{corr}}$ is set to 1.

$$C_{\theta,\text{corr}} \geq \frac{2\theta_C}{11} \tag{7.19}$$

To estimate the blade loading parameter, the blade-to-blade velocity difference is required, see equation (7.20). The blade loading parameter, L, is then given by equation (7.21).

$$\Delta C = \frac{2\pi(r_3 C_{\theta 3} - r_4 C_{\theta 4})}{Z L_s} \tag{7.20}$$

$$L = \frac{\Delta C}{C_3 - C_4} \tag{7.21}$$

Similar to θ_C, the performance has been noted to deteriorate for $L > \frac{1}{3}$. A correction factor $C_{L,\text{corr}}$ is introduced according to the relation in (7.22).

$$C_{L,\text{corr}} \geq 3L \tag{7.22}$$

With divergence angle, blade loading, and correction factors introduced the blockage factor can be defined, see equation (7.23) through (7.26).

$$B_4 = \frac{L_s\left[K_1 + K_2(\bar{C}_R^2 - 1)\right]}{w_4} \tag{7.23}$$

$$K_1 = 0.2\left(1 - \frac{1}{C_{L,\text{corr}} C_{\theta,\text{corr}}}\right) \tag{7.24}$$

$$K_2 = \frac{2\theta_c}{125 C_{\theta,\text{corr}}}\left(1 - \frac{2\theta_c}{22 C_{\theta,\text{corr}}}\right) \tag{7.25}$$

$$\bar{C}_R = \frac{1}{2}\left(\frac{C_{m3}\cos\alpha_{b4}}{C_{m4}\cos\alpha_{b3}} + 1\right) \tag{7.26}$$

Skin Friction

The loss coefficient for the skin friction of an airfoil is given by (7.27). It is taken from fully developed pipe-flow and corrected with the thickness of the boundary layer,

δ. The boundary layer thickness is estimated using flat-plate correlations and further approximated by taking the value at mid-passage, see equation (7.28). The hydraulic diameter, d_H, in equation (7.27) is taken as the average values of the hydraulic diameter at throat and exit of a cascade passage. The hydraulic diameter is calculated using equation (2.40).

$$LC_{\mathrm{SF}} = \frac{4C_f}{(\frac{2\delta}{d_H})^{0.25}}\left(\frac{\bar{C}}{C_3}\right)^2 \frac{L_s}{d_H} \tag{7.27}$$

$$\delta = \frac{5.142 C_f L_s}{2} \tag{7.28}$$

Incidence Loss

The incidence loss represents the losses stemming from flow adjustment at entry to the cascade passage. At entry, the flow needs to be adjusted both with respect to the blade angle and the throat area. The optimum incidence is the incidence which would yield the lowest losses. It is defined in equation (7.29). The flow angle at throat is calculated from A_3 and A_{th}, both of which are known for a specified geometry.

$$\cos\alpha^* = \sqrt{\cos\alpha_{3b}\cos\alpha_{\mathrm{th}}} = \frac{C_{m3}}{C_3^*} \tag{7.29}$$

At entry to the passage the flow-area is both contracted due to introduction of the vanes and expanded from the flow turning. The incidence loss coefficient, see equation (7.30), is a balancing of these two concepts and the model approximates the loss as 80% of a sudden expansion loss in addition to the reduction in flow area.

$$LC_{i0} = 0.8\left(\frac{C_3^* - C_{\mathrm{th}}}{C_3}\right)^2 + \left(\frac{Zt_{b3}}{2\pi r_3}\right)^2 \tag{7.30}$$

Wake Mixing Loss

At exit to the vane passage there is a sudden increase in area. In this region the flow has separated from the blade due to boundary layer growth. The velocity of the separated flow is estimated from the inlet velocity and C_θ from the blockage calculations, see equation (7.31).

$$C_{\mathrm{sep}} = \frac{C_3}{1 + 2C_\theta} \tag{7.31}$$

The meridional velocity in the wake of the vane is given by the velocity triangle in which the tangential velocity is given by the conservation of angular momentum:

$$C_{m,\text{wake}} = \sqrt{C_{\text{sep}}^2 - C_{\theta 4}^2} \tag{7.32}$$

The mixed meridional flow is given by continuity from the core flow and the change in flow area:

$$C_{m,\text{mix}} = \frac{A_4 C_{m4}}{2\pi r_4 b_4} \tag{7.33}$$

The losses associated with mixing of the wake and the core flow can then be estimated using equation (7.34).

$$LC_{\text{mix}} = \left[\frac{C_{m,\text{wake}} - C_{m,\text{mix}}}{C_3}\right]^2 \tag{7.34}$$

Fluid Deviation

The angle of the flow leaving the diffuser differs from the vane exit angle by the deviation. To close the system of equations describing the performance of vaned diffusers, the deviation and thus the flow angle must be estimated. Models for fluid deviation have been studied thoroughly for axial compressors and they are commonly used in vaned diffuser calculations as well. Both Aungier [13] and Japikse [22] implement the deviation model by Howell [21], given in equation (7.35). The point of maximum camber ($\frac{a}{c}$) is 0.5 for NACA65 profiles. For circular arcs they need to be calculated from the generated geometry. The solidity (σ) is given by equation (7.36).

$$\delta^* = \frac{\theta[0.92(\frac{a}{c})^2 + 0.02\alpha_{4b}]}{\sqrt{\sigma} - 0.02\theta} \tag{7.35}$$

$$\sigma = \frac{Z(r_4 - r_3)}{2\pi r_3 \cos\bar{\alpha}_b} \tag{7.36}$$

Another option to calculate the fluid deviation is to use Carter's rule [9], described below in equation (7.37).

$$\begin{aligned} \delta* &= \frac{m\theta}{\sqrt{\sigma}} + x \\ m &= 0.23\left(2\frac{a}{c}\right)^2 + \frac{{\alpha_5}^*}{500} \end{aligned} \tag{7.37}$$

7.3.2 Off-Design Mass-flow

To predict the off-design performance, the choking and stall-limits of the design must be known. As choking will not be a factor in the design-program for the pump, only stall will be considered. The stall-limit of the vaned diffusor is described in Aungier [13] through the parameter K given by equation (7.38). K is evaluated between inlet and throat and the average value is taken, hence the approximation.

$$K = -r\frac{\partial \sin\alpha}{\partial r} \approx \frac{r_3}{h_{th}}\left[\frac{\sin\alpha_3}{\sin\alpha_{th}} - 1\right] \tag{7.38}$$

An additional parameter K_0 is introduced in order to implement Mach-number effects in centrifugal compressors, see equation (7.39). K_0 tends towards zero for small Mach-numbers which will be the case in pump-analysis due to the high speed of sound in liquids.

$$K_0 = \frac{M_3^2 \cos^2\alpha_{3b} \sin\alpha_{3b}}{1 - M_3^2 \cos^2\alpha_{3b}} \tag{7.39}$$

The stall limit has empirically been found to be well approximated by the criteria $K + K_0 = 0.39$, according to Aungier [13].

Incidence Loss

The value for K at which stall ensues yields a corresponding flow angle α_{3s} which makes it possible to estimate a loss coefficient for the off-design incidence loss based on the velocities [13]. At velocities lower than stall-velocity, the losses are related to the velocity at optimum incidence through equation (7.40).

$$LC_i = 0.8\left[\frac{C_3 - C_3^*}{C_3}\right]^2 \tag{7.40}$$

If, on the other hand, the velocity is higher than stall-velocity the loss coefficient is given

by equation (7.41) in which it is assumed that 80% of the ideal pressure recovery is lost.

$$LC_i = 0.8\left[\frac{C_{\text{th}}^2}{C_3^2}\left(\left(\frac{C_3}{C_{3,\text{stall}}}\right)^2 - 1\right) + \frac{(C_{3,\text{stall}} - C_3^*)^2}{C_{3,\text{stall}}^2}\right] \tag{7.41}$$

Fluid Deviation

At off-design the deviation must be adjusted for the change in incidence. Aungier implements a method derived from the data presented by Johnsen and Bullock [23] which expresses the relationship between deviation and incidence according to equation (7.42).

$$\frac{\partial\delta}{\partial i} = \exp\left[\sigma\left((1.5 - \frac{\alpha_{3b}}{60}) - 3.3\right)\right] \tag{7.42}$$

7.4 Design

This chapter has previously dealt with the basic principles, geometric construction of airfoils, and the performance of an already set design. A design procedure is required, however, to generate a geometry for a given flow. Much of the flow structures in a pump is dictated by the impeller and subsequent components are usually designed for the flow delivered by the impeller at design point.

7.4.1 Procedure

The design procedure follows the path shown in figure 7.3

Initial Guesses

The design process starts with a selection of geometric quantities at position 3, diffuser leading edge:

- r_3
- b_3
- α_{3b}

A good starting point would be to select the same height of the diffusor as at impeller tip and a sufficiently large vaneless space. According to Rodgers [24], the minimum radius

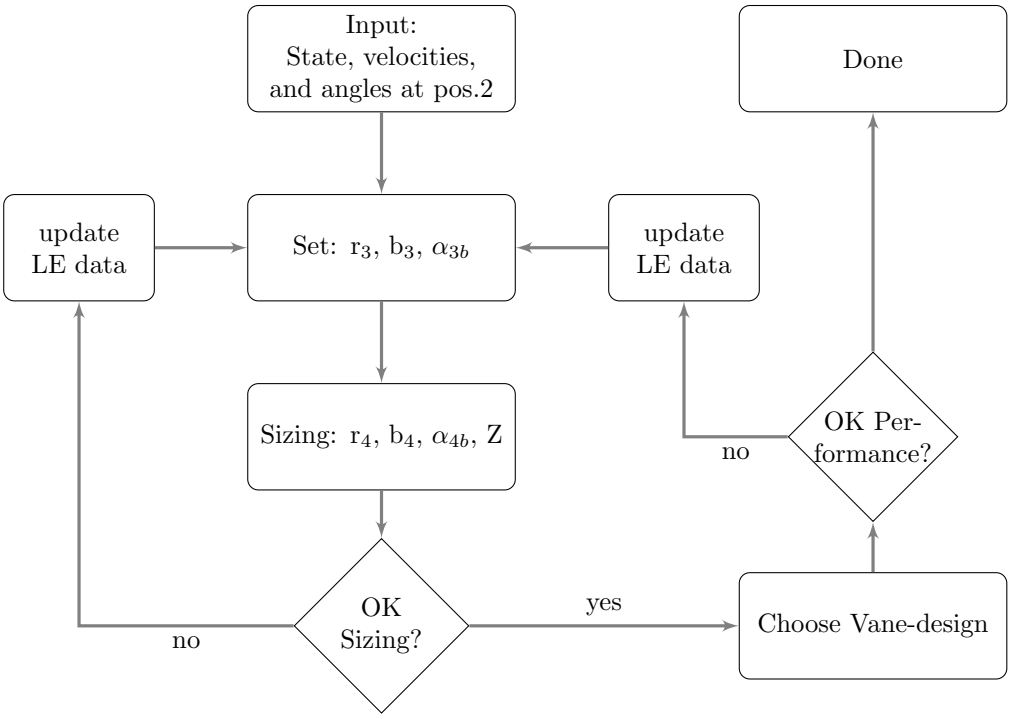

Figure 7.3: Design Procedure vaned diffusers

ratio for the vaneless space lie in the range 1.1 to 1.15. The blade angle at the leading edge is usually specified from the absolute flow angle leaving the impeller with some design angle of attack. Japikse [22] suggests an AoA around 5-6° if NACA65 airfoils are used.

Sizing

There might be restrictions affecting the designer when the overall shape of the vaned diffuser is to be selected. The radial length of the pump might be a limiting factor and the number of vanes dictated by the number of impeller blades as to avoid resonance. Analysis of resonance is usually conducted in a later part of the design phase.

Too short of a vaned diffuser with too few blades will lead to poor guidance of the flow. A long vaned diffuser with many vanes, however, will lead to large friction losses and blockage of the flow. A trade-off is required.

The parameters to be decided are:

- r_4
- b_4

- Z
- α_{4b}

The blade angle at the trailing edge can be initially estimated using the correlation presented by Horlock, according to Japikse [22], where the camber angle was correlated to lift coefficient of a NACA65 airfoil. A rough approximation of the correlation presented suggests:

$$\theta \approx 20 C_{L_0}$$

A designer may use the correlations presented in equations (7.19) and (7.22) to evaluate the parameters chosen so as not to exceed the limits. The solidity of of the vaned diffuser can also guide the designer towards good starting values. Senoo et. al [25] detail the benefit of low solidity cascades in their study. Additional information that strengthens the claims made by Senoo et. al are presented in Japikse [22].

In preliminary design the width of the cascade exit can be set equal to the width at the leading edge. The number of vanes should be an uneven number and, as mentioned earlier, be set as to avoid the natural frequencies of the impeller blades at the specified rotational speed.

Vane Design

When the overall flow path and size are chosen, the designer may choose a suitable airfoil profile and construct the geometry in accordance with the method described in section 7.2. Once the geometry has been constructed the performance can be evaluated using the method described above.

Chapter 8

Return Channel

The basic functionality of the return channel is to bring the flow from one stage of the pump to the next. Furthermore, the flow entering the next stage should be without swirl, which is an additional target in the design of the return channel. The reasoning behind the no-swirl aspiration lies in the Euler turbomachine equation (2.26), with positive swirl-components reducing the work-input of the impeller.

There are variants of return channels available, not implemented in the design tool, where a vaned diffuser is continued over the bend and transformed into de-swirl vanes. This type of return channel system is more advanced and not thoroughly covered in the open literature.

8.1 Basic Principles

8.1.1 Purpose of Return Channel

The aim of the return channel is to supply the inlet of the next stage with the working fluid, preferably with no swirl. This process should be done with as low loss as possible.

8.1.2 Detailed Return Channel Geometry

The flow is guided through a bend, a 180° turn, before being introduced to the vaned section, which aims to remove all swirl from the flow. Following the vaned section lies the 90° bend, turning the flow from a radially inwards direction, to an axial direction, into the next stage. An overview of the return channel can be seen in figure 8.1.

In the current study, only an initial design of the return channel is generated, due to the lack of models evaluating differences in designs. The geometry generated can be extracted and further manipulated using other software for a more in depth analysis e.g. using CFD.

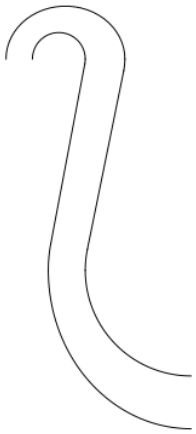

Figure 8.1: Meridional view of the return channel.

8.1.3 Flow Structures

The flow in the return channel is dominated by secondary flows. Vortices as big as the channel width may exist due to boundary layer roll-up of fluid in front of vane leading edge, according to Japikse [2].

The swirl in the flow coming into the return bend aids in the turning of the flow in the 180° bend. Visualise a purely radial flow at diffuser exit, a high pressure can then be imagined along the outer perimeter of the bend with separation and low pressure at the inner perimeter. Adding swirl to the flow could have a smoothing effect, creating better adhesion to the inner perimeter. This can be seen in data presented by Japikse [2], see figure 8.2. A certain level of swirl gives a minimum loss coefficient for a prescribed bend geometry. If the swirl is increased above this level the loss coefficient also increases. This is most likely due to the longer flow path required and the associated frictional losses.

As mentioned in chapter 2, conservation of tangential momentum states that rC_θ is constant if no forces are involved. This implies an increase in tangential velocity when radius is reduced. The flow physics are therefore in opposition to the desired end state of the return channel, in contrast to the vaneless diffuser.

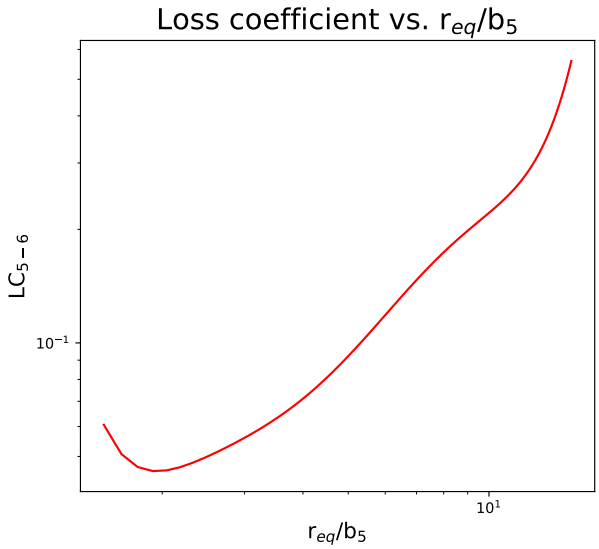

Figure 8.2: LC_{5-6} as a function of r_{eq}/b_5. Reworked from data by [26] presented in [2].

8.2 Performance

The losses here are, as usual, defined from the dynamic pressure. The reader should now realise the importance of a good diffusion prior to the return channel, to reduce the amount of dynamic head entering the return channel. If a designer were to employ an inferior diffuser but still have the same loss coefficient in the return channel, the absolute loss would be greater since dynamic head entering return channel is larger.

8.2.1 Modelling of First Bend

Using the data from the experiment performed by Rothstein [26], see figures 8.2 and 8.3, the loss-coefficient for the bend and the flow angle after the bend can be approximated using curve-fitting. The equivalent radius of the bend is calculated in equation (8.1).

$$r_{\text{eq}} = \frac{r_5}{\cos \alpha_5} \tag{8.1}$$

8.2.2 Modelling of Deswirl Vanes

As mentioned above in section 8.1.2, Japikse [2] proposes two sets of deswirl vanes to reduce the swirl of the flow. Some studies including different setups of return channels has yielded empirical data that could be utilised, in the same manner as for the 180°

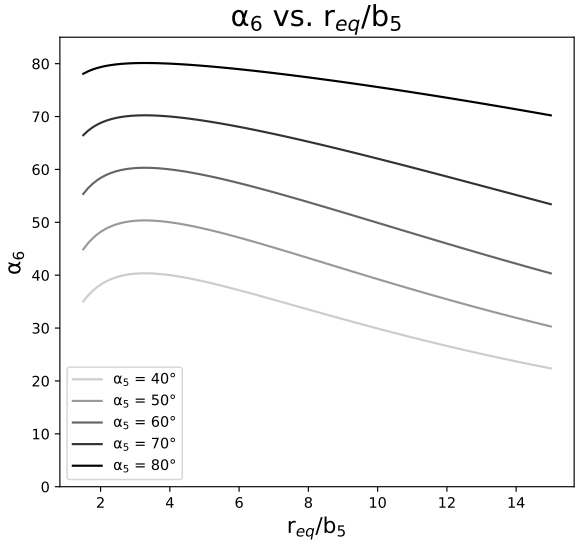

Figure 8.3: Flow angle out of bend can be determined from this graph. Reworked from data by [26] presented in [2].

bend, to determine the performance of the vaned section.

Another mean of modelling the losses and performance is presented by Aungier [27]. Many similarities to Aungier's description of vaned diffuser performance, discussed in section 7.3, can be seen. However, the bend of the return channel causes flow distortions which affects the interactions between fluid and return channel downstream. This bend is not present in a vaned diffuser, and therefore this performance modelling of incidence on the vaned section will differ.

Aerodynamic area blockage factors are estimated in two ways, see equations (8.2) and (8.3), κ_{ave} is the average curvature of the vanes. Equation (8.2) is an estimate utilising inviscid flow and the average radius of curvature of the crossover bend. The estimation done in equation (8.3) is based of blockage due to stall. The estimation that yields the minimum aerodynamic area blockage factor is used.

$$B_6 = \frac{(\kappa_{\text{ave}} b_6)^2}{12 + (\kappa_{\text{ave}} b_6)^2} \tag{8.2}$$

$$B_6 = \frac{r_{\max} b_{\max}}{r_6 b_6} \tag{8.3}$$

When the flow angle in the vane throat is equal to the flow inlet angle, the incidence loss is assumed to be at a minimum, according to Aungier [27]. Since area blockage is not directly utilised in return channel analysis, the minimum loss incidence angle is corrected to account for aerodynamic entrance blockage, described in equation (8.4).

$$\tan(90 - \alpha^*) = (1 - B_6) \tan\left[90 - \arcsin\left(\frac{A_{\text{th}}}{A_6}\right)\right] \tag{8.4}$$

The loss coefficient stemming from incidence of the flow, can now be determined, see equation (8.5).

$$LC_i = 0.8\left[1 - \frac{C_{m6}}{C_6 \sin(90 - \alpha^*)}\right]^2 \tag{8.5}$$

The skin friction, due to viscous shear forces on the perimeter of the channels, are described in equation (8.6). The friction coefficient may be estimated by either Haalands or Colebrook, see section 2.6.2. The hydraulic diameter d_H is estimated in a similar way done in performance of vaned diffuser, see section 7.3.

$$LC_{SF} = \left(\frac{4L_s C_f}{d_H}\right)\left(\frac{C_{\text{ave}}}{C_6}\right)^2 \tag{8.6}$$

The average velocity, needed to estimate the skin friction loss coefficient, is based on the average of the maximum of C_6 and C_{th}, and C_7. See equation (8.7).

$$\begin{aligned} C &= \max(C_6, C_{\text{th}}) \\ C_{\text{ave}} &= \frac{C + C_7}{2} \end{aligned} \tag{8.7}$$

The loss due to blade loading, described by the blade loading loss coefficient, is modelled in equation (8.9). It is based on the blade-to-blade velocity difference, calculated from vane re-circulation in equation (8.8).

$$\Delta C = \frac{2\pi(r_6 C_{\theta 6} - r_7 C_{\theta 7})}{Z L_s} \tag{8.8}$$

$$LC_{\text{BL}} = \left[\frac{\Delta C}{6C_6}\right]^2 \tag{8.9}$$

In a similar fashion to the impeller blade loading, mentioned for relative velocities in section 5.4.2, the maximum velocity on the vane surface is approximated through equation (8.10). It is assumed to occur halfway along the passage, in accordance with Aungier [27].

$$C_{\max} = \frac{C_6 + C_7}{2} + \Delta C \tag{8.10}$$

The separation velocity, the velocity where boundary layer is assumed to separate is assumed to be $C_{\text{sep}} = \frac{C_{\max}}{2}$ if $C_{\max} > 2C_7$. Otherwise the separation velocity is set to C_7.

The velocity after mixing of the wake, following the vane, is approximated by equation (8.11).

$$C_O = \sqrt{\left(\frac{C_7 A_7}{A_O}\right)^2 + C_{\theta 7}^2} \tag{8.11}$$

Where the flow areas are described below in equation (8.12). A_7 accounts for blockage of vanes, whilst A_O is assumed to be just after the trailing edge of the vanes, and therefore described by the complete circumferential area.

$$\begin{aligned} A_7 &= \left(2\pi r_7 - \frac{Zt_7}{\cos\alpha_7}\right) b_7 \\ A_O &= 2\pi r_7 b_7 \end{aligned} \tag{8.12}$$

The mixing of the wake and primary flow results in some losses, as described in earlier chapters. However, in the return channel the loss will be described by a loss coefficient, given by equation (8.13).

$$LC_{\text{mix}} = \left[\frac{C_{\text{sep}} - C_O}{C_6}\right]^2 \tag{8.13}$$

The actual flow angle leaving the vaned section can be estimated in the same manner as for the vaned diffuser, see section 7.3.

8.2.3 Modelling of Second Bend

The final task of the return channel is to turn the flow into the axial direction towards the impeller eye of the next stage. The loss associated with this turning is described in Aungier [27] and calculated through equation (8.14). It is under the assumption that the flow is turned 90°, i.e. from the radial direction to the axial direction.

$$LC_O = 0.1\left(\frac{C_{m7}}{C_6}\right)^2 \tag{8.14}$$

8.3 Design

8.3.1 First Bend

The first bend, which turns the flow 180° is defined by a circular arc on the hub side and an ellipse on the shroud side.

8.3.2 De-swirl Vanes

The de-swirl vanes are situated in a section described by straight line segments. The de-swirl vanes themselves may be described in a multitude of ways. Japikse [2] proposes two methods on how to remove the swirl of the flow and the construction of the camberlines. The first way proposed is to linearly reduce the tangential velocity from an inlet tangential velocity to a desired value. The other way of achieving de-swirl of the flow is by linearly reducing the tangential momentum, rC_θ. The thickness distribution of the first two of these cascades have the thickness distribution described by NACA65-series profile.

CCR

The circumferential component reduction (CCR) cascade, yields a linear change in the tangential velocity component. The camber coordinate θ is described in equation (8.15). $R_7 = r_7/r_6$, $R_i = r_i/r_6$ and i is denoting a local condition. P is the fraction of initial angular momentum left in the cascade. θ is given in radians.

$$\theta_i = \frac{(R_i - 1)\left(R_7 + R_i \frac{P-1}{2} - \frac{P+1}{2}\right)}{(R_7 - 1)\tan(90 - \alpha_{6b})} \tag{8.15}$$

Additionally, Japikse [2] features a study on CCR cascades performed by Japikse and Osborne. CCR was chosen in the study as it was hypothesised that it would provide more uniform turning of the flow over the passage. A correlation for the losses as a function of the diffuser outlet flow angle, for the different return channels, was developed. The effect of incidence onto the de-swirl vane was also evaluated.

MMR

Another cascade mentioned by Japikse is a cascade which linearly reduces the angular momentum rC_θ. This is called a moment of momentum reduction (MMR) cascade. The camber line for this vane is described in equation (8.16).

$$\theta_i = \frac{(R_7 - P)\ln R_i - (1 - P)(R_i - 1)}{(R_7 - 1)\tan(90 - \alpha_{6b})} \tag{8.16}$$

Japikse [2] mentions a study performed by Sulaiman, where the MMR cascade was utilised in different return channels to evaluate the performance. One critical conclusion was that, even though the MMR cascade was designed to remove all swirl, a significant swirl could remain. Hence, some overturning may be required.

Aungier

A third set of airfoil is described by Aungier [27]. This set of airfoil is shown in figure 8.4. The geometric description of this airfoil is similar to the vanes described for vaned diffuser. The blade angle is described in equation (8.17). The camber line coordinate, θ, is calculated in equation (8.18). Dimensionless parameters described by radii are seen in equations (8.19) and (8.20). Constants are described in equation (7.14), but are repeated below in equation (8.21) with notations appropriate to the return channel. The following equations apply to all radii greater than r_{7sh}. Below this radius a constant blade angle camber line is used.

The thickness distribution used is described in equation (8.22). In a similar manner as described for the camber line, this is only utilised for radii greater than r_{7sh}. For radii less than this a constant thickness is employed. The chord is defined from leading edge to the point of the vane at the radius r_{7sh}.

$$\tan\alpha_b = -A - By - 2Cy^2 - 3Dy^3 \tag{8.17}$$

$$\theta = A\ln(y) + B(y - 1) + C(y^2 - 1) + D(y^3 - 1) \tag{8.18}$$

$$Y = \frac{r_{7sh}}{r_6} \tag{8.19}$$

$$y = \frac{r}{r_6} \tag{8.20}$$

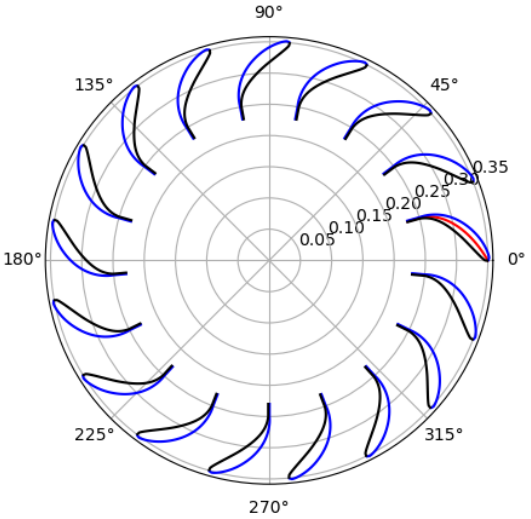

(a) Top view of de-swirl vanes. Note that flow is going radially inwards. The camber line (red) is drawn for one of the vanes.

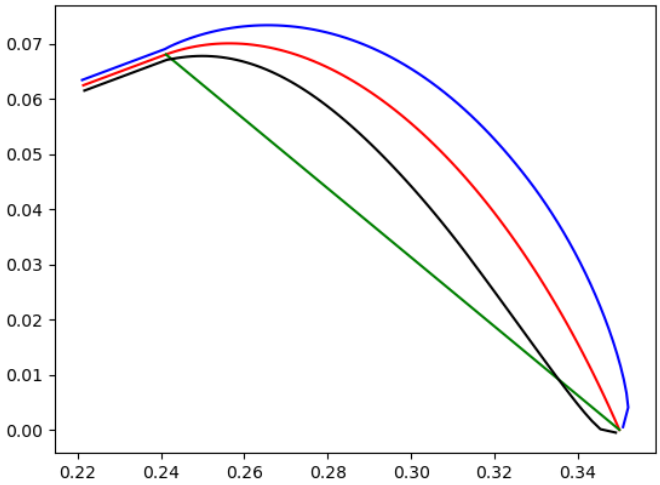

(b) A single de-swirl vane. The green line is the chord. The last part is described by a straight segment with constant width.

Figure 8.4: View of de-swirl vanes, from Aungier's construction.

$$
\begin{aligned}
D &= \frac{(\tan\alpha_{6b} - \tan\alpha_{7b})(K_6 + K_7 - 2)}{3(Y-1)^3} \\
C &= \frac{(\tan\alpha_{6b} - \tan\alpha_{7b})(K_7 - K_6)}{4(Y-1)^2} - \frac{9D(Y+1)}{4} \\
B &= \frac{K_6(\tan\alpha_{6b} - \tan\alpha_{7b})}{Y-1} - 4C - 9D \\
A &= \tan\beta_6 - B - 2C - 3D
\end{aligned}
\tag{8.21}
$$

$$
\begin{aligned}
t &= t_0 + (t_{\max} - t_0) y_t^e \\
t_0 &= t_6 + (t_7 - t_6)\frac{x}{c} \\
y_t &= \frac{x}{x_m}, \quad \text{for } x < x_m \\
y_t &= \frac{1 - x/c}{1 - x_m/c}, \quad \text{for } x > x_m \\
e &= \sqrt{\frac{0.4 x_m}{c}}\left[0.95\left(1 + \frac{x}{c}\right)(1 - y_t) + 0.05\right]
\end{aligned}
\tag{8.22}
$$

8.3.3 Second Bend

The second bend, turning the flow 90° to axial direction is described by a circular arc on the shroud side and an ellipse on the hub side.

8.4 Off-Design Considerations

At off-design conditions the flow will approach the bend with a flow angle different from the design conditions. At low mass-flows the diffuser, provided that it has not stalled, will deliver a higher than design flow angle to the return channel. At high mass-flows this angle will, correspondingly, be lower. If the pump features a vaned diffuser it may provide better guidance for the flow leaving the diffuser, resulting in a flow closer to the design conditions for the return channel. The flow deviation at off-design may be modelled utilising Carters rule, shown below in equation (8.23). This may result in a flow having swirl at the end of the return channel. This swirl will affect the performance of the upcoming stage. The same equation can be used when designing, to iteratively obtain a vaned section yielding a desired level of swirl, often zero.

$$
\begin{aligned}
\delta* &= \frac{m\theta}{\sqrt{\sigma}} + x \\
m &= 0.23\left(2\frac{a}{c}\right)^2
\end{aligned}
\tag{8.23}
$$

Chapter 9

Volute

The volute is situated after the diffusor in the last stage of the pump. Occasionally, the volute is regarded as part of the diffusor, or alternatively, the diffuser regarded as part of the volute. The purpose of the volute is to gather the flow leaving the diffusing elements and send it towards the exit of the pump with as low loss as possible. This chapter starts with a description of the volute geometry which is necessary to grasp the flow-structure inside the volute. The chapter ends with a model predicting the performance of the volute and design aspects.

9.1 Basic Principles

9.1.1 Detailed Volute Geometry

Figure 9.1 shows the general layout of a single vane volute with a circular cross-section in the rθ-plane in which the impeller is rotating anti-clockwise. The flow enters the volute circumferentially at position 6 and leaves tangentially at section 8. This results in an uneven circumferential mass-flow distribution as the fluid elements closest to section 8 need not travel as far in the volute as the fluid-elements entering the volute at a smaller θ-coordinate. To accommodate this increase in mass-flow there is a need for increased flow area along the circumferential direction. The point in the volute where the θ-coordinate is zero, i.e. where the smallest flow area occurs, is called *cut-water* or *tongue*, see figure 9.1.

The performance of a volute is evaluated by the increase in static pressure and the loss in total pressure, as mentioned in section 2.4.2. The loss arise from wall friction, shear forces between fluid elements as they mix in the flow, and exit/entry loss. These are complicated 3D-phenomena involving vortex structures and they will be described in later sections in this chapter. However, to understand the flow field and the origin of the vortex structures one should first consider the different geometric aspects of the volute.

A designer need to navigate among the main geometric parameters to find a combination

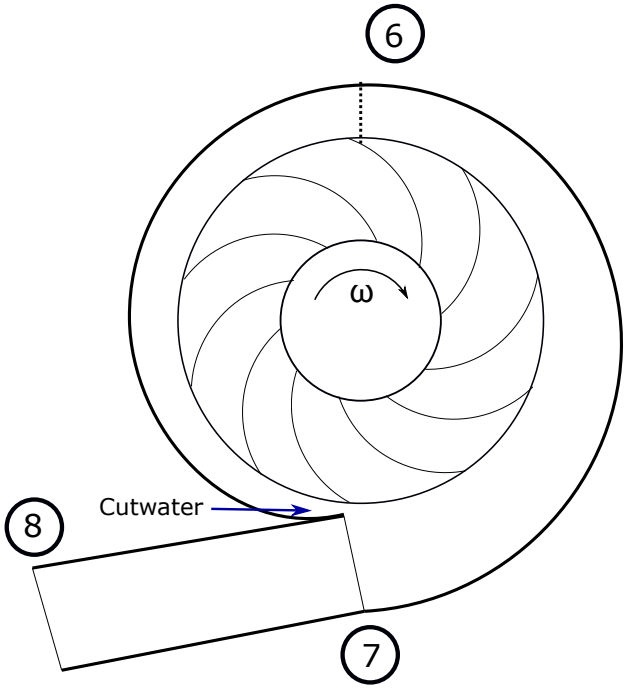

Figure 9.1: Top-view of a volute

that yields the best performance [14]. The parameters are:

- the connection to the diffuser
- the shape of the cross-sections
- change in flow area
- size of the volute

Connection to the Diffuser

Volutes are commonly defined as internal, external, or central [28]. The difference between external and internal volutes lies in how much space the volute occupies in the radial direction. An internal volute folds behind the impeller in the axial direction whereas an external volute continues radially outward after the diffuser, thus taking up more space in the radial direction. Figure 9.2a shows a principle sketch of an internal volute and figure 9.2b an external. It can be seen that the centre-radius for the internal

volute lies at a smaller radius than the diffuser exit radius and that the centre-radius for the external volute lies at a larger radius. A central, or semi-external, volute is one with its centre-radius located at the same radius as the diffuser exit radius. The decrease in radius for internal volutes results in an acceleration of the flow. This acceleration of the flow is unwanted as it removes some of the static pressure recovered in the diffuser [14]. Furthermore, a bend is required after the diffuser for internal volutes which increases the total pressure loses. External volutes, then, would appear the more attractive choice strictly from a performance perspective. If the radial space is a limiting factor, however, internal or central volutes might be the better option.

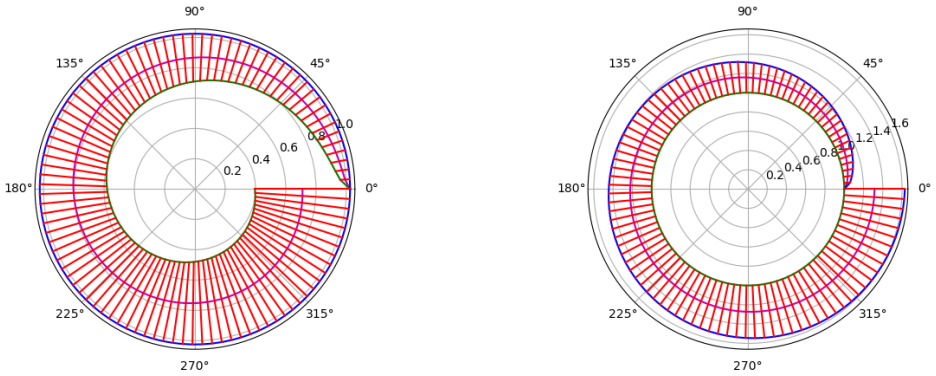

(a) Internal **(b)** External

Figure 9.2: Axial view of internal and external volutes from the developed design program.

Another aspect of the connection between the diffuser and the volute is how the flow enters the volute. If the entering flow is tangential to the cross-section the design is said to be overhung. If, on the other hand, the flow is directed towards the middle of the cross-section the design is termed symmetric. Figure 9.3 shows the schematic of an overhung and a symmetric volute. From numerous test performed in a study by Chen et. al. [29] it has been shown that overhung volutes yield better performance than symmetric volutes. Reasons for this will be discussed later in this chapter. Note that both internal and external volutes could use either overhung or symmetric designs. Just as intermediate volutes are a mixture between internal and external volutes, there is an option to mix the overhung and symmetric designs. The parameter a designer can try to optimise in such a configuration is how much from the centre of the cross-section the flow is directed, i.e. the eccentricity. Recognising that symmetric volutes result in lower overall efficiency than overhung designs, Heinrich and Schwarze [30] performed a numerical investigation into eccentric volute cross sections. Their result showed that an eccentricity of 0.85 was the optimum for overall performance, where an eccentricity of 1 or -1 would yield completely tangential inlet flow.

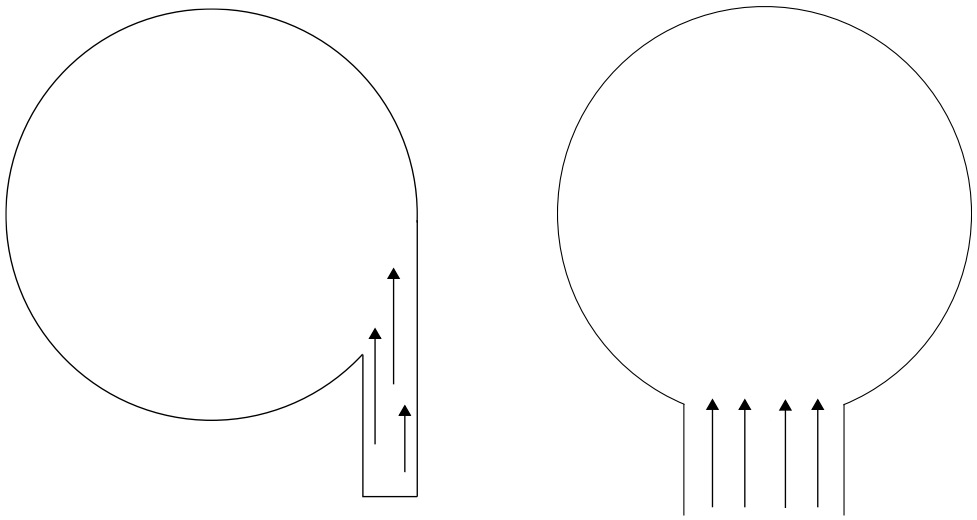

(a) Overhung **(b)** Symmetric

Figure 9.3: Tangential view of overhung and symmetric volutes.

Shape of Cross-Sections

Besides choosing between internal/external and overhung/symmetric volutes a designer has to decide upon the shape of the cross-sections. The options are rectangular, circular, or elliptic [14]. For readers familiar with aerodynamic design the intuitive choice might be the circular or elliptical designs. Mishina and Gyobo [31] investigated rectangular and circular cross-sections for tangential inflow volutes which showed a small favour for circular cross-sections. Ayder et. al. [32] conducted experiments on volutes with elliptical and rectangular cross-shapes. The results showed better performance for the rectangular volutes which the authors attribute to the rectangular volute being better adapted to the impeller and vaneless diffuser. The conclusion one can draw from these studies is that circular/eliptical shapes generally perform better than rectangular ones and that the most important factor is that the system is designed as a whole.

Flow Area

Apart from studying the shape of the cross-sections, Mishina and Gyobo [31] investigated how the loss was affected by area distribution. Through trial-and-error they found the optimum area distribution and related that to the area distribution obtained from an analysis employing conservation of angular momentum. The effect of area-distribution was shown to have more impact on loss-coefficient than choice of cross-sectional shape. Their study also showed a clear drop in performance when moving from external to internal volutes.

Besides deciding upon the proper area distribution, the designer is tasked with choosing the overall size of the volute. The choice between a larger/smaller volute is closely linked to the desired effects at off-design conditions. Larger volutes generally provide a larger operating range for high mass-flows but are sensitive to surge at low mass flows. Furthermore, at rotational speeds exceeding design large volutes show unsteady flow behaviour. Small volutes are stable at all rotational speeds but lack the operating range of large volutes, dropping rapidly in pressure-ratio for increased mass-flows [14]. The volutes behaviour at design and off-design conditions will be detailed later in this chapter.

9.2 3D Flow Structures

The through-flow velocity in the volute (C_T) is primarily made up of the tangential flow leaving the diffusor ($C_{\theta 6}$), with absolute flow angles generally around 60-70°. C_T is what drives the fluid-element through the volute and out of the pump. This leaves the radial velocity component, C_{r6}, which is often modelled as completely lost. Consider a fluid element entering an overhung volute close to the cut-water. As there are no other fluid-elements in the volute, the fluid elements fill the flow area completely. The radial velocity component of this initial flow encounters a wall and can safely be assumed to be lost due to frictional forces and dissipation. Hence, these initial fluid elements only have tangential velocity. As these fluid-elements travel along their respective streamlines, the flow area increases and other fluid-elements are fed into the flow. As we are dealing with an overhung volute the radial velocity components of the added flow enters tangentially to the original streamline. The added flow starts swirling around the original streamline, creating a vortex tube. What was a tangential-radial flow has transformed into a tangential flow with swirl. This process continues throughout the volute, each step in the circumferential direction adds a vortex-tube with ever increasing radius around the original streamline.

9.2.1 At Design Mass-Flow

From the previous explanation of the flow structure it can be understood that the swirl-component of the flow depends on C_{r6}. At design operation C_{r6} is constant out of the diffusing elements as there are no disturbances to the flow. Hence, the resulting swirl velocity inside the volute would be uniform assuming no loss, as seen in figure 9.4a. This corresponds to a free-vortex flow. However, this flow structure cannot exist as the velocity gradients in the centre would generate large shear forces. A real structure would approach the shape depicted in figure 9.4b, with a linear decrease in swirl towards the centre. Thus, a vortex tube experience a decrease in swirl as it moves through the volute. This is intuitive as there is a continuous mixing of the flow where kinetic energy is continuously dissipated. Experiments have validated this flow structure inside the volute

and has shown that the swirl-velocity is close to uniform at the outer vortex tubes, i.e. low initial dissipation of the kinetic energy.

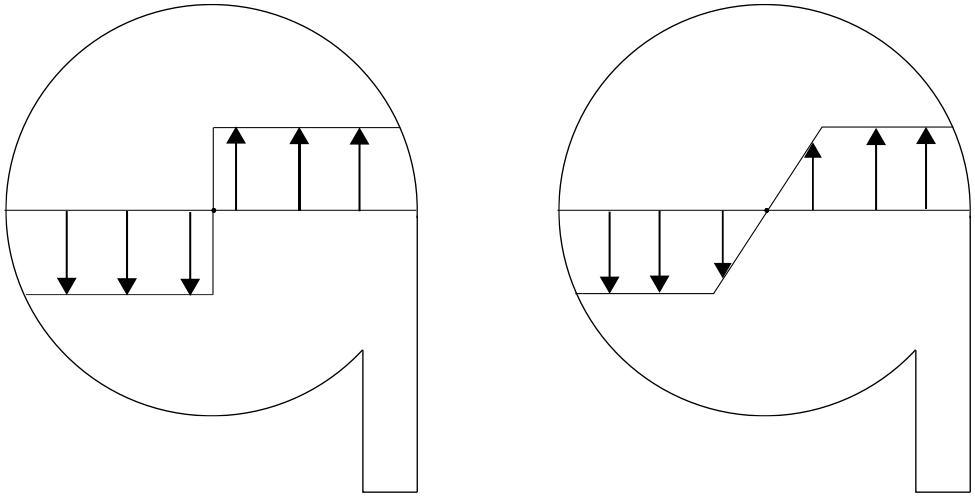

(a) Ideal **(b)** Real

Figure 9.4: Cross-section of volute with swirl velocities at design mass-flow. Reworked from Braembussche [17]

Due to the energy dissipation, the total pressure is lower at the centre of the cross-section. From radial equilibrium and energy balance, equation (9.1) and (9.2), it can be shown that the decrease in total pressure and swirl velocity leads to a lower static pressure and an increase in tangential velocity towards the centre of a cross-section.

$$\frac{dp}{dr} = \rho \frac{C_{\text{swirl}}^2}{r} \tag{9.1}$$

$$\rho \frac{V_{\text{tan}}^2}{r} = p_0 - p - \rho \frac{C_{\text{swirl}}^2}{r} \tag{9.2}$$

9.2.2 At Off-Design Mass-Flow

The flow in the volute at off-design conditions is a key piece of the puzzle in the understanding of why a pump behaves in a certain way during off-design operations.

Low Mass-Flows

At lower than design mass-flow the tangential velocity out of the impeller is increased and the radial velocity reduced compared to design conditions. This is due to continuity and increased diffusion in the impeller combined with constant blade speed. The increase in tangential velocity implies an increase in C_T, as $C_{\theta 6}$ fed into C_T. Continuity between volute inlet and exit, however, demands a lower C_T than at design-conditions. Hence, $C_{\theta 6}$ is decelerated upon entry to the volute which increases the static pressure. As velocities and pressures need to be continuous throughout the volute there is a build-up in static pressure between start and exit of the volute. With a circumferential increase in static pressure towards volute exit, there is an accompanying decrease in radial velocity.

High Mass-Flows

At higher than design mass-flow the tangential velocity out of the impeller is decreased and the radial velocity increased compared to design conditions. A low tangential velocity implies a low C_T, but as more fluid needs to pass through the geometry of the volute for a given time, C_T needs to be larger than at design mass-flow. Hence C_T needs to accelerate through the volute which leads to a decrease in static pressure. Through the same analogy as in the low mass-flow case (continuous pressure-field), the static pressure will be highest at the start of the volute and lowest at volute exit. The circumferential distribution of mass-flow will be low where the static pressure is high and thus C_{r6} will increase from volute start to exit.

Implications for Cross-Sections

The link between C_{r6} and swirl-velocity in vortex tubes was described earlier in this chapter. At off-design mass-flows, C_{r6} was seen to decrease/increase from start to end of the volute. The swirl-velocity of a vortex tube, then, will be larger towards the centre of the cross section for low mass-flows and smaller towards the centre for high mass-flows. Assuming isentropic flow, the cross-sectional velocity distributions would approach the shapes shown in figures 9.5a and 9.6a, respectively. However, as at design-conditions, the shear-forces at the centre would be too great. The distribution instead approaches the ones depicted in figures 9.5b and 9.6b.

9.3 Performance

With knowledge about the flow structure inside the volute, the assumptions made in the prediction of performance of the volute becomes more intuitive. The performance of the volute can be described by an increase in static pressure and an inevitable decrease in

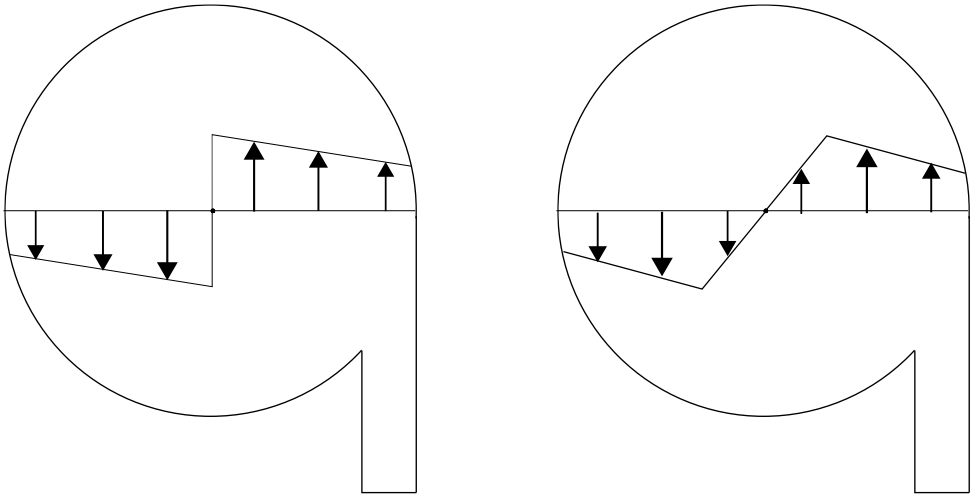

(a) Ideal **(b)** Real

Figure 9.5: Cross-section of volute with swirl velocities at low mass-flow.

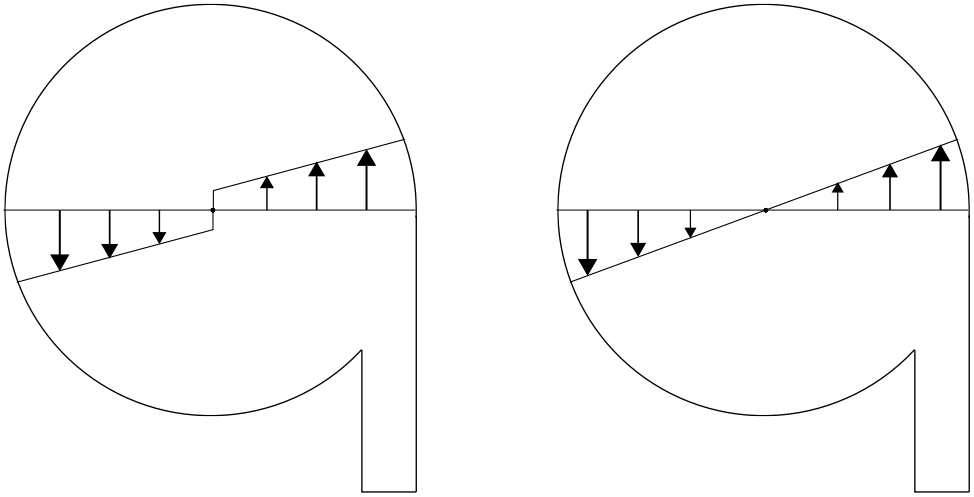

(a) Ideal **(b)** Real

Figure 9.6: Cross-section of volute with swirl velocities at high mass-flow.

total pressure. These are described by the static pressure recovery coefficient $C_{P,5-7}$ and the total pressure loss coefficient LC_{5-7}. These have already been presented in section 2.4.2 but are re-iterated here for clarity, see equations (9.3) and (9.4).

$$C_{p,5-7} = \frac{p_7 - p_5}{p_{05} - p_5} \tag{9.3}$$

$$LC_{5-7} = \frac{p_{05} - p_{07}}{p_{05} - p_5} \tag{9.4}$$

Japikse [33] presented a method for estimating the loss-coefficient and it has been improved by Weber and Koronowski [28]. The model includes:

- LC_m, meridonal velocity loss
- LC_θ, tangential velocity loss
- LC_f, frictional loss
- LC_e, exit loss

The accumulated loss coefficient is given by:

$$LC_{5-7} = LC_m + LC_\theta + LC_f + LC_e \tag{9.5}$$

9.3.1 Meridional Loss

The meridional component of the loss predicts how much of the meridional kinetic energy entering the volute is lost. Relating this to the flow structure described in section 9.2 means that some of the kinetic energy associated with the swirl is destroyed by the shear forces. LC_m can be calculated through equation (9.6). Selecting $F_1 = 1$ makes the assumption that all of the swirl has dissipated i.e. all of the meridional velocity has been lost. This is a common (and pessimistic) assumption in predicting the volute performance [22].

$$LC_m = F_1 \frac{C_{m5}^2}{C_5^2} \tag{9.6}$$

9.3.2 Tangential Loss

The tangential component of the loss depends on whether the through-flow velocity accelerates or decelerates through the volute i.e. if the mass-flow is higher or lower than design. Considering the swirl-velocities detailed in 9.2.2 reveals the reasons for this. For an accelerating flow, the swirl-velocities in the centre of the cross-section where found to be small. Small swirl-velocities require only a small level of dissipation (low kinetic energy loss) in order to reach a forced vortex structure. A decelerating flow, on the other

hand, where found to yield higher swirl-velocities towards the centre of the cross-section and thus require a lot of dissipation to reach a forced vortex structure, according to Braembussche [14]. For geometries where the central position of the cross-section increases from start to end of the volute ($r_5 < r_6$) some free vortex diffusion is possible. To allow for this in the loss-model Japikse [22] introduces another correction factor, F_2. The tangential loss coefficient for decelerating flows is described by equation (9.7). For accelerating flow, the loss is assumed negligible ($F_2 = 0$) and for decelerating flow the loss is modelled like sudden expansion loss ($F_2 = 1$).

$$LC_\theta = F_2 \left(\frac{r_5}{r_6}\right)^2 \frac{C_{\theta 5}^2 (1 - A_5/A_7)^2}{\frac{1}{2}\rho C_5^2} \tag{9.7}$$

9.3.3 Frictional Loss

The frictional loss is modelled by a friction coefficient dependent on the Reynolds number and wall roughness, the hydraulic diameter of the volute and the length of the fluid path. The friction coefficient is usually taken from pipe-flow charts [14]. Equation (9.8) shows the definition for the loss coefficient.

$$LC_f = C_f \frac{L_s}{d_H} \tag{9.8}$$

9.3.4 Exit Loss

The exit loss, according to Weber and Koronowski [28], is modelled as a conical diffuser, see equation (9.9). The opening angle from the volute to exit should not exceed 10-11° so as to avoid flow separation. For moderate opening angles a constant value of 0.15 for F_3 is proposed. For values of fully separated flow, F_3 may reach values exceeding 1.

$$LC_e = F_3 \frac{\frac{1}{2}\rho (C_{T5} - C_{T6})^2}{\frac{1}{2}\rho C_5^2} \tag{9.9}$$

Aungier [13] suggests that the proceeding exit loss from Weber and Koronowski is to optimistic and instead proposes an exit loss coefficient according to equation (9.10).

$$LC_e = \left(\frac{C_6 - C_7}{C_5}\right)^2 \tag{9.10}$$

9.4 Design

The description of volute flow shows that external slightly eccentric overhung volutes are preferable if the available space allows it. Apart from basic geometric choices, the main task in designing a volute is to specify the circumferential variation in cross-sectional area. Aungier [13] describes two approaches: the simple area schedule (SAS) and the conservation of angular momentum (CAM-model). In SAS-design the area of the fully collected flow is specified and the cross-sectional area varies linearly.

9.4.1 CAM-model

The conservation of angular momentum combined with the continuity equation specifies the cross-sectional area as a function of mean passage radius r_c, see equation (9.11).

$$\begin{aligned} r_c C &= r_5 C_{\theta 5} \\ \rho_c A_c C_c &= \rho_5 A_5 C_{m5} \\ A_c &= \theta \frac{r_c b_5}{\tan \alpha_5} \end{aligned} \tag{9.11}$$

The CAM-model can be updated with predictions about loss in angular momentum due to e.g. friction. Karassik [34] suggests a correction factor in the magnitude 0.9 to 0.95 which can be implemented for a more realistic model.

9.4.2 Implementation

Restrictions of r_c may be found if, for instance, the shape of the cross-sections are defined or some other restrictions put on the overall geometry of the pump. The distribution of r_c in the design-tool is calculated from predefined cross-sections and symmetry.

Undersized volutes are associated with a loss penalty, according to Aungier [13], and a sizing parameter (SP) may be introduced to enlargen the volute somewhat. Values of SP in the range 1-1.2 are common.

Chapter 10

Hub-to-Shroud Analysis

10.1 Basic Principles

Chapters 4 and 5 detail the flow inside the impeller and preliminary flow models. The output from a design-program operating on the principles described in chapter 3 and 5 is the axisymmetric geometry at cross-sections 1 and 2, with reference to figure 1.1. The preliminary design does not provide information about the streamlines between station 1 and 2. However, this is of great importance in the design and a common tool to use in the preliminary phase (pre-CFD) is a quasi-three-dimensional flow analysis [13], sometimes referred to as the streamline curvature method (SCM). Wu [35] is commonly referenced as the creator of the quasi-three-dimensional flow analysis and his ideas have been implemented in numerous commercial codes. Before CFD, quasi-three-dimensional flow analysis was the primary tool used in the design of turbomachinery. The techniques of Wu guided the advances within radial turbomachines between the 1950's and 1980's. In the original report by Wu he presents two axisymmetric stream surfaces on which the flow field is calculated. These are termed the S1 and S2 surfaces, see figure 10.1. The S1 surface lies between two blade rows and the S2 surface lies in the hub-to shroud plane. The S2 surface is the most common starting point in preliminary design. Japikse [22] deems the additional detail supplied by the S1 surface unnecessary in relation to the added complexity and recommends that designers move on to viscid 3D solvers after the S2 surface have been solved. The S2 stream surface, also known as the hub-to-shroud plane, was prioritised and this chapter details the derivation and implementation of the SCM-equations on this plane.

10.1.1 Purpose of SCM

The designers choice of pressure ratio, swirl parameter, and blade angles decide the overall geometry of the impeller in the preliminary design. The models, however, provide no information about how section 1 and 2 is connected, or how the velocity changes between these sections. The velocity distribution on the S2 surface provides information about the blade loading which, through empirical correlations and previous experience,

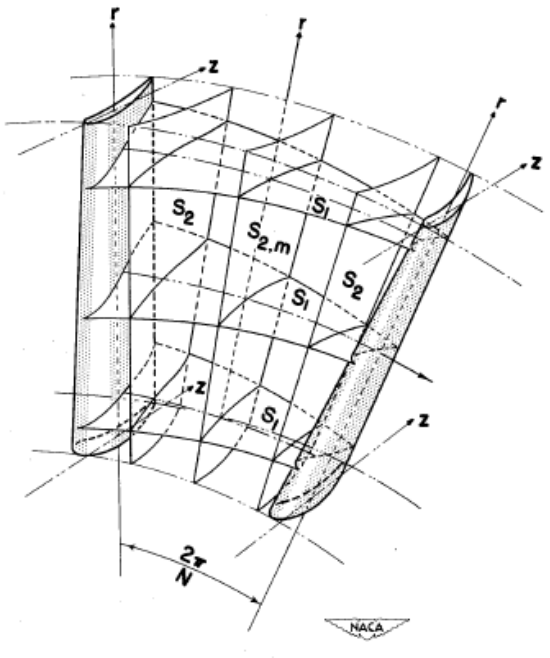

Figure 10.1: S1 and S2 surfaces in quasi-three-dimensional analysis, from Wu [35].

can guide the designer towards good aerodynamic design. Blade loading is normally evaluated through the local blade loading coefficient and the local rate of diffusion [22]. The blade loading coefficient is given by the change in relative velocity divided by the average value: $\Delta W/\bar{W}$.

The rate of diffusion and the resulting pressure field within the flow passage must be within certain limits. If the rate of diffusion is to high, i.e. sharp increases in pressure along the hub- and shroud contours, the boundary layers will grow leading to an increase of the secondary flows [22]. Large secondary zones imply a relatively small primary zone and inefficient work-input to the fluid. Restricting the rates of diffusion along hub and shroud, then, is an essential part of the design process. Knowledge about boundary layer growth within the impeller is required and some models for this have been presented, for instance by Aungier [13]. In absence of such models, empirical data and experience will have to suffice. The purpose of the hub-shroud-analysis, then, is to evaluate blade- and passage profiles through trial-and-error until a candidate geometry for CFD has emerged.

10.1.2 Flow Description

The problem to be solved on S2 is described by the Navier-Stokes equations. In the preliminary design, only the inviscid parts of these equations are considered, what is known as the Euler equations. The continuity equation is re-iterated here on vector notation, see equation (10.1).

$$\frac{\partial \rho}{\partial t} + \vec{\nabla} \cdot (\rho \vec{C}) = 0 \tag{10.1}$$

The first part of equation (10.1) represents the temporal term and it is neglected during steady state, i.e. when there is no change to the flow over time. The momentum Euler equation can be derived from Newtons second law and has been presented in numerous texts, for instance Young [7] or Anderson [3]. It is presented here in equation (10.2) on vector notation. The steady momentum Euler equation is given in equation (10.3).

$$\rho \left[\frac{\partial \vec{C}}{\partial t} + (\vec{C} \cdot \vec{\nabla}) \vec{C} \right] = -\vec{\nabla} p + \vec{F} \tag{10.2}$$

$$(\vec{C} \cdot \vec{\nabla}) \vec{C} = -\frac{1}{\rho} \vec{\nabla} p + \vec{f} \tag{10.3}$$

The derivation of the acceleration and force terms for the impeller fluid flow will be detailed in section 10.3. The pressure terms can be elaborated through radial equilibrium. Consider the fluid element shown in figure 10.2, it is described in cylindrical coordinates by (r, θ, z). A balance of forces on the surface of the fluid yields the expression in equation (10.4) [36].

$$C_r \frac{dC_r}{dr} + C_z \frac{dCr}{dz} - \frac{C_\theta}{r} = -\frac{1}{\rho} \frac{dp}{dr} \tag{10.4}$$

The second Gibbs equation can be differentiated with regard to dr, see equation (10.5). Rewriting the enthalpy in terms of total enthalpy and velocity allows for an expression connection the velocity distribution to the work transfer and entropy generation. The rewritten version of the radial equilibrium equation is shown in equation (10.6) [36], in which quantities are assumed constant in the θ-direction.

$$\frac{1}{\rho} \frac{dp}{dr} = \frac{dh}{dr} - T \frac{ds}{dr} \tag{10.5}$$

$$\frac{dh_0}{dr} - T \frac{ds}{dr} = -C_z \frac{dC_r}{dz} + C_z \frac{dC_z}{dr} + C_\theta \frac{dC_\theta}{dr} + \frac{C_\theta^2}{r} \tag{10.6}$$

The flow physics presented in this section shows that the velocity field in the hub-shroud-analysis is a matter of modelling the fluid acceleration and force-terms. In order to implement these models, a discretisation of the impeller geometry is needed.

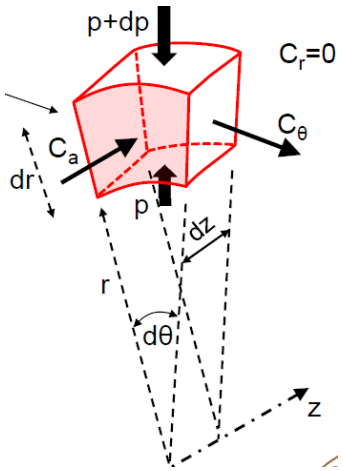

Figure 10.2: Radial equilibrium of a fluid element in cylindrical coordinates (Courtesy of Magnus Genrup).

10.2 Geometric Description

A well-defined geometry lies at the heart of the hub-shroud-analysis. This section seeks to introduce the reader to the domain used in later part of this chapter.

10.2.1 Intrinsic Coordinates

The SCM utilises one key aspects of streamlines: there is no velocity-component normal to a streamline as streamlines are defined as being tangent to the velocity vector [7]. When performing computations on streamlines it is helpful to define a coordinate system that follows the streamline. These coordinates are known as intrinsic coordinates, given in (m, n, θ). Figure 10.3 shows how the intrinsic coordinates can be expressed in terms of cylindrical coordinates given the local flow angle, ϕ.

Also shown in figure 10.3 is q, t, and γ, which is the quasi-normal to the streamline, the orthogonal direction to the quasi-normal, and their angle to the radial and axial direction respectively. Quasi-normals are used to describe the flow field from a supplied geometry.

The relative flow direction w is described by m and the relative flow angle β. Since the only components of velocity lies in the $m\theta$-plane, so does w. Since no fluid can pass through the blades, w will follow the blades if incidence and deviation are neglected. However, there are models to incorporate incidence and deviation within the computational domain, for instance Aungier [13].

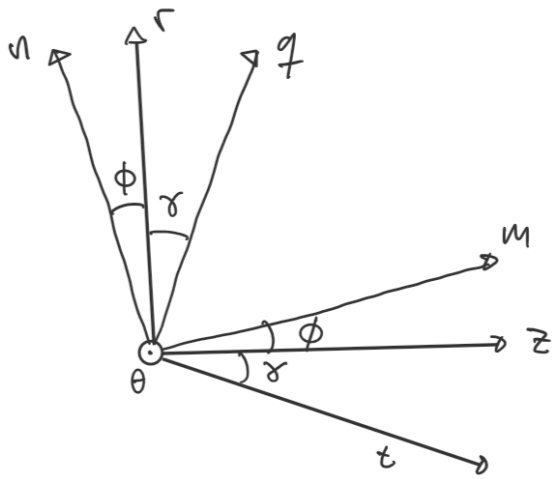

Figure 10.3: Relationship between intrinsic coordinates, cylindrical coordinates, and ϕ.

10.2.2 Lean/Rake

Apart from the hub- and shroud contours, the blades are what defines the computational domain on the S2 surface. The blades can be tilted somewhat in the tangential direction, and this angle is often termed lean or rake. This implies that two corresponding points on the hub- and shroud surfaces do not share the same θ-coordinate. Lean/rake is represented by ε, shown in figure 10.4. The e-direction can be described as q rotated ε degrees around t.

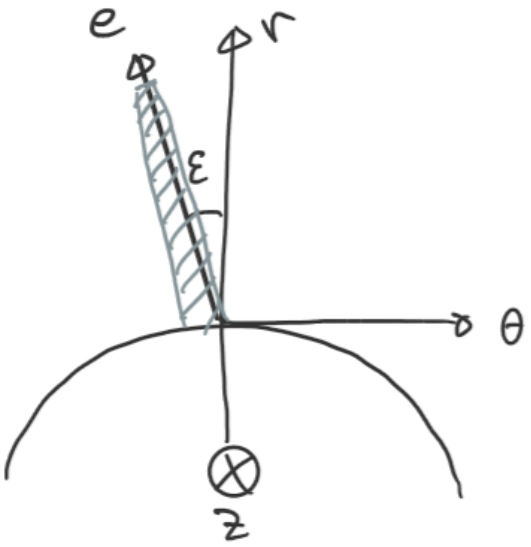

Figure 10.4: Description of lean angle.

The force exerted by the blades on the fluid acts normal to the blade surface. As the w and t directions both lie tangential to the plane, the direction normal to the blade

surface, p is given by the cross-product shown in equation (10.7), and the unit vector in p-direction is obtained by normalising.

$$\begin{aligned} \vec{N}_p &= \vec{e}_w \times \vec{e}_t \\ \vec{e}_p &= \frac{\vec{N}_p}{|N_p|} \end{aligned} \tag{10.7}$$

10.2.3 Differentiation of Unit-vectors

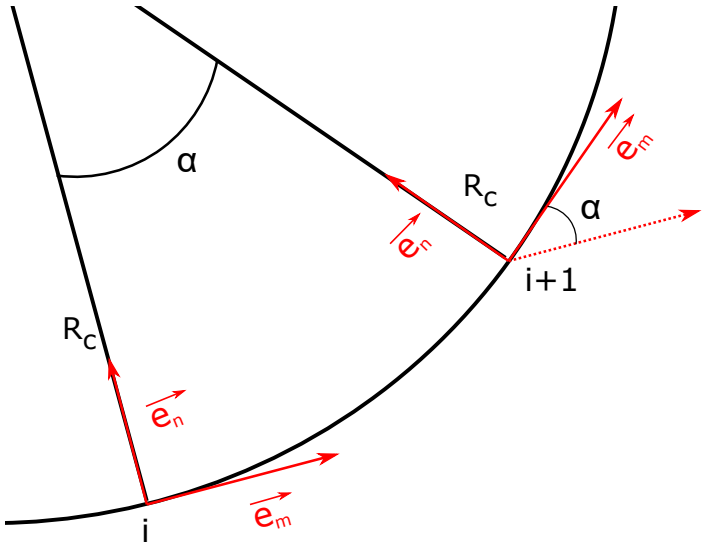

Figure 10.5: Differentiation of meridional unit vector.

When moving from point i to $i+1$ along a streamline, a distance Δm, the meridional direction changes, from $\vec{e}_{m_i}$ to $\vec{e}_{m_{i+1}}$. This change can be seen as a rotation around the θ-axis, which is orthogonal to the paper. Let us now describe the unit vectors in directions from point i, in intrinsic coordinates (n, θ, m).

$$\vec{e}_{m_i} = [0, 0, 1] \qquad \vec{e}_{m_{i+1}} = [\sin\alpha, 0, \cos\alpha]$$

Note that both vector has the length of unity, as they are unit-vectors.

To obtain the relative change of the direction from point i to $i+1$ the diffence is taken.

$$\Delta\vec{e}_m = \vec{e}_{m_{i+1}} - \vec{e}_{m_i} = [\sin\alpha, 0, \cos\alpha - 1]$$

The trigonometric expressions can be rewritten by utilising Taylor expansion:

$$\sin\alpha = \alpha - \frac{\alpha^3}{3!} + \frac{\alpha^5}{5!} - \frac{\alpha^7}{7!} + \ldots$$
$$\cos\alpha = 1 - \frac{\alpha^2}{2!} + \frac{\alpha^4}{4!} - \frac{\alpha^6}{6!} + \ldots$$

Truncating terms of second order and greater yields the following expression of the relative change of the meridional direction.

$$\Delta\vec{e}_m = [\alpha, 0, 0]$$

The change in the unit vector is meridional direction is described by the angle α in the normal direction, n. The change of the meridional unit vector over the change in distance may be desribed as:

$$\frac{\Delta\vec{e}_m}{\Delta m} = \frac{[\alpha, 0, 0]}{\Delta m} = \frac{\alpha\vec{e}_n}{\Delta m}$$

The distance along the streamline, Δm can be described by a circular arc, with the angle α and the radius R_c.

$$\Delta m = \alpha R_c$$

Combined with the expression above, yields.

$$\frac{\Delta\vec{e}_m}{\Delta m} = \frac{\alpha\vec{e}_n}{\alpha R_c} = \frac{\vec{e}_n}{R_c}$$

The example is derived from a streamline having a macroscopic curvature, thus making it easy to visualise. However, if the limit of the fraction is taken one obtains the partial derivative seen below. It should be obvious that this equation is true for an arbitrary streamline.

$$\frac{\partial\vec{e}_m}{\partial m} = \frac{\vec{e}_n}{R_c}$$

10.3 Governing Equations

With the geometry fully defined, the acceleration and force terms can be derived.

10.3.1 Acceleration

The acceleration term in the steady momentum equation was given by:

$$(\vec{C} \cdot \vec{\nabla})\vec{C}$$

in which the velocity vector and the nabla operator in cylindrical coordinates is given by [3]:

$$\begin{aligned}\vec{C} =& C_m\vec{e}_r + C_\theta\vec{e}_\theta + C_z\vec{e}_z \\ \vec{\nabla} =& \frac{\partial}{\partial r}\vec{e}_r + \frac{1}{r}\frac{\partial}{\partial \theta}\vec{e}_\theta + \frac{\partial}{\partial z}\vec{e}_z\end{aligned}$$

Expanding the acceleration terms yields the following expression:

$$\left[(C_m\vec{e}_r + C_\theta\vec{e}_\theta + C_z\vec{e}_z)\left(\vec{e}_r\frac{\partial}{\partial r} + \vec{e}_\theta\frac{1}{r}\frac{\partial}{\partial \theta} + \vec{e}_z\frac{\partial}{\partial z}\right)\right](C_m\vec{e}_r + C_\theta\vec{e}_\theta + C_z\vec{e}_z)$$

Within the blade impeller, the fluid is best described by the relative velocity. Below the components of velocity is related from the absolute frame to the relative frame.

$$\begin{aligned}C_m &= W_m \\ C_\theta &= W_\theta + \omega r\end{aligned}$$

The nabla-operator in intrinsic coordinates are given by

$$\vec{\nabla} = \vec{e}_m\frac{\partial}{\partial m} + \frac{\vec{e}_\theta}{r}\frac{\partial}{\partial \theta} + \vec{e}_n\frac{\partial}{\partial n}$$

The acceleration, for steady state, is shown in the left-hand-side of equation (10.2). Applying the nabla operator to the velocity vector, all given in intrinsic coordinates, results in the following expression.

$$\vec{a} = (\vec{W}\cdot\vec{\nabla})\vec{W} = \vec{e}_m W_m \frac{\partial W_m}{\partial m} + W_m^2 \frac{\partial \vec{e}_m}{\partial m} + \vec{e}_\theta W_m \frac{\partial (W_\theta + \omega r)}{\partial m} + W_m (W_\theta + \omega r)\frac{\partial \vec{e}_\theta}{\partial m} + \frac{(W_\theta + \omega r)}{r} W_m \frac{\partial \vec{e}_m}{\partial \theta} + \vec{e}_m \frac{(W_\theta + \omega r)}{r}\frac{\partial W_m}{\partial \theta} + \frac{(W_\theta + \omega r)^2}{r}\frac{\partial \vec{e}_\theta}{\partial \theta} + \frac{(W_\theta + \omega r)}{r}\vec{e}_\theta \frac{\partial (W_\theta + \omega r)}{\partial \theta}$$

By assuming axi-symmetric flow, i.e. no variation in tangential direction, and utilising the following expressions below, equation (10.8) is obtained.

$$\frac{\partial \vec{e}_m}{\partial m} = \frac{\vec{e}_n}{R} \qquad \frac{\partial \vec{e}_m}{\partial \theta} = 0 \qquad \frac{\partial \vec{e}_\theta}{\partial m} = 0 \qquad \frac{\partial \vec{e}_\theta}{\partial \theta} = -\vec{e}_r$$

$$\vec{a} = \vec{e}_m W_m \frac{\partial W_m}{\partial m} + \vec{e}_n \frac{W_m^2}{R_c} + \vec{e}_\theta W_m \frac{\partial (W_\theta + \omega r)}{\partial m} - \vec{e}_r \frac{(W_\theta + \omega r)^2}{r} \tag{10.8}$$

The acceleration in the quasi-normal direction may now be calculated as the scalar-product between the unit vector and acceleration.

$$a_q = \vec{e}_q \cdot \vec{a} = \sin(\phi + \gamma) W_m \frac{\partial W_m}{\partial m} + \cos(\phi + \gamma)\frac{W_m^2}{R_c} - \cos(\gamma)\frac{(W_\theta + \omega r)^2}{r}$$

The acceleration can, with use of the Euler equations, be written as below, when applied in quasi-normal direction.

$$a_q = \frac{-1}{\rho}\frac{\partial p}{\partial q} + F_q$$

Where the pressure gradient can be rewritten in a similar fashion as above, utilising Gibbs and the definition of total enthalpy. The force-term, however, will be derived below.

10.3.2 Force

The acceleration in the tangential direction can be described, utilising the Euler momentum equation. Since axi-symmetry is assumed, the pressure gradient in tangential direction is zero, $\frac{-1}{\rho}\frac{\partial p}{\partial \theta} = 0$. Thus resulting in:

$$a_\theta = f_\theta$$

This specific force equates to the turning of the flow in tangential direction, and can therefore be found from the change in velocities.

In the meridional direction the following expression is reached.

$$a_m = \frac{-1}{\rho}\frac{\partial p}{\partial m} + f_m$$

$$W_m \frac{\partial W_m}{\partial m} - \frac{(W_\theta + \omega r)^2}{2}\sin(\phi) =$$
$$T\frac{\partial s}{\partial m} - \frac{\partial h_0}{\partial m} + W_m \frac{\partial W_m}{\partial m} + \left(W_m \tan(\beta) + \omega r\right)\left(\tan(\beta)\frac{\partial W_m}{\partial m} + W_m \frac{\partial \tan(\beta)}{\partial m} + \omega^2 r \sin(\phi)\right) + f_m$$

The specific force applied to the fluid by the blades, f_p are acting normal to the blade surface, in the direction given by $\vec{e}_p$. f_p may be described by components in the intrinsic coordinate system.

$$f_{n,p} = \vec{f}_p \cdot \vec{e}_n$$

$$f_{\theta,p} = \vec{f}_p \cdot \vec{e}_\theta$$

Since the tangential specific force can be found through the tangential acceleration, all forces may be calculated if the directions are known.

Finally the force in the quasi-normal direction may be calculated as

$$f_q = \sin(\phi + \gamma) f_m + \cos(\phi + \gamma) f_n$$

10.4 Modelling

The section above describes the inviscid flow terms to be caluclated in the hub-to-shroud analysis. The geometry needs to be discretized in order to implement the equations in computer code and some of the quantities within the flow require models to provide a good estimation.

10.4.1 Discretization

The impeller is discretized according to figure 10.6. The quasi-orthogonals go in the j-direction and the streamlines move in the i-direction. The computational nodes are the intersections between the streamlines and the quasi-orthogonals. The hub represents j=0 and the shroud j=n, where n is the number of streamlines. The impeller inlet represents i=0, and the outlet i=k, where k is the number of quasi-orthogonals. The area generated between four computational points, for instance [i,j], [i,j+1], [i+1,j], and [i+1,j+1] is termed a *stream-tube*.

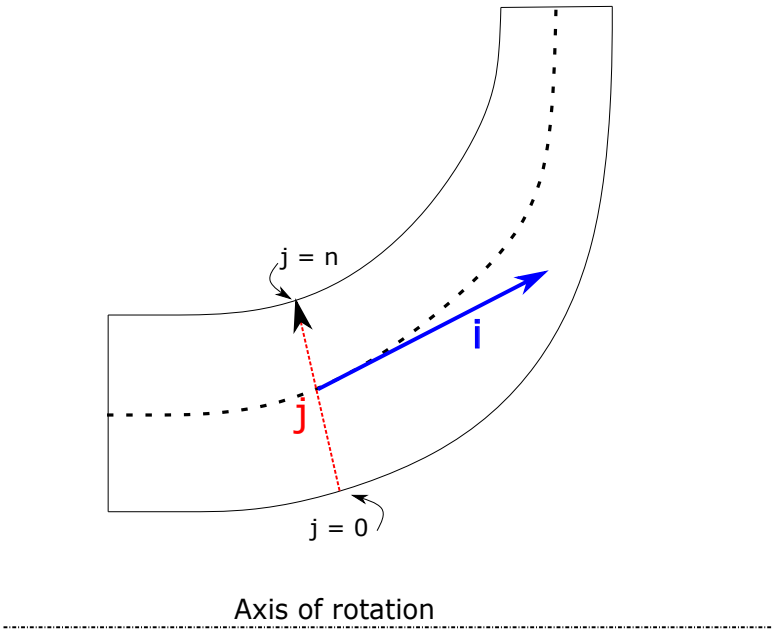

Figure 10.6: Discretization of impeller geometry.

The hub-, and shroud contours are normally specified through Bezier curves [22]. This allows the designer to specify both angles at leading-, and trailing edge, as well as the curvature. For more information about how the Bezier polynomials can be implemented, the reader is directed to appendix B. The points created along hub and shroud are then moved to be equidistant, and the quasi-orthogonals can be created by connecting respective points on the hub- and shroud contours [13]. Figure 10.7 shows how Bezier curves and quasi-normals can be implemented in a design program.

The starting point for the calculation procedure, described below, can then be initiated by creation of the initial streamlines. For this, the number of desired streamlines must be provided by the designer. The initial computational points are then distributed along the

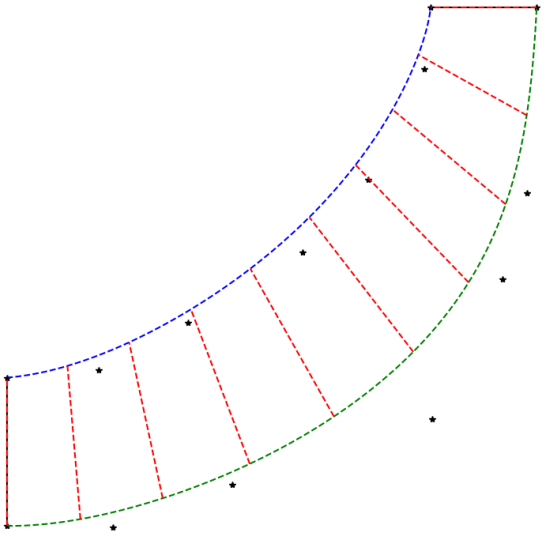

Figure 10.7: Hub(green) - and shroud(blue) contours with Bezier points and generated quasi-normal(red).

quasi-normal to give equal flow area for each stream-tube. This is done by placing the computational points on the RMS-value.

The curvature can be computed for each node on the hub- and shroud contours, as was shown in section 10.2. Along streamlines inside the impeller, however, the curvature cannot be computed as easily. A linear approximation between the contours of hub-and shroud have therefore been implemented.

10.4.2 Entropy Generation

In order to close the system of equations described in sections above a model is required for the generation of entropy, both along the quasi-normal and the meridional direction. A simple model mentioned by Casey [37] is to model the entropy generation with a specified polytropic efficiency. Another model mentioned by Casey is the dissipation loss coefficient to estimate the viscous losses.

10.5 Calculation Procedure

The implementation of the equations described in section 10.3 and the discretized geometry described in section 10.4 follow the procedure shown in figure 10.8. The computations starts with a calculation of the inlet condition and a two-zone model, following the procedures described in chapters 3 and 5. This fixes the inlet and outlet

geometry of the impeller as well as the state at inlet. The rothalpy of each streamline can thus be computed.

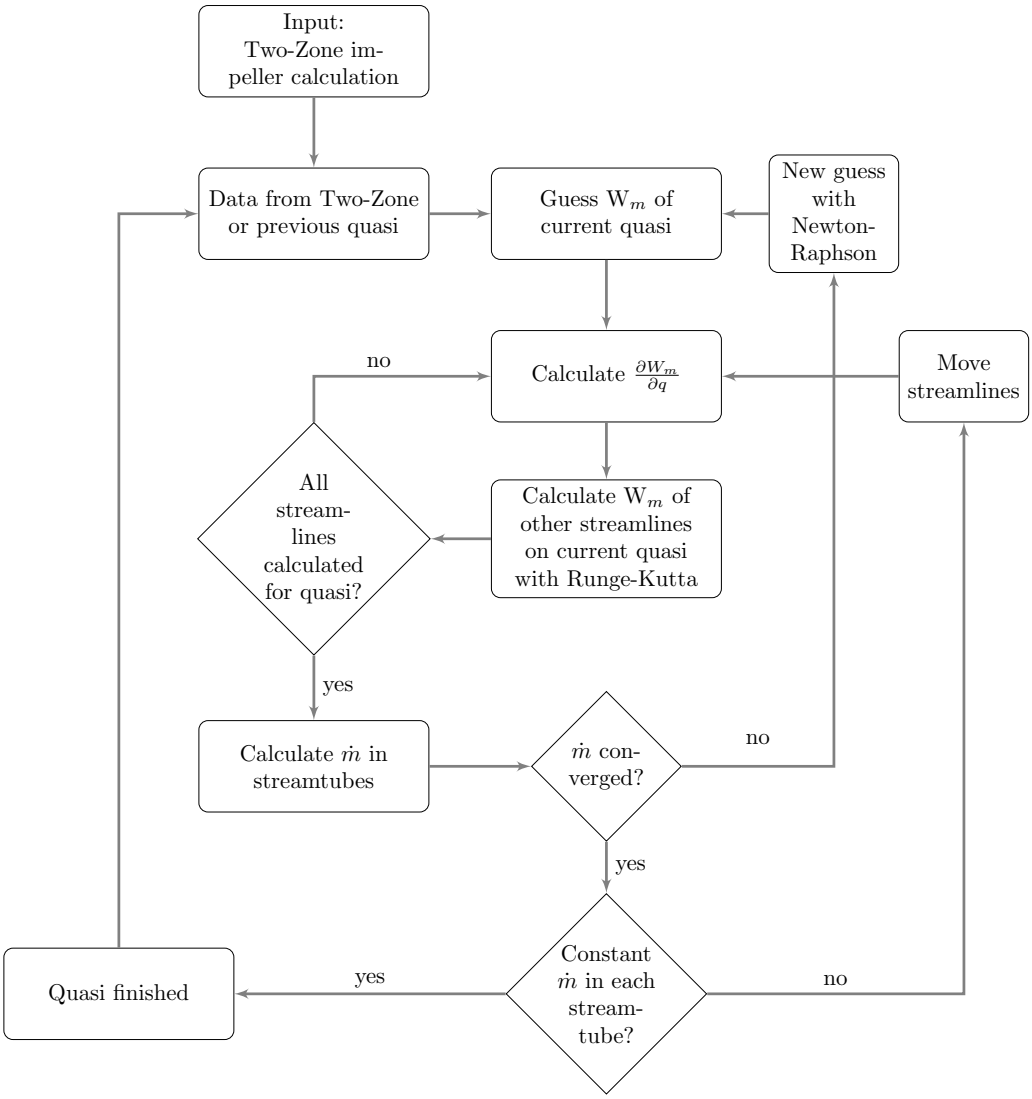

Figure 10.8: Calculation procedure for the hub-shroud analysis.

The second step in the procedure is to guess the meridional velocity in a node on the quasi-orthogonal one position ahead in the impeller ($W_{m,i+1,j}$). A good starting guess would be the meridional velocity of the current point on the same streamline ($W_{m,i,j}$). With an assumption about W_m the derivative $\frac{\partial W_m}{\partial q}$ can be calculated, which provides the meridional velocity of the adjacent streamline. In the code developed by the authors this calculation is made using a Runge-Kutta integration. This procedure follows for each node along the quasi-normal.

Once W_m has been calculated for each node, the mass-flow of each individual stream-tube

can be calculated, summed, and checked against the prescribed total mass-flow. This provides a means of validating the initial guess of W_m. W_m is updated in the code developed by the authors using the Newton-Rahpson method.

When the mass-flow has converged, the position of each computational node can be evaluated. If the mass-flow inside a stream-tube ($\dot{m}_{st}$) differs from $\dot{m}_{st}$ upstream, the distance between two nodes must be updated. If the mass-flow inside a stream-tube has changed it implies that there has been flow across a streamline, which violates the definition of a streamline. The re-positioning of nodes means that the computation must start from the top, but the values of W_m are kept from the last iteration as a first guess.

With converged W_m, $\dot{m}$, and $\dot{m}_{st}$ the calculation procedure is finished for the current quasi-normal. The data from the current-quasi-normal becomes the input value for the next quasi-normal.

Chapter 11

Validation

The developed program needs to be validated in order to be trusted as a preliminary design-tool. Validation is preferably done against a myriad of experimental data, to ensure flexibility. However, due to lack of experimental data during this thesis, validation is conducted against a theoretical pump developed in a similar tool. Further testing and tweaking of the program during use is essential to have a versatile and accurate program.

11.1 Validation against Japikse

The validation is conducted against an example given by Japikse [2]. The program is therefore validated against another computational program. However, the results from Japikse are deemed to be a good benchmark. In the data presented by Japikse, the density of the fluid is calculated to be around 2300 kg/m^3. The density is found from dynamic pressure and kinetic energy. Through this knowledge the pump performance in head may be calculated, and reasonable input data chosen to match the given case. Other fluid properties, e.g. viscosity, are not known, but assumed to be similar to water as that is the fluid stated.

All of the initial data is not readily available. Total pressure at plenum, is calculated backwards from the loss coefficient. From this estimated pressure, the sought pressure ratio is found by dividing the result at impeller tip with the plenum pressure. Mass flow is also estimated, calculated from the provided volume flow and estimated density. An estimation of blade thickness was made to 1 mm, which is deemed reasonable. Input data used is shown in table 11.1.

The relative error is calculated according to equation (11.1).

$$\text{Relative Error} = \left| \frac{\text{Our Value} - \text{Reference Value}}{\text{Reference Value}} \right| \tag{11.1}$$

11.1.1 Sources of Error

There are a few sources of error in the validation process. The most prominent sources are presented below:

- Small errors in each component are likely to add up. Another way of presenting this validation could have been component-wise. However, it was thought to be a better validation if the program as a whole was tested.
- The reference pump did not converge to exactly $\lambda_{2m} = 4.35$. This might cause some of the discrepancies. Furthermore, this raises questions about the numerical tolerances in the reference program.
- The lack of information both in design input and numerical controls may introduce sources of error, stemming from slightly different data.
- All of the models implemented in the developed design-program may not be exactly the same as for the program behind the reference pump. Important to note is that all models are merely approximations of reality.

Parameter	Value	Unit
r_{1h}	0.0857	m
σ_b	0.2	(-)
N	1000	RPM
$\dot{m}$	315	kg/s
incidence_h	2.61	°
incidence_m	2.66	°
incidence_t	2.68	°
$\lambda_{2m,\text{desired}}$	4.35	(-)
Pressure ratio	4.253889	(-)
ϕ_1	40	°
AK	1.07	(-)
LC_{01}	0.1	(-)
$BLCK_1$	0.03	(-)
β_{2b}	-67.5	°
r_5/r_2	1.36	(-)
b_5/b_2	1	(-)
p_{00}	79701.7	Pa
T_{00}	310.93	K
LC_{01}	0.1	(-)

Table 11.1: Input data for validation of pump-design

11.1.2 Inlet

Results from the inlet portion are presented in table 11.2. Overall the relative errors are small.

Parameter	Our	Reference	Unit	Rel. Error [%]
r_{1t}	0.159	0.158	m	0.63
NPSH	3.80	3.80	m	0
C_{1t}	4.00	4.07	m/s	1.7
W_{1t}	17.12	17.03	m/s	0.53
β_{1t}	-76.5	-76.2	°	0.39
C_{1m}	3.73	3.80	m/s	1.8
W_{1m}	13.88	13.84	m/s	0.29
β_{1m}	-74.4	-74.1	°	0.40
C_{1h}	3.49	3.56	m/s	2.0
W_{1h}	9.63	9.65	m/s	0.21
β_{1h}	-68.8	-68.4	°	0.58

Table 11.2: Comparison for inlet data

11.1.3 Impeller

The results regarding the impeller are seen in table 11.3. Note that the developed program converges on the value $\lambda_{2m} = 4.35$, the desired value. This is not the case for the reference data.

Parameter	Our	Reference	Unit	Rel. Error [%]
r_2	0.222	0.224	m	0.89
b_2	0.080	0.080	m	0
p_{2p}	260438	257055	Pa	1.3
p_{02p}	329887	324803	Pa	1.6
W_{2p}	13.16	14.19	m/s	7.3
p_{02s}	484760	485091	Pa	0.068
W_{2s}	2.14	2.28	m/s	6.1
p_{2m}	263789	261401	Pa	0.91
p_{02m}	344740	339042	Pa	1.7
W_{2m}	11.15	11.65	m/s	4.3
σ_{2m}	0.763	0.807	(-)	5.5
λ_{2m}	4.35	4.33	(-)	0.46

Table 11.3: Comparison for impeller data

11.1.4 Vaneless Diffuser

The data for the vaneless diffuser will be givan at three different radial locations. The first corresponds to inlet to vaneless diffuser, see table 11.4. The second at the mid-radius, table 11.5, and the last one at outlet, table 11.6. The radial locations do not line up perfectly. due to differences in previous components.

The large relative error for the losses are likely due to the difference in friction coefficients. For the reference pump a value of 0.006 compared to the calculated value in our design tool of 0.0047. The friction coefficient is calculated in equation (6.9), and the difference is likely due to different Re, stemming from different fluid properties.

Parameter	Our	Reference	Unit	Rel. Error [%]
C_m	2.86	2.81	m/s	1.8
C_θ	12.45	12.16	m/s	2.4
T	310.95	310.98	K	0.0096
p	263789	261401	Pa	0.91
p_0	344739	339042	Pa	1.7
α	77.05	76.98	°	0.09
C_p	0	0	(-)	0
LC	0	0	(-)	0
$(rC_\theta)_i/(rC_\theta)_{2m}$	1	1	(-)	0

Table 11.4: Comparison for vaneless data at radial location r = 0.222 m for our designed pump and r = 0.224 m for the reference pump.

Parameter	Our	Reference	Unit	Rel. Error [%]
C_m	2.43	2.40	m/s	1.3
C_θ	10.44	10.17	m/s	2.7
T	310.95	310.99	K	0.013
p	286294	282985	Pa	1.2
p_0	343331	337543	Pa	1.7
α	76.92	76.76	°	0.21
C_p	0.278	0.278	(-)	0
LC	0.017	0.021	(-)	19
$(rC_\theta)_i/(rC_\theta)_{2m}$	0.99	0.987	(-)	0

Table 11.5: Comparison for vaneless data at radial location r = 0.2616 m for our designed pump and r = 0.2644 m for the reference pump.

Parameter	Our	Reference	Unit	Rel. Error [%]
C_m	2.10	2.08	m/s	0.96
C_θ	9.00	8.71	m/s	3.3
T	310.95	310.99	K	0.013
p	300217	296175	Pa	1.4
p_0	342323	336344	Pa	1.8
α	76.79	76.54	°	0.33
C_p	0.45	0.448	(-)	0.45
LC	0.030	0.037	(-)	19
$(rC_\theta)_i/(rC_\theta)_{2m}$	0.980	0.975	(-)	0.51

Table 11.6: Comparison for vaneless data at radial location r = 0.3015 m for our designed pump and r = 0.3048 m for the reference pump

11.1.5 Vaned Diffuser

The reference pump does not have a vaned diffuser, and thus it could not be validated against. However, there is a reference compressor in Japikse [22] that feature a vaned diffuser with 11 NACA65-0406 airfoils. The solidity, loss-coefficient, and pressure recovery are similar to the vaned diffuser developed in the developed program.

11.1.6 Volute & Return Channel

Due to lack of information regarding the volute, e.g. shape and model, it is omitted from the validation.

The reference pump does not contain a return channel, which is why this part of the developed program cannot be validated. However, the performance of return channels designed are on par with experimental performance-data presented in [2].

Chapter 12

Conclusions

12.1 Conclusions

A tool for preliminary design of radial pumps, named *RaPID* (**Ra**dial **P**ump **I**nitial **D**esign), has been developed. The tool is able to produce designs with a variety of components to choose from with satisfactory results, as shown in chapter 11. The speed of design generation and off-design analysis is quick. It takes only seconds to read, run the calculations, and produce a report presented in either excel or as a text-file.

With increasing computational power, full 3D simulations become increasingly accessible, even for simple problems. However, old and proven methods utilised when computers were quite weak, should not be underestimated. In these preliminary designs, only the most vital aspects of the flow are considered. If a pump is designed poorly in respect to these vital aspects, the project as a whole will suffer since it is more costly to use a trial-and-error approach during 3D-simulations. The benefit of a trustworthy and rapid design tool, then, should not be overlooked. Once an accepted preliminary design is obtained, it may be transferred to 3D simulations to alter details not accessible in 1D or 2D simulations. The designer should use the most suitable tool available for the current phase of the design process.

12.2 Future Work

The models presented in this text can be developed further. They rely on empirical data and assumptions about the flow. With more knowledge about flow structures in radial turbomachinery and more empirical data it is possible to create more accurate models that can improve the preliminary design.

One assumption about the flow made in this text is that it is axi-symmetric. Models describing flow-interactions between impeller, diffuser, and volute that look at non-symmetric flow structures could give the designer a better insight into how the pump

would perform at off-design mass-flows. Such models are available in the open literature, see for instance [14].

A handful of possible topics that could improve the preliminary design tool are:

- Connect the output data from the return channel to the input data of a following stage, thus having the possibility to easily design a multistage pump. This step has to be done manually in the current program.
- Two-zone model applied to the vaneless difuser, see for example Japikse and Dubitsky [38].
- A impeller-diffuser-volute response model
- Parallelisation, mainly for faster off-design computation. However, if more sophisticated models are to be implemented, it might be necessary to incorporate parallel processing to keep computational times low.

Bibliography

[1] C. Anderson, *Wind Turbines: Theory and Practice*. Cambridge University Press, 2020, ISBN: 9781108478328.

[2] D. Japikse, W. D. Marscher and R. B. Furst, *Centrifugal Pump Design and Performance*. 2006, ISBN: 0-933283-09-1.

[3] J. Andersson, *Fundamentals of Aerodynamics*. McGraw-Hill, 2011.

[4] H. Versteeg and W. Malalasekera, *An Introduction to Computational Fluid Dynamics: The Finite Volume Method*. Pearson Education Limited, 2007, ISBN: 9780131274983.

[5] E. M. Greitzer, C. S. Tan and M. B. Graf, *Internal Flow: Concepts and Applications*. Cambridge University Press, 2004.

[6] Y. A. Cengel and M. A.Boles, *Thermodynamics an Engineering Approach*, 8th ed. 2 Penn Plaza, New York, NY 10121: McGraw-Hill Education, 2015, ISBN: 978-981-4595-29-2.

[7] D. Young, *Introduction to Fluid Mechanics*. Wiley, 2012, ISBN: 9780470902158.

[8] *Liquid Rocket Engine Turbopump Inducers. NASA SP-8052*. 1971, vol. 8052.

[9] S. L. Dixon and C. A. Hall, *Fluid Mechanics and Thermodynamics of Turbomachinery*. 2014, ISBN: 978-0-12-415954-9.

[10] E. S. Taylor, "Film notes for secondary flow", Massachusetts Institute of Technology, Report 21612, 1968.

[11] M. Johnson, "Secondary flow in rotating bends", *Journal of Engineering for Power*, vol. 100, pp. 553–560, 1978.

[12] J. Daily and R. Nece, "Chamber dimension effects on induced flow and frictional resistance of enclosed rotating disks", *Journal of Basic Engineering*, vol. 82, pp. 217–230, 1978.

[13] R. Aungier, *Centrifugal Compressors: A Strategy for Aerodynamic Design and Analysis*. ASME Press, 2000, ISBN: 9780791800935.

[14] R. Van den Braembussche, *Design and Analysis of Centrifugal Compressors*, ser. Wiley-ASME Press Series. Wiley, 2019, ISBN: 9781119424109.

[15] J. D. Stanitz, "One-dimensional compressible flow in vaneless diffusers of radial-, and mixed-flow centrifugal compressors including effects of friction, heat transfer and area change", Lewis Flight Propulsion Laboratory, Technical Note 2610, 1952.

[16] W. Jansen, "Rotating stall in a radial vaneless diffuser", *Journal of Basic Engineering*, vol. 86, pp. 750–758, 1964.

[17] P. Fringe and R. Van den Braembussche, "A theoretical model for rotating stall in the vaneless diffuser of a centrifugal compressor", *Journal of Engineering for Gas Turbines and Power*, vol. 107, pp. 507–513, 1985.

[18] Y. Senoo and Y. Kinoshita, "Influence of inlet flow conditions and geometries of centrifugal vaneless diffusers on critical flow angle for reverse flow", *Journal of Fluid Engineering*, vol. 99, pp. 98–102, 1977.

[19] R. H. Aungier, "A systematic procedure for the aerodynamic design of vaned diffusers", *ASME FED*, vol. 69, pp. 27–34, 1988.

[20] S. Lieblein, "Analysis of experimental low-speed loss and stall characteristics of two-dimensional compressor blade cascades", Lewis Flight Propulsion Laboratory, Technical Note RM E57A28, 1957.

[21] A. R. Howell, "Fluid dynamics of axial compressors", *Proceedings of the Institution of Mechanical Engineers*, vol. 153, no. 1, pp. 441–452, 1945.

[22] D. Japikse, *Centrifugal Compressor Design and Performance*. 1996, ISBN: 978-0-933283-03-9.

[23] I. Johnsen, R. Bullock, N. Aeronautics, S. Space Administration and L. R. C. Technical Information Division, *Aerodynamic Design of Axial-flow Compressors: Ed*. U.S. Government Printing Office, 1965.

[24] C. Rodgers, "The Performance of Centrifugal Compressor Channel Diffusers", ser. Turbo Expo: Power for Land, Sea, and Air, V001T01A003, vol. Volume 1: Turbomachinery, Apr. 1982.

[25] Y. Senoo, H. Hayami and K. Utsunomiya, "Application of a low-solidity cascade diffuser to transonic centrifugal compressor", *Journal of Turbomachinery*, vol. 112, pp. 25–29, 1990.

[26] E. Rothstein, *Experimentelle und theoretische Untersuchung der Strömungsvorgänge in Rückführkanälen von Radialverdichterstufen, insbesondere solcher mit geringen Kanalbreiten*. Fakultät für Maschinenwesen der Rheinisch-Westfählischen Technischen Hochschule Aachen, 1984.

[27] R. H. Aungier, "Aerodynamic design and analysis of vaneless diffusers and return channels", Turbo Expo: Power for Land, Sea, and Air, vol. Volume 1: Aircraft Engine; Marine; Turbomachinery; Microturbines and Small Turbomachinery, May 1993.

[28] C. R. Weber and M. E. Koronowski, "Meanline Performance Prediction of Volutes in Centrifugal Compressors", ser. Turbo Expo: Power for Land, Sea, and Air, vol. Volume 1: Turbomachinery, Jun. 1986.

[29] H. Chen, D. Tong and X. Wang, "Vortices and performance of internal and external volutes", Jun. 2015.

[30] M. Heinrich and R. Schwarze, "Genetic optimization of the volute of a centrifugal compressor", 2017.

[31] H. Mishina and I. Gyobu, "Performance Investigations of Large Capacity Centrifugal Compressors", ser. Turbo Expo: Power for Land, Sea, and Air, vol. Volume 1A: General, Apr. 1978.

[32] E. Ayder and R. Braembussche, "Numerical analysis of the 3d swirling flow in centrifugal compressor volutes", May 1993.

[33] D. Japikse, "Advanced diffusion levels in turbocharger compressors and component matching.", *I Mech E Conference Publications (Institution of Mechanical Engineers)*, pp. 143–155, Jan. 1982.

[34] I. Karassik, *Pump Handbook*, ser. Mechanical engineering. McGraw-Hill, 1976, ISBN: 9780070333017.

[35] C. Wu, P. Beck and U. S. N. A. C. for Aeronautics, *A General Theory of Three-dimensional Flow in Subsonic and Supersonic Turbomachines of Axial-, Radial-, and Mixed-flow Types*, ser. Technical note. National Advisory Committee for Aeronautics, 1952.

[36] D. Japikse and N. Baines, *Introduction to Turbomachinery*, ser. A Concepts ETI Book Series. Concepts ETI, 1994, ISBN: 9780933283060.

[37] M. Casey and C. Robinson, *Radial Flow Turbocompressors*. Cambridge University Press, 2021, ISBN: 9781108416672.

[38] O. Dubitsky and D. Japikse, "Vaneless diffuser advanced model", *Journal of Turbomachinery*, vol. 130, 2008.

[39] J. Hoffman and S. Frankel, *Numerical Methods for Engineers and Scientists, Second Edition,* Taylor & Francis, 2001, ISBN: 9780824704438.

Appendix A

State Function

Equations of state (EOS) was introduced in chapter 2 and it was noted that two thermodynamic properties was required to fix the state. Once the state is fixed the other properties linked to the state can be determined using EOS. There are software available, e.g. REFPROP, that lets the user insert state-properties and receive any other thermodynamic property or dependant property of the state. The state must be fully defined by the input properties.

Using EOS-software is useful when the number of state calculations are limited. The EOS-calculations require significant computational effort and as the number of calls to the software increase so does the computational time. With large number of state-calculations it is often more efficient to access the properties of a state through property tables. One common file-type that contains property tables are RGP-files (Real Gas Property). RGP-files have a predictable structure which make them easy to implement.

The thermodynamic properties in a RGP-file are sorted by temperature and pressure. The file contains both single phase properties and saturation properties. The thermodynamic properties available, besides temperature and pressure, are:

- Specific enthalpy, h
- Specific entropy, s
- density, ρ

The dependent properties available in a RGP-file are:

- Specific heat at constant pressure, c_p
- Specific heat at constant volume, c_v
- Speed of sound, a
- Dynamic viscosity, μ
- Thermal conductivity, k

In order for the program to use RGP-files instead of an EOS-software the program must be able to read the files and interpolate between values. The program should be able to find all of the properties no matter which thermodynamic properties are given. The trivial case is when T and p are known, as the tables are already sorted by T and p. Any other set of thermodynamic properties require table inversion, which is a more sophisticated search. The search that involves the most computations is to supply h, s, or ρ to find the other properties of the state, e.g T = T(h, s).

The problem with table-inversion was solved in a recursive manner, to minimise the computational time and effort. The algorithm that searches through the tables divides the table into quadrants and checks whether one of the input properties lie within one of these quadrants. If it does, the algorithm checks weather the other input property also lies within the aforementioned quadrant. If both values are found within a quadrant, that specific quadrant is subdivided into 4 new quadrants and the process starts anew. One key aspect of the search is that tables are continuous, this enables the algorithm to determine whether the sought value exists within a certain quadrant.

The search-algorithm stops when the two input properties are found in, or between, four points in the table. Then, bi-linear interpolation is used to yield an estimation of the thermodynamic-state and return the sought properties.

Appendix B

Bezier Curves

A Bezier curve is a curve defined by N points, and gives a curve described by a polynomial of order N-1. I.e. two points give a straight line, three points gives a second degree curve etc. For a general Bezier curve, the curve starts in the first control point and ends in the last point. It is guided by the other points, but does not generally pass through them. The easiest way of describing the process of obtaining the Bezier curve, is to start with two points. The Bezier curve can easily be obtained from linear interpolation from the first point to the other, described below in equation (B.1)

$$Q(t) = P_0(1-t) + P_1 t \qquad 0 \leq t \leq 1 \tag{B.1}$$

When adding an additional point, the complexity is increased. Between the first and second point a line is described, as done above. Similarly is done between the second point and the third point. Now, the Bezier curve may be obtained from linear interpolation, from the two already interpolated lines, as described below in equations (B.2). It should be clear to the reader that a simple substitution of the Q-expressions into the third line of equation (B.2) will result in a single, second-order polynomial, seen in equation (B.3).

$$\begin{aligned} Q_0(t) &= P_0(1-t) + P_1 t & 0 \leq t \leq 1 \\ Q_1(t) &= P_1(1-t) + P_2 t & 0 \leq t \leq 1 \\ R(t) &= Q_0(1-t) + Q_1 t & 0 \leq t \leq 1 \end{aligned} \tag{B.2}$$

$$R(t) = P_0(1-t)^2 + 2P_1 t(1-t) + P_2 t^2 \tag{B.3}$$

The reader should now have a clear picture of how a greater number of points form a Bezier curve, i.e. through a recursive process of linear interpolation until a single curve is left. If a fourth point were to be added to the example above, three Q-expressions would be obtained, which in turn results in two R-expressions. These two expressions can then be used to obtain a single third-order polynomial, which describes the single Bezier curve.

Appendix C

Numeric Methods

C.1 Newton-Raphson

The Newton-Raphson method utilises the derivative of the function to estimate the next guess in the iteration. It is one of the most popular method for solving non-linear equations due to its fast and reliable convergence [39]. The convergence-rate is quadratic.

$$x_{i+1} = x_i - \frac{f(x_i)}{f'(x_i)} \tag{C.1}$$

The drawback of the Newton-Raphson model is that the derivative must be calculated, which adds a computational point from the start. The method can be visualised according to figure C.1.

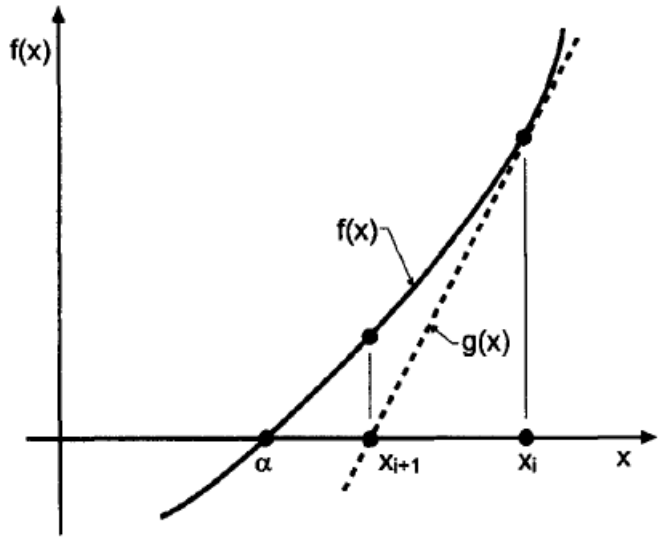

Figure C.1: Newton-Raphson method, from Hoffman [39].

C.2 Runge-Kutta

Differential equations are encountered in many fields. In this thesis they were introduced in chapter 6. To solve differential equations numerically the Runge-Kutta method was used. This text relies upon the work by Hoffman [39].

Consider equation (C.2), where a non-linear first order ordinary differential equation (ODE) is given.

$$y' = \frac{dy}{dt} = f(t, y) \tag{C.2}$$

If the initial value is known for the equation, the solution can be estimated through marching through the solution one step at the time. A simple approach of doing this is assuming the function to be piece-wise linear, i.e. holding the slope constant from point n to $n + 1$, based on the slope value of point n.

$$y_{n+1} = y_n + \Delta y \tag{C.3}$$

where:

$$\Delta y = y'(y_n)\Delta t \tag{C.4}$$

However, by using this method, the time step, Δt, must be kept small to minimise the errors. The fourth order Runge-Kutta method is shown in equation (C.5), where the next step value is described by a weighted sum of all four Δy.

$$y_{n+1} = y_n + \frac{1}{6}\left(\Delta y_1 + 2\Delta y_2 + 2\Delta y_3 + \Delta y_4\right) \tag{C.5}$$

The differences, Δy, are described at different points between t_n and t_{n+1}, where the midpoint differences are weighted heavier. The differences are described below in equation (C.6).

$$\begin{aligned}
\Delta y_1 &= \Delta t\, f(t_n,\ \ y_n) \\
\Delta y_2 &= \Delta t\, f\left(t_n + \frac{\Delta t}{2},\ \ y_n + \frac{\Delta y_1}{2}\right) \\
\Delta y_3 &= \Delta t\, f\left(t_n + \frac{\Delta t}{2},\ \ y_n + \frac{\Delta y_3}{2}\right) \\
\Delta y_4 &= \Delta t\, f(t_n + \Delta t,\ \ y_n + \Delta y_1)
\end{aligned} \tag{C.6}$$

The ODEs presented in chapter 6 for the diffuser are shown below for simplicity. They can be solved in a similar manner as mentioned above, with the exception that they depend on each other. The equations can either be solved simultaneously in a matrix or sequentially, the latter was chosen by the authors.

$$\frac{dp}{dr} = \rho\left(\frac{C_\theta^2}{r} - C_m\frac{dC_m}{dr} - C_f\frac{C^2\cos(\alpha)}{b\sin(\phi)}\right) \tag{C.7}$$

$$\frac{dC_\theta}{dr} = -\frac{1}{C_m}\left(\frac{C_m C_\theta}{r} + C_f\frac{C^2\sin(\alpha)}{b\sin(\phi)}\right) \tag{C.8}$$

$$\frac{dC_m}{dr} = -C_m\left(\frac{1}{\rho}\frac{d\rho}{dr} + \frac{1}{b}\frac{db}{dr} + \frac{1}{r}\right) \tag{C.9}$$

To solve the flow state in each point, but most importantly at the last point, i.e. outlet from the diffuser, these equations are solved iteratively with the Runge-Kutta method.

Since this is an initial valued problem, the flow state, and fluid state, is completely known at inlet to the diffuser. Each of the three ODEs above can be evaluated at station 2. An approximation can be made at the mid-way point similar to equations (C.3) and (C.4), between the start point and next point. The same ODEs are evaluated at this mid-point, but with new values. Next, new derivatives are obtained. These are used to acquire new values at the mid-point. From these values a third set of derivatives are calculated and from these, values of the next point are approximated. These values are used at this point to get a fourth set of derivatives.

At this stage, four set of derivatives exist. These are used in a weighted average to obtain the difference of the current point and the next one, see equations (C.5) and (C.6). This means that the next point is now approximated. The same procedure can now be repeated until the final radius is reached.